

Application of image processing and statistical analysis to model patient outcomes in  
cochlear implantation and epilepsy surgery

By

Srijata Chakravorti

Dissertation

Submitted to the Faculty of the  
Graduate School of Vanderbilt University  
in partial fulfillment of the requirements  
for the degree of

DOCTOR OF PHILOSOPHY

in

Electrical Engineering

May 14, 2021

Nashville, Tennessee

Approved:

Prof. Benoit M. Dawant, PhD

Prof. Jack H. Noble, PhD

Prof. Robert F. Labadie, MD, PhD

Prof. Richard Alan Peters, PhD

Prof. Ipek Oguz, PhD

Copyright ©2021 by Srijata Chakravorti

All Rights Reserved

# TABLE OF CONTENTS

	Page
LIST OF TABLES . . . . .	vii
LIST OF FIGURES . . . . .	ix
LIST OF ABBREVIATIONS . . . . .	xii
Chapter	
1 Introduction . . . . .	1
1.1 Cochlear Implantation . . . . .	2
1.1.1 Hearing Outcomes and role of Positioning . . . . .	3
1.1.2 Image Quality . . . . .	4
1.2 Laser Interstitial Thermal Therapy for Epilepsy . . . . .	7
1.3 Goals and Contributions of this Dissertation . . . . .	8
2 Cochlear implant phantom for evaluating computed tomography acquisition parameters . . . . .	11
2.1 Introduction . . . . .	12
2.2 Methods . . . . .	17
2.2.1 Construction of the Phantom . . . . .	18
2.2.2 Dataset . . . . .	18
2.2.3 Localization of Cochlear Implant Arrays . . . . .	21
2.2.4 Registration . . . . .	21
2.2.4.1 Point-based rigid body registration . . . . .	21
2.2.4.2 Mutual information based rigid body local image registration . . . . .	23

2.2.5	Electrode Localization Errors . . . . .	24
2.3	Results . . . . .	26
2.3.1	Evaluation of Automatic Cochlear Implant Array Localization Using the Phantom . . . . .	29
2.3.1.1	Automatic localization errors . . . . .	35
2.3.1.2	Effect of acquisition parameters . . . . .	36
2.3.2	Modeling Expected Errors based on Image Quality . . . . .	40
2.4	Conclusions . . . . .	41
2.5	Acknowledgements . . . . .	42
3	Further Evidence of the Relationship Between Cochlear Implant Electrode Posi- tioning and Hearing Outcomes . . . . .	44
3.1	Introduction . . . . .	45
3.2	Materials and Methods . . . . .	48
3.3	Results . . . . .	50
3.4	Discussion . . . . .	53
3.4.1	Precurved (a.k.a. Perimodiolar) Electrodes . . . . .	53
3.4.2	Implications for Precurved (a.k.a. Perimodiolar) Electrodes . . . . .	55
3.4.3	Lateral Wall (a.k.a. Straight) Electrodes . . . . .	56
3.4.4	Implications for Lateral Wall (a.k.a. Straight) Electrodes . . . . .	56
3.4.5	Implications for Surgical Procedures . . . . .	57
3.4.6	Limitations . . . . .	58
3.5	Conclusions . . . . .	59
3.6	Acknowledgements . . . . .	59
4	Effects of precurved cochlear implant position on open-set word recognition out- comes . . . . .	60
4.1	Introduction . . . . .	61

4.2	Material and Methods . . . . .	63
4.2.1	Dataset . . . . .	63
4.2.2	Features Computed from CT Images . . . . .	64
4.2.3	Analysis . . . . .	65
4.3	Results . . . . .	66
4.3.1	Relationship between features and outcome . . . . .	66
4.3.2	Analyzing modiolar distance . . . . .	68
4.3.3	Tip Insertion Depth and Apical Mean Modiolar Distance . . . . .	68
4.3.4	Linear Regression . . . . .	69
4.4	Discussion . . . . .	72
4.4.1	Effects of Demographics . . . . .	72
4.4.2	Effect of Position . . . . .	73
4.4.3	Simulation . . . . .	74
4.5	Conclusions . . . . .	75
4.6	Acknowledgments . . . . .	76
5	Identifying effects of surgical targeting in laser interstitial thermal therapy for mesial temporal lobe epilepsy . . . . .	77
5.1	Introduction . . . . .	78
5.2	Methods . . . . .	79
5.2.1	Study design . . . . .	79
5.2.2	Participants . . . . .	79
5.2.3	Data collection . . . . .	80
5.2.4	Ablation cavity quantification . . . . .	81
5.2.5	Image Normalization and Segmentation . . . . .	81
5.2.6	Volume of ablation . . . . .	84
5.2.7	Statistical analysis of clinical variables . . . . .	86
5.2.8	Statistical analysis of ablation location . . . . .	86

5.3	Results . . . . .	88
5.3.1	Seizure outcomes . . . . .	88
5.3.2	Complications . . . . .	89
5.3.3	Volume of ablation for mesial structures . . . . .	90
5.3.4	Ablation location . . . . .	91
5.4	Discussion . . . . .	92
5.4.1	Patient factors . . . . .	92
5.4.2	Surgical factors . . . . .	93
5.4.3	Complications . . . . .	96
5.4.4	Limitations . . . . .	96
5.5	Conclusion . . . . .	97
5.6	Acknowledgements . . . . .	98
5.7	Supplementary Information: Calculation of Engel I Probability Maps . . . . .	98
6	Summary and Future Work . . . . .	103
	REFERENCES . . . . .	109

## LIST OF TABLES

Table	Page
2.1 Image Dataset . . . . .	20
2.2 Effect of electrode spacing on localization errors. . . . .	29
2.3 Effect of HU range during reconstruction . . . . .	29
2.4 Effect of Orientation . . . . .	30
2.5 Effect of Resolution . . . . .	31
2.6 Effect of Dose . . . . .	32
2.7 Summary of effects of CT parameters on localization accuracy . . . . .	33
2.8 Standard Linear Model fit with intercept of average localization error values.	41
3.1 Straight and precurved arrays included in the study . . . . .	49
3.2 Summary of factors included in each GLM . . . . .	51
3.3 Pearson correlation coefficients between factors and audiological scores . .	52
3.4 Model specifications for precurved arrays . . . . .	52
3.5 Model specifications for straight arrays . . . . .	53
4.1 Patient demographics, position features, and outcomes . . . . .	65

4.2	Precurved arrays included in the study . . . . .	65
5.1	Average Node Errors distribution . . . . .	85
5.2	Patient demographics and characteristics relative to seizure outcomes . . . .	87
5.3	Reported complications based on retrospective chart review . . . . .	90

## LIST OF FIGURES

Figure	Page
1.1 Parts of a CI system . . . . .	3
1.2 Effect of beam orientation in CT . . . . .	5
1.3 CT image quality . . . . .	6
1.4 Intraoperative and postoperative MR T1 images of a LITT procedure . . . . .	8
2.1 CI array implanted in the left ear . . . . .	13
2.2 Measurements of electrode position demonstrated on a specimen . . . . .	14
2.3 Method of processing the phantom images to obtain localization errors. . . . .	17
2.4 CI phantom . . . . .	19
2.5 Visual verification of registration accuracy . . . . .	25
2.6 Image-Based Localization Errors across A1 and A2 . . . . .	27
2.7 Effect size values for image-based localization errors across A1 and A2 . . . . .	30
2.8 Results from Automatic Electrode Localization . . . . .	34
2.9 Automatic and Image-Based Localization Errors . . . . .	37
2.10 Automatic Localization Errors . . . . .	38

2.11	Effect size values for automatic localization errors across A1 and A2 (Auto I)	39
2.12	Effect size values for automatic localization errors across A1 and A2 (Auto II)	39
3.1	CI positioning measures	50
4.1	Correlation of Continuous Demographic Features with CNC scores	66
4.2	Correlation of Continuous Position Features with CNC scores	67
4.3	Effect of Categorical Position Features on CNC scores	67
4.4	Correlation of Different Modiolar Distance Features with CNC scores	68
4.5	Correlation of Tip Insertion Depth with Apical Mean Modiolar Distance	70
4.6	Analysis of relative importance of tip insertion depth and apical mean modiolar distance	71
4.7	Multiple Linear Regression Model	71
4.8	Variation of mean predicted outcome with the change of the important position factors	75
5.1	Subject Selection Flowchart	80
5.2	Accuracy of nonrigid registration at predicting hippocampal borders from preoperative MRI	84
5.3	Work flow for LITT ablation image-processing	85

5.4	Rates of Engel I outcome . . . . .	88
5.5	Heat map of the distribution of ablations . . . . .	91
5.6	PPV and NPV . . . . .	101
5.7	Theoretical ablation zones . . . . .	102

## LIST OF ABBREVIATIONS

AB	Advanced Bionics
ABA	Adaptive Bases Algorithm
AED	Antiepileptic Drug
AHC	Amygdalohippocampal Complex
ANE	Average Node Error
ASE	Average Surface Error
ATL	Anterior Temporal Lobectomy
BKB-SIN	Bamford-Kowal-Bench Sentences in Noise
BM	Basilar Membrane
CI	Cochlear Implant
CNC	Consonant-Nucleus-Consonant
CO	Cochlear Devices
CRST	Clinical Rating Scale for Tremor
CT	Computed Tomography
DRE	Drug Resistant Epilepsy
EADC	European Alzheimer's Disease Consortium
EEG	Electroencephalography
ET	Essential Tremor
FAS	Focal Aware Seizures
FIAS	Focal Impaired Awareness Seizures
FLE	Fiducial Localization Error
FTC	Focal to Bilateral Tonic-Clonic Seizures
GLM	Generalized Linear Model
HIFU	High Frequency Focused Ultrasound
HL	Hearing Loss

HU	Hounsfield Units
iEEG	Intracranial Electroencephalography
IRB	Institutional Review Board
LITT	Laser Interstitial Thermal Therapy
ME	Med-EI
MI	Mutual Information
MRI	Magnetic Resonance Image
mTLE	Mesial Temporal Lobe Epilepsy
NIDCD	National Institute on Deafness and Other Communication Disorders
NPV	Negative Predictive Value
OR	Odds Ratio
PET	Positron Emission Tomography
PhCT	Philips CT Scanner
PPV	Positive Predictive Value
rHS	Radiographic evidence of Hippocampal Sclerosis
rms	Root Mean Square
RW	Round Window
SiCT	Siemens CT Scanner
SNR	Signal-to-Noise Ratio
ST	Scala Tympani
SUDEP	Sudden Unexplained Death in Epilepsy
SV	Scala Vestibuli
TRE	Target Registration Error
XCT	Xoran CT Scanner

# Chapter 1

## INTRODUCTION

Image guided minimally invasive surgery is considered one of the safest and most precise methods of performing surgical interventions. Not only does a minimally invasive approach reduce risks associated with open surgery, image guidance also allows precise targeting which helps avoid collateral damage to healthy tissue. Currently image guidance can be integrated into every step of patient care. Preoperative scans aid in surgical planning, intraoperative scans provide feedback during surgery, and postoperative imaging provides data which can be analyzed to improve future surgical procedures. The widespread adoption of image guidance has been largely possible due to the development of automatic image processing methods. Two examples of automatic image processing methods that are heavily involved in image guided therapy are image registration, and image segmentation. The registration of patient anatomy to a labeled reference atlas helps overcome issues of patient variability in terms of physiology and pathology. Aligning patient images to a common atlas image enables the identification of structures, aids surgical targeting, and in general provides a means to compare data across different patients and institutions. Image segmentation enables identification of anatomy as well as tracking the state of the targeted anatomy pre-, intra- and post-operatively. Automatic segmentation algorithms eliminate the time and labor cost associated with manual segmentation by experts and ensure consistency of results.

The best evaluation of the efficiency of a surgical intervention are the patient outcomes. Image guided surgeries are ideal subjects for outcomes analysis, because the associated imaging data provides a rich array of features describing details of the physiological results of the surgery. This dissertation primarily focuses on the analysis of preoperative and post-operative images, and their correlation with outcomes, in two specific minimally invasive

image guided interventions – cochlear implantation and laser interstitial thermal therapy (LITT) for mesial temporal lobe epilepsy (mTLE). We will briefly discuss these surgical methods and our aims in the following sections 1.1 and 1.2.

## **1.1 Cochlear Implantation**

The cochlea is a fluid-filled spiral bony structure in the inner ear that plays a key role in converting mechanical sound waves to electrical impulses for sound perception. Sound waves entering the outer ear set up traveling waves in the cochlear fluid, which are converted to electrical signals by the hair cells of the organ of Corti [1]. The auditory nerve conducts this signal to the brain, and this entire process produces the phenomenon of hearing. In cases where the hair cells are damaged, the sound to nerve signal transformation is interrupted and the patient perceives this as hearing loss.

Cochlear implants (CIs) are neuroprosthetics that are widely considered the standard of care treatment for patients with at least a moderate sloping to profound sensorineural hearing loss. According to the National Institute on Deafness and Other Communication Disorders (NIDCD) [2], over 324,200 people worldwide have received CIs. The central component of a CI is an electrode array that has to be surgically implanted into the inner ear (Fig. 1.1) through the round window after temporal mastoidectomy. The array is connected to an internal receiver coil embedded under the skin at the surface of the skull. Externally, a microphone and a CI processor are worn behind the ear while a transmitting coil is connected to the skull at the same position as the receiver. The processor converts the sound picked up by the microphone into electrical signals that is transmitted to the internal receiving coil and then on to the implanted electrodes. The activated electrodes stimulate the surviving nerve cells of the spiral ganglia bypassing the damaged cochlea and produce the sensation of sound.

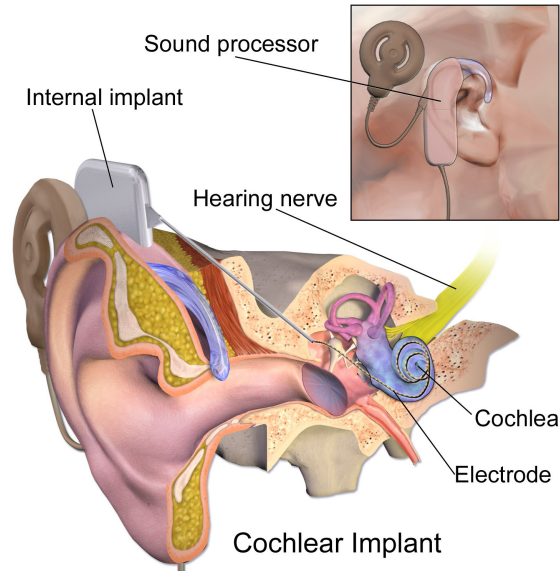


Figure 1.1: The CI consists of several internal and external components described in this figure. The internal components are the electrode array and the internal implant. The microphone, sound processor and transmitting coil constitute the external parts. Image retrieved from Wikimedia [3].

### 1.1.1 Hearing Outcomes and role of Positioning

Most recipients experience impressive improvement in their hearing with CIs, with average speech recognition scores in quiet approximately at 60% correct for Consonant-Nucleus-Consonant (CNC) monosyllabic word scores and 70% for AzBio sentence recognition tests in quiet [4–7]. However, despite their remarkable effectiveness, patient outcomes suffer from unexplained variability [8] and many studies have been conducted to determine the causes. Besides factors like duration of deafness before CI implantation [8–14] and length of CI use [9, 15–17], studies have found that the final CI position also has a significant association with hearing outcomes. However, there are still conflicting conclusions among these studies about which specific factors of positioning affect hearing outcomes. For example, while most studies agree that scalar translocation of the electrode array across the basilar membrane from scala tympani (ST) to the scala vestibuli (SV) is strongly correlated with poor hearing outcomes [8, 18–22], certain studies report no correlation between

outcomes and positioning of the array in ST [23, 24]. There are also disagreements regarding the effect of insertion depth. While a number of studies [19, 21, 25, 26] come to the conclusion that there is a positive correlation between monosyllabic word scores and insertion depth of the most basal electrode, other studies [27, 28] do not find any significant correlation, and certain other analyses [8, 20] report a negative correlation of outcomes with insertion depth. There are several possible reasons for the lack of consensus, including the fact that the effect might differ for straight and precurved arrays and it's possible that the relationship is not monotonic. Undoubtedly, there is a need for further large-scale studies to clarify the relationship between positioning and outcomes, which we undertake in Chapters 3 and 4.

One factor that has limited large scale analysis of these relationships is the difficulty in post-operative imaging. CI electrodes and the anatomy of interest are so small that they are difficult or impossible to directly visualize. Electrode position is also not known intra-operatively because the surgeon must thread the array through a very small opening into the cochlea (usually the round window membrane), and it is not possible to predict the final position of the array in the cochlea. Post-implantation high resolution Computed Tomography (CT) imaging is the best modality for this application and provides the resolution necessary to visually identify electrode position, albeit with an unknown degree of accuracy depending on image acquisition parameters.

### **1.1.2 Image Quality**

The accuracy of any image processing algorithm is invariably affected by the image quality. We can define CT image quality by four parameters – orientation of the subject in the scanner, Hounsfield Unit (HU) range of reconstruction of the image, image resolution, and dose of the scan. Orientation of the subject in the scanner, for example, may cause the beams to pass through teeth or receiver coils along with the CI electrodes and worsen beam hardening artifacts. Fig. 1.2 shows three scans of the same phantom in the same scanner

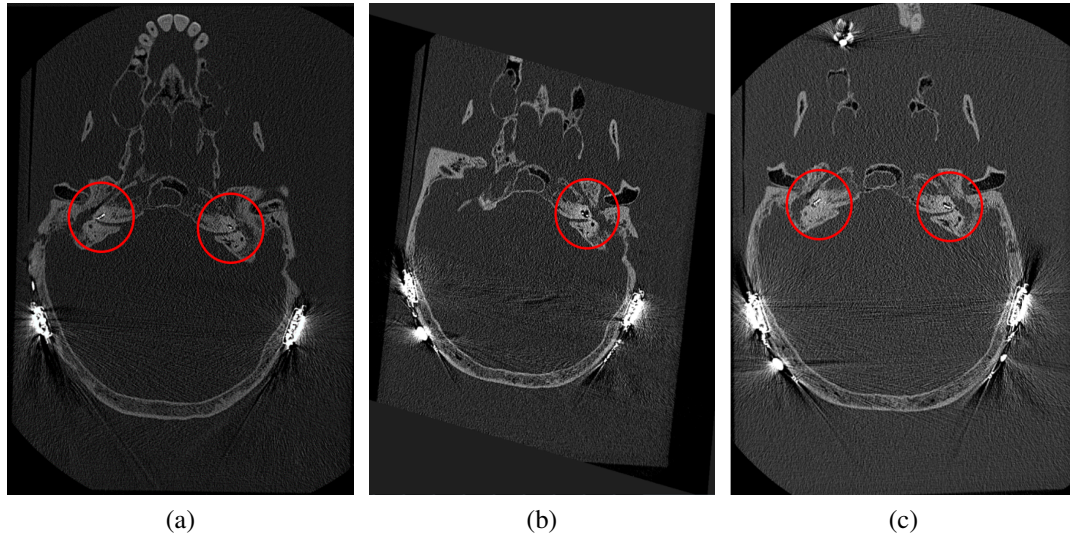
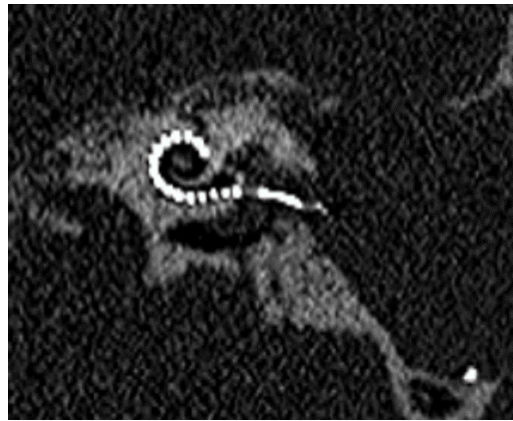


Figure 1.2: Changing the orientation of the subject in the scanner leads to varied degree of beam hardening artifacts on the electrodes, identified here by the red circles.

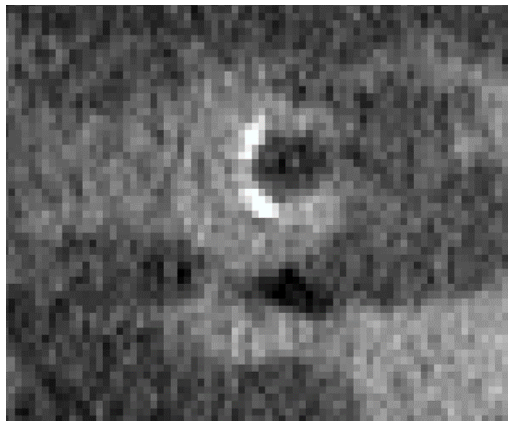
with different orientations. Electrodes lying in the plane of the receiver coils are more affected by beam hardening artifacts and the extent is different in all three orientations. It is evident that in the orientation Fig. 1.2b, the electrode array on the left side of the head is not on the same plane and is therefore unaffected by this particular artifact. Reconstruction with extended HU uses a larger intensity encoding range, whereby the metallic electrodes have a higher contrast against other radiodense materials like bone. The same array reconstructed with extended HU in Fig. 1.3b has a much better contrast with the surrounding bone and between individual electrodes when compared to the limited HU reconstruction in Fig. 1.3a. Resolution is another critical image acquisition parameter that controls the voxel size. Since the CI electrodes are small enough to occupy a voxel or less, and the inter-electrode spacing is close to a voxel length, lower resolution scans can significantly distort the image of electrodes. This is evident in how difficult it is to visually identify the separate contacts in the the low resolution image Fig. 1.3c compared to the high resolution version of the same 2D slice in Fig. 1.3d. Finally, dose – parametrized by radiation exposure per rotation – is usually indicative of the level of noise in the image. Low dose images like



(a) Limited HU image



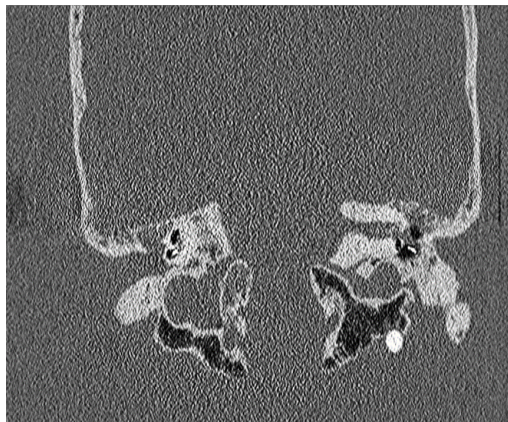
(b) Extended HU Image



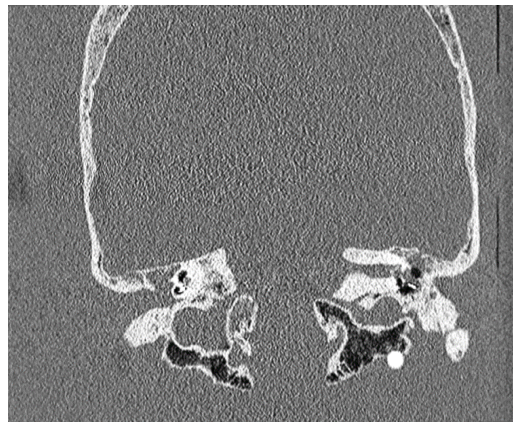
(c) Low Resolution Image (0.69 mm voxel diagonal)



(d) High Resolution Image (0.35 mm voxel diagonal)



(e) Low Dose Image (351 mAs exposure)



(f) High Dose Image (500 mAs exposure)

Figure 1.3: The ability to identify individual electrodes against high intensity bone and from adjacent electrodes depends on image parameters like HU range of reconstruction (Figs. 1.3a and 1.3b), resolution of the reconstruction (Figs. 1.3c and 1.3d), and the dose of the scan (Figs. 1.3e and 1.3f).

Fig. 1.3e can make it difficult to distinguish electrodes from each other and from bone, a task that is easier in a higher dose image like Fig. 1.3f. The variability of image quality makes it important to quantify the sensitivity of image processing algorithms to changes in image parameters. Besides enabling quality control of our dataset, it will also help make our algorithms more robust, and we investigate the sensitivity in Chapter 2.

## 1.2 Laser Interstitial Thermal Therapy for Epilepsy

Approximately 30 million people worldwide suffer from recurrent disabling seizures due to partial onset epilepsy, which is characterized by seizures arising from a single focal point in the brain [29]. Mesial temporal lobe epilepsy (mTLE) is among the most commonly reported variants of focal epilepsy, accounting for 17-31% of all surgical procedures done for epilepsy [30]. Although a number of antiepileptic drugs (AEDs) are available to control seizures, 20-40% of all patients suffer from drug-resistant epilepsy, in which seizures persist despite administering adequate doses of 2 AEDs [31]. The most common treatment for pharmaco-resistant epilepsy is a resection of the epileptogenic region – commonly a standard anterior temporal lobectomy in case of mTLE.

Recently, a minimally invasive alternative to open resection known as laser interstitial thermal therapy (LITT) has gained prominence for epilepsy treatment. Guided by an Magnetic Resonance Imaging (MRI) scanner, surgeons can ablate the epileptogenic focus in the brain with great accuracy using the thermal energy of a laser probe. Usually an occipital incision is used as the probe entry point (Fig 1.4a) to target the long axis of the hippocampus. After the procedure is complete, a contrasted postablation T1 is performed to determine the extent of ablation (Fig. 1.4b).

Despite the relative safety and convenience, studies report lower efficacy in terms of seizure freedom (53-60%) [33, 34] for LITT than for open resective procedures (66-70%) [35]. It is imperative to understand not only the patient-specific factors, but also the surgical factors that contribute to the variability in outcomes, especially the roles of the location

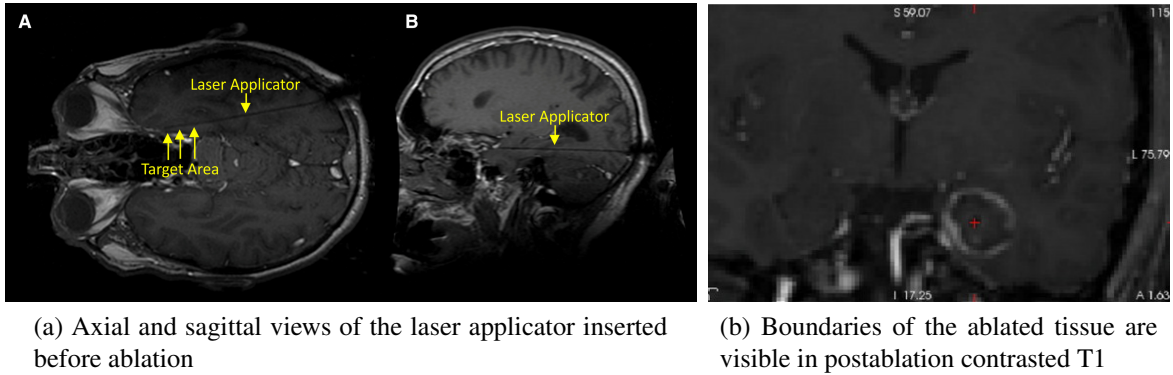


Figure 1.4: Intraoperative and postoperative MR T1 images of a LITT procedure. Figure adapted from [32].

and the volume of tissue ablated. However, it has not been easy to analyze postoperative outcomes because individual centers only treat a small number of patients [34, 36, 37]. A successful analysis will require a multi-institutional dataset that has sufficient statistical power to enable investigation of the effects of all the pertinent factors on outcomes. Moreover, anatomic differences such as the presence of varying degrees of radiographic evidence of hippocampal sclerosis (rHS) make it difficult to draw conclusions about ablations across patients. Resolving anatomic differences requires selecting appropriate nonrigid registration techniques and evaluating the associated errors to ensure that we can compare data from different patients and scanners. In Chapter 5 we discuss how to overcome these problems and investigate the role of different patient specific and surgical targeting factors.

### 1.3 Goals and Contributions of this Dissertation

The primary goal of this dissertation is to establish innovative image processing pipelines for outcomes analysis from surgical data in order to provide insight that can aid image guided surgery. This need arises because despite their general adoption, there is a considerable variability reported in patient outcomes in both these treatments. There is a significant number of CI recipients who experience poor speech recognition outcomes, for example,

and this variability in outcomes has been the subject of extensive study over the years [8, 9]. LITT for mTLE results in seizure freedom in 53-60% cases [33, 34] compared to 66-70% for open temporal lobe resection [35]. The sources of outcome variability can be broadly divided into two types – patient-specific factors and surgical factors. While subject selection does affect the population outcomes, there is considerable unexplained variance in outcomes that can only be attributed to surgical techniques. Positioning is a surgical factor that has consistently emerged as a key indicator of outcomes. For example, in LITT ablation, the position of the laser catheter has been shown to affect outcomes [38–40]. In studies with CIs, scalar translocation of the electrode array has been associated with poor outcomes [8, 18–22] while modiolar proximity for curved arrays has been linked to better outcomes [8, 24]. The concept that positioning of surgical intervention affects outcomes is intuitive, but in many cases it is not evident how to accomplish optimal positioning. Furthermore, differences in device type can greatly change the concept of ideal positioning.

In this dissertation, novel applications of image processing techniques combined with statistical analysis tools are used to quantify the relationship of patient outcomes to positioning. The studies broadly follow a pattern of four steps – (a) the selection and validation of appropriate image processing methods for the surgical problem; (b) semi-supervised image processing to extract positioning information from image datasets; (c) statistical analysis on the data derived from imaging; and (d) generalizable inference that contributes to patient counseling, device choice and surgical techniques. The specific contributions are summarized below:

**Chapter 2** discusses the development of a phantom to validate the performance of automatic electrode localization for CIs in CT images with diverse image quality. We created a phantom implanted with CIs, scanned it at different image acquisition parameters in different scanners, and estimated the electrode localization errors associated with image quality. This is an important step to make sure we know the accuracy limits of automatic algorithms in finding the positions of CI electrodes before that data can be used to investigate corre-

lations between positioning and outcomes. Understanding the error associated with image quality enables us to select our datasets better and improve algorithms in the future.

**Chapter 3** determines and quantifies the role of CI positioning factors in affecting hearing outcomes. We used robust segmentation algorithms, including a validated localization algorithm from chapter 2, to find CI electrode locations with respect to patient anatomy in a large dataset. We then use statistical modeling techniques to quantify outcomes for recipients of both straight and precurved CIs.

**Chapter 4** expands on the work of chapter 3 by focusing exclusively on precurved arrays. Using validated segmentation algorithms and various data analysis techniques, we exhaustively examine the associations between the outcome and predictor variables. After controlling for significant demographic covariates, we identify the role of good apical positioning of CIs as a significant predictor of good outcomes.

**Chapter 5** determines the optimal location for good patient outcomes in LITT for mTLE. This is challenging because of the limited data available at individual institutions as well as the inter-patient and inter-scanner variability. We developed methods to normalize the images and estimate the expected error. Thereafter we analyzed the role of ablation volume and location by modeling the ablation in terms of conditional probabilities.

**Chapter 6** provides a summary of the dissertation work and discusses possible future work.

## Chapter 2

### COCHLEAR IMPLANT PHANTOM FOR EVALUATING COMPUTED TOMOGRAPHY ACQUISITION PARAMETERS

Srijata Chakravorti<sup>1</sup>, Brian J. Bussey<sup>2</sup>, Yiyuan Zhao<sup>1</sup>, Benoit M. Dawant<sup>1</sup>, Robert F.  
Labadie<sup>3</sup>, Jack H. Noble<sup>1</sup>

<sup>1</sup> Department of Electrical Engineering and Computer Science, Vanderbilt University

<sup>2</sup> Department of Radiology, Medical Center North, 1161 21st Ave South, Nashville

<sup>3</sup> Department of Otolaryngology-Head and Neck Surgery, Vanderbilt University Medical  
Center

---

This chapter has been adapted from the publication “Cochlear implant phantom for evaluating computed tomography acquisition parameters”, Journal of Medical Imaging, 4(04), 1, and has been reproduced with the permission of the publisher and all co-authors: <https://doi.org/10.1111/epi.15565>

## 2.1 Introduction

Cochlear Implants (CIs) are neuroprostheses designed to restore hearing to patients with profound sensorineural hearing loss. They induce the sensation of sound by directly stimulating the surviving spiral ganglion nerve cells of the inner ear. An electrode array that is surgically implanted into the inner ear (Fig. 2.1) is connected by a wire leading to an internal receiver coil embedded under the skin at the surface of the skull. A CI processor worn behind the ear transforms sound detected by a microphone into electrical signals to be sent through a transmitter coil to the internal receiver and implanted electrodes. Outcomes are remarkable for most recipients, with average speech recognition approximately at 60% and 70% correct for Consonant-Nucleus-Consonant (CNC) words and AzBio sentence recognition tests, respectively [4–7, 41]. Despite this success, outcomes are highly variable, and a significant number of recipients still experience poor speech recognition outcomes.

The position of the electrode array within the cochlea is not generally known intraoperatively because the surgeon must thread the array through a very small opening into the cochlea [usually the “round window (RW) membrane”], and it is not possible to visualize or estimate the final position of the array in the cochlea. However, recent studies have relied on postimplantation imaging studies to detect final electrode position and have indicated that there is a correlation between the position of the electrodes relative to intracochlear anatomy and the ultimate hearing outcome of the patient [8, 18–20, 23, 26, 42, 43]. For example, it is now well known that arrays that cross the basilar membrane separating the scala tympani and scala vestibuli (see Fig. 2.2) cavities of the cochlea are associated with poorer outcomes [8, 20, 26, 43]. However, further study of the relationship between position and outcomes is warranted because: (a) there are still conflicting conclusions among studies about which other specific factors of positioning affect hearing outcomes. For example, Holden et al.[8] show that a deeper insertion negatively affects outcome. This, however, contradicts previous studies [19, 26] that have reported a positive correlation be-

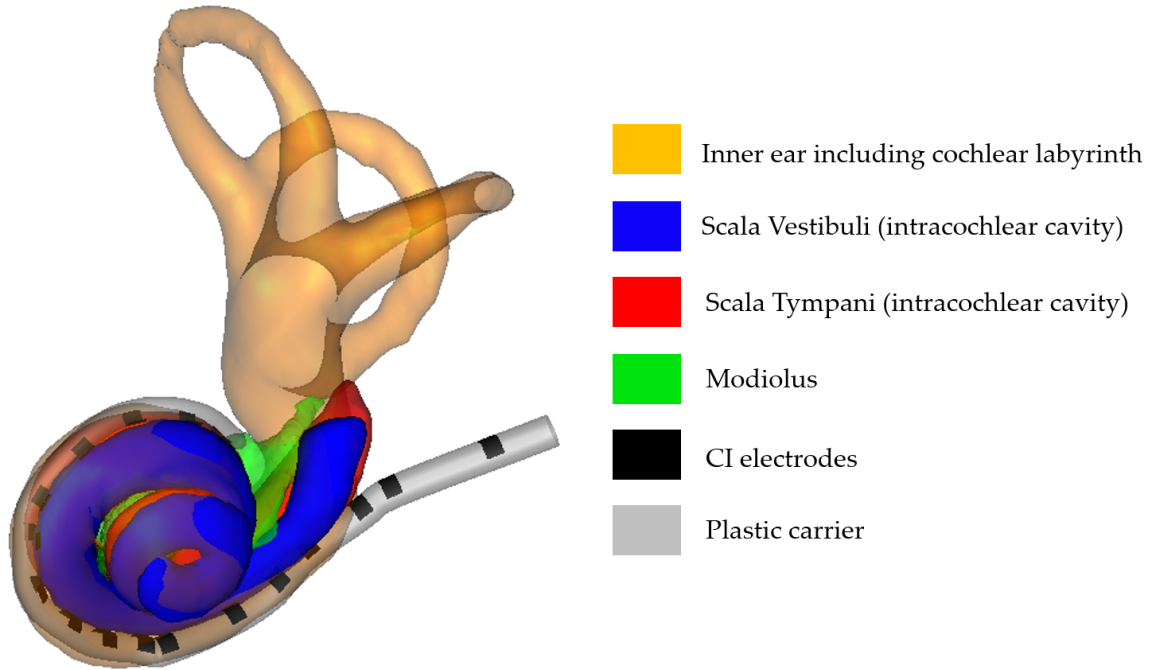


Figure 2.1: CI array implanted in the left ear. In order, the yellow structure is the inner ear, the blue and red surfaces are the scala vestibuli and scala tympani intracochlear cavities, respectively, and the green structure is the modiolus. CI electrodes are shown in black, and the plastic carrier is shown in gray.

tween speech recognition and depth of insertion. And (b) most studies have not had access to a set of accurate automatic analysis tools to localize the anatomy and electrodes and thus have only analyzed small datasets, focusing only on the coarse measures of electrode position that can be manually quantified, such as whether or not an obvious scalar translocation occurs. Our long-term goal is to perform a large-scale crossinstitutional study to more comprehensively and precisely analyze the relationship between electrode position and outcomes than has ever been done before. We will collect precise measures of electrode position, such as the distance from each electrode to the modiolus, the distance from each electrode to the basilar membrane, and the angular insertion depth of each electrode relative to the RW membrane (see Fig. 2.2). This project is enabled by algorithmic techniques we have developed that permit accurately identifying the anatomical structures that are not directly visible in Fig. 2.2 and methods to identify each of the electrodes [44, 45],

which would otherwise require substantial effort to manually identify. Because we aim to perform these analyses with thousands of images of subjects that have been acquired from a large number of institutions, it will involve processing images acquired from different scanners and with different imaging protocols that we do not control. Since the accuracy of our algorithmic techniques will be highly dependent on the imaging protocol, we are currently interested in learning the relationship between common acquisition parameters and the accuracy of our algorithms. In this study, we have developed a phantom that will permit evaluating the relationship between acquisition parameters and the accuracy of our electrode localization techniques. Results from this phantom will permit controlling for expected electrode localization accuracy as a function of acquisition parameters in our dataset and to determine if images with certain acquisition parameters should be withheld from our analyses. In a future study, we plan to develop a phantom for our anatomy localization algorithms, which are also sensitive to acquisition parameters.

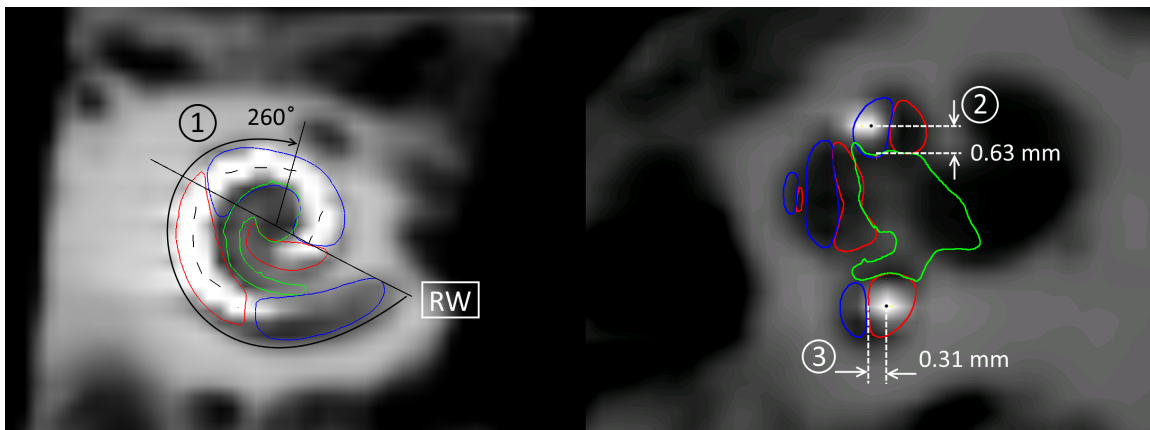


Figure 2.2: Measurements of electrode position demonstrated on a specimen implanted with an Advanced Bionics Mid-Scala array. The red structure is the scala tympani, the blue structure is the scala vestibuli, and the green structure is the modiolus (following the color scheme of Fig. 1). The measures of interest to us are (1) angular insertion depth relative to the RW membrane, (2) distance of each electrode to the modiolus, and (3) distance of each electrode to the basilar membrane. Scalar translocation of the electrode array can also be observed as the array is initially in the scala tympani (red) but then crosses the basilar membrane into the scala vestibuli (blue) at greater insertion depths.

While the focus of our study is evaluating how algorithms perform on images that are

acquired at many sites where we do not control acquisition parameters, it is important to note that many studies have been aimed at developing CI-specific image acquisition protocols. For example, it has been shown that CI electrodes can be localized even in simple two-dimensional radiographs of the skull, provided an appropriate projection is chosen. This is the principle of cochlear view [46], which allows localization of the individual electrodes to a good degree of accuracy, although it is limited in describing the positions of the electrodes in terms of the surrounding anatomy, which is critical for the analyses we would like to accomplish. Using multiple radiographs can improve the accuracy of electrode localization somewhat by adding a third dimension. For example, x-ray stereophotogrammetry [47] can fuse information from a stereo pair of radiographs to locate the positions of the electrodes in three-dimensions (3-D). Computed tomography (CT) imaging offers the best view of electrode position by providing a 3-D view of the temporal bone area on which the electrode positions can be estimated. Techniques for electrode localization have been explored on cone beam CTs[48] as well as spiral CTs [18, 19, 42, 49]. Currently, postimplantation high-resolution CT imaging is the modality accepted as the standard for this application and provides the resolution necessary to visually identify electrode arrays. Standard CT protocols can be prone to beam hardening artifacts when radiodense materials like CI electrodes are present in the field-of-view. However, digital image processing methods exist to improve the image quality available from commercial scanners. For example, iterative reconstruction methods can reduce beam hardening effects and image deblurring [50, 51] can optimize the resolution of spiral CT slices retrospectively, thereby allowing more accurate electrode localization.

As discussed above, using high-quality CT images available today, it is possible for experienced surgeons to make rough estimations of angular depth, modiolar proximity, and scalar translocation or lack thereof. However, this manual approach is impractical for analyzing large datasets of CT images, and we aim to achieve more precise localization than is feasible manually and more than what would be possible by visual examination. Thus, our

goal in this study is to develop and use a phantom to evaluate the relationship between CT acquisition parameters and the accuracy of our electrode localization algorithms because, while we have shown our methods work well with high-quality CT scans, the accuracy of our techniques with the range of CTs that have been acquired at many outside institutions is unknown.

The primary imaging parameters of interest are the CT image Hounsfield unit (HU) reconstruction range, resolution (parameterized by the voxel diagonal length), CT dose (parameterized by the exposure per rotation), and orientation of the subject in the scanner. Reconstructions with extended HU have a greater intensity encoding range and are expected to provide greater contrast to the metallic electrodes against the surrounding high-intensity bony tissue or noise. Resolution is an important parameter given that the CI contacts typically occupy less than a voxel's volume, and the spacing between contacts is often close to a voxel length even in high resolution scans. A lower dose CT image might have significant beam hardening artifacts that increase noise and make it difficult to distinguish electrodes from each other and from dense bone. Beam hardening is also influenced by the orientation of the head in the scanner because some orientations may lead to beams that pass through dense structures, such as the teeth or receiver coils in addition to the CI electrodes, which would worsen the artifact. By varying these four CT parameters and estimating the resulting localization errors on the phantom, we can obtain bounds on the expected error as a function of these CT parameters. While it is obvious that the highest quality parameters should permit the best possible localization, our aim is not to find an optimized protocol but rather to develop a system for calculating expected localization error bounds on any CT acquisition protocol for any given localization method. A secondary benefit of this phantom is that it could significantly aid the development and implementation of highly accurate automatic electrode localization methods, which would permit large-scale analysis of the relationship between electrode position and outcomes. A better understanding of this relationship could have implications for future hardware design and improvements in

surgical techniques. This may also have important implications for clinical applications, such as techniques proposed for selecting personalized CI processor settings for patients based on electrode position to improve hearing outcomes [52].

## 2.2 Methods

A phantom was created using a skull implanted with CIs in its left and right ears. Several scans of this phantom were acquired from different scanners and using different acquisition parameters. Each image provides an estimate of the location of each electrode. Every electrode was localized in each image by averaging multiple manual localizations of the centroid of the electrode by experts. The different images were then coregistered to a chosen reference image, in which a ground truth was defined by experts, also through repeated electrode localization measurements. Localization errors were calculated with reference to this ground truth. These procedures, summarized in Fig. 2.3, are described in the following subsections.

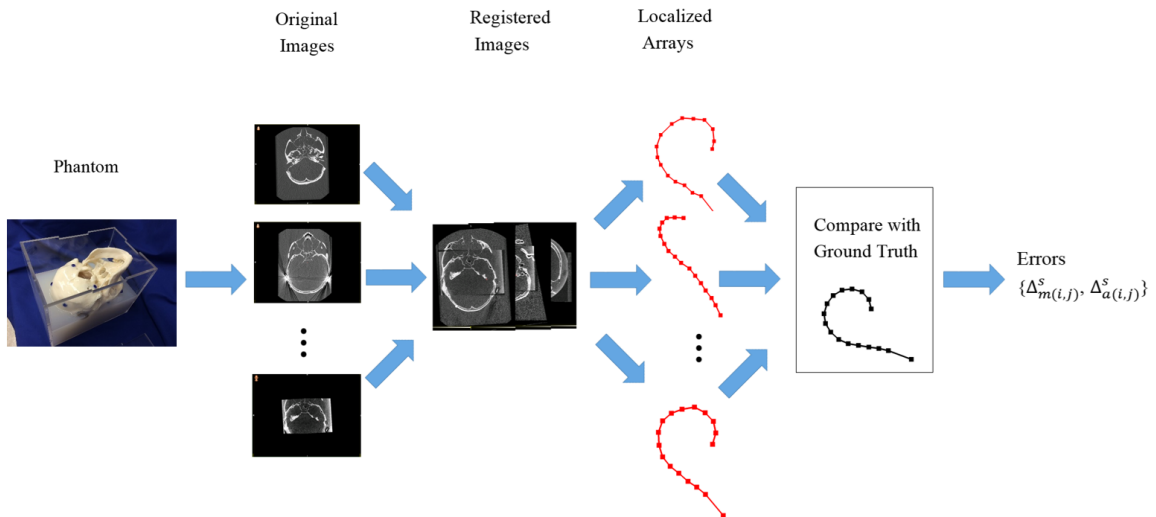


Figure 2.3: Method of processing the phantom images to obtain localization errors.

### **2.2.1 Construction of the Phantom**

The phantom was created using a cadaveric skull implanted with CIs in both ears. The left ear of the skull was implanted with an Advanced Bionics (AB) (Valencia, California) 1J device (A1), whereas the right ear was implanted with an AB Mid-Scala device (A2). The skull was then enclosed in a plexiglass box (Fig. 2.4). The box and cranial cavity were subsequently filled with silicone (Ecoex 00-10 supersoft silicone rubber, Reynolds Advanced Materials) after removing air bubbles using a vacuum chamber, and the silicone was allowed to cure. Silicone rubber is used to mimic the properties of soft tissue in a CT image. Both A1 and A2 are arrays with 16 active contacts and 1 nonstimulating contact at the proximal end of the array that serves as a marker, which indicates that the full insertion depth of the array has been reached when the marker reaches the cochlea entry site. A1 has a larger electrode spacing between active contacts (1.1-mm pitch) than A2 (0.95-mm pitch), and this leads to different degrees of image contrast between the contacts in the phantom’s images.

For registration purposes, eight fiducial marker spheres from Brainlab (Munich, Germany), each of diameter 8 mm, were embedded and glued into the skull and were spaced so that the centroid of the fiducial distribution approximately corresponds to the centroid of the skull. These markers can be seen in blue in Fig. 2.4 and have high intensity in CT images sufficiently contrasted against surrounding tissues to be reliably used for point-based registration.

### **2.2.2 Dataset**

The phantom was scanned in different CT scanners with different acquisition parameters 14 different times (Table 2.1), providing us with 28 images of CI arrays. Philips scanners are abbreviated as “PhCT,” Siemens scanners as “SiCT,” and Xoran scanners as “XCT.” All images marked with a superscript of (E) had extended HU reconstructions, and

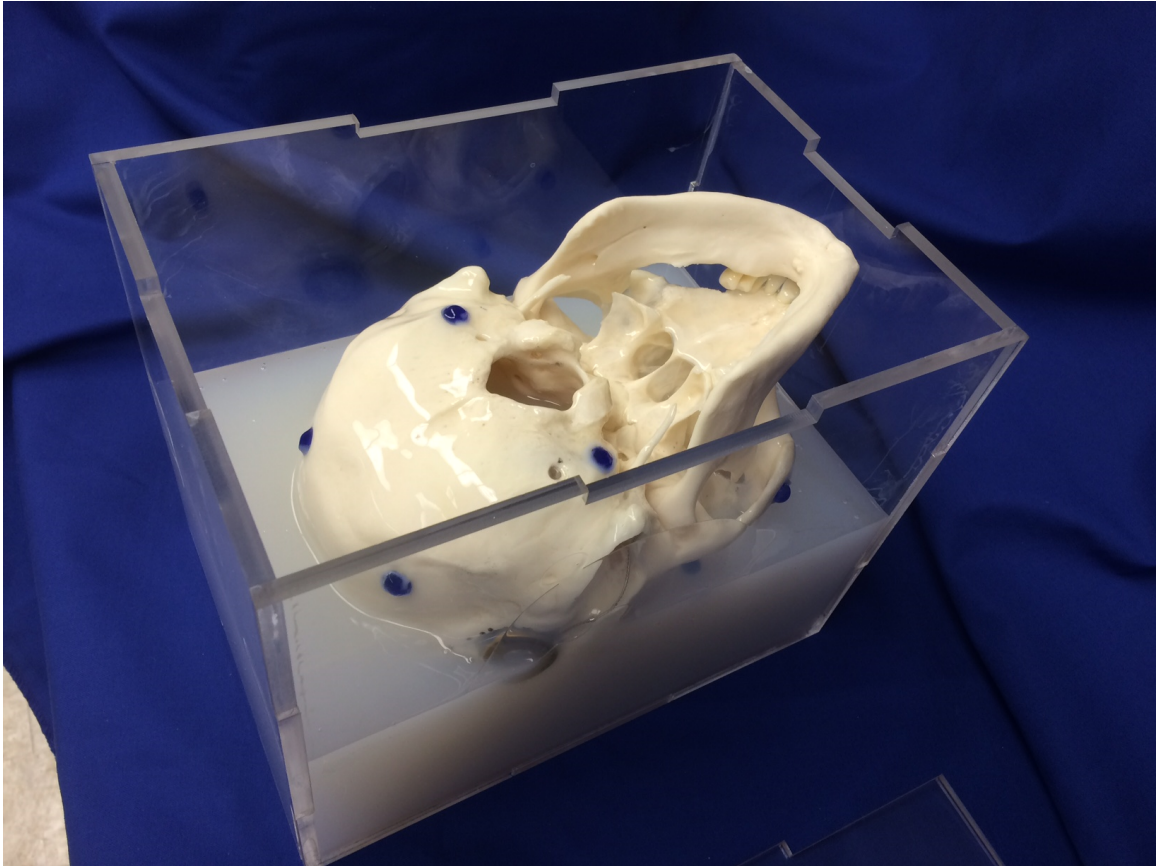


Figure 2.4: CI phantom shown during construction with the plexiglass box only partly filled with silicone rubber. Most of the inferior half of the skull is still visible above the silicone.

all other images have limited HU ranges. In every case, a filtered backprojection algorithm was used for the CT reconstruction. Since the layer of silicone rubber surrounding the skull is thicker than skin, the phantom has higher radioabsorption than an actual patient, and the images contain more noise than standard clinical images. This ensures that the phantom represents the worst case scenario and we obtain the upper bounds of localization error a particular localization algorithm can generate.

For the next sections, we group the images having resolution between 0.35 and 0.45 mm as “high res,” those in the range 0.45 to 0.55 mm as “mid res,” those at 0.5 to 0.65 mm as “low res,” and finally, the ones more than 0.65 mm as “very low res.” In a similar way, “low dose” refers to less than 250 mAs exposure value, “mid dose” refers to an exposure

Table 2.1: Image Dataset

Number	Scanner	Image	Voxel Diagonal (mm)	Exposure (mAs)	kVp
1	PhCT Brilliance 64	$V_1^{(E)}$	0.462	500	120
2	PhCT Brilliance 64	$V_2^{(E)}$	0.478	500	120
3	PhCT Brilliance 64	$V_3^{(E)}$	0.478	500	120
4	PhCT Brilliance 64	$V_4^{(E)}$	0.468	351	120
5	PhCT Brilliance 64	$V_5^{(E)}$	0.563	350	120
6	SiCT SOMATOM Definition Flash	$M_1^{(E)}$	0.581	395	120
7	XCT MiniCAT	$X_1^{(E)}$	0.346	58.8	125
8	XCT MiniCAT	$X_2^{(E)}$	0.346	58.8	125
9	XCT xCAT	$X_3^{(E)}$	0.693	57.6	120
10	PhCT iCT 128	$V_1$	0.446	500	120
11	PhCT iCT 128	$V_2$	0.460	280	120
12	PhCT iCT 128	$V_3$	0.591	280	120
13	PhCT iCT 128	$V_4$	0.540	280	120
14	SiCT SOMATOM Definition Flash	$M_1$	0.388	395	120

range of 250 to 375 mAs, and “high dose” refers to an exposure of 375 to 500 mAs.

### 2.2.3 Localization of Cochlear Implant Arrays

The centroid of each electrode in the CI arrays was localized multiple times by three expert raters on all the images in the dataset based on their intensity difference from surrounding bone and tissue. Each electrode roughly has the appearance of a high intensity blob in the image. The centroid of this blob can be visualized in three orthogonal views – axial, sagittal and coronal – to localize the electrode. This process is then repeated one to four times by each of the experts for each electrode for a total of 6 to 10 localizations of each electrode by all experts. It takes an expert about 2 to 3 min to complete a single localization of the electrode array, making it a very time consuming process. The averages of the multiple sessions were used to represent the best estimation of electrode position for the respective images. Based on the image quality of  $V_2^{(E)}$  and the fact that the raters had the best repeatability in determining the electrode position in this image, it was chosen to serve as the ground truth of the dataset.  $V_2^{(E)}$  will thus be the reference for registration (see Table 2.1) and will henceforth be referred to as  $V_{ref}$ . The ground truth of the CI arrays is defined as the average of 10 manual localizations by experts on this reference image.

### 2.2.4 Registration

#### 2.2.4.1 Point-based rigid body registration

Our first approach to coregister all the images was point registration using the fiducial markers embedded in the skull phantom. The eight markers were manually localized by an expert rater. Using their positions in the images, 10 out of the 14 CT scans are registered to the reference image  $V_{ref}$  by a point-based rigid body registration technique[53]. The other three images [ $X_1^{(E)}$ ,  $X_2^{(E)}$ , and  $X_3^{(E)}$ ] cannot be registered with this method because some of the markers are not visible in the field of view. This registration step ensures that

the automatically localized CI arrays are effectively in the same image space as the ground truth arrays, allowing a direct comparison of the automatic localization procedure against the ground truth.

Because this registration is a crucial step for the performance evaluation, the errors in this step must also be taken into consideration. For unbiased results, the registration errors should be much smaller than the localization errors on average. The fiducial markers are 8 mm in diameter, which is 16 times larger in dimension than the slice width in the coarsest image, which is important because larger fiducials lead to lower fiducial localization error (FLE), leading to lower target registration errors (TRE). With fiducials of this size, it can be reasonably assumed that the localization of the marker centroids is robust against the image quality variations that affect the CI electrodes, which occupy less than a voxel in size. We, therefore, assume that the errors associated with locating the centroids of the fiducials, the FLE, in all the scans are isotropic, independent, and normally distributed. We use a standard registration error analysis approach [54] to calculate the overall fiducial registration error (FRE):

$$\langle FLE^2 \rangle \approx \frac{1}{M} \sum_{m=1}^M \frac{N}{N-2} \times FRE^2(m) \quad (2.1)$$

where  $M$  is the number of pairwise registrations,  $N$  is the number of fiducial markers which remains constant for all registrations  $m$ . With this estimate of  $\langle FLE^2 \rangle$ , the Target Registration Error (TRE) at the positions of the CI contacts, marked by the ground truth arrays, can be calculated:

$$\langle TRE^2(\mathbf{r}) \rangle \approx \frac{1}{N} \left( 1 + \frac{1}{3} \sum_{k=1}^3 \frac{d_k^2}{f_k^2} \right) \times \langle FLE^2 \rangle, \quad (2.2)$$

where  $\mathbf{r}$  is the position of the target in image space,  $d_k$  is the distance of the target calculated from the principal axis  $k$ , and  $f_k$  is the root mean square (rms) distance of all  $N$  fiducials from the same  $k^{th}$  principal axis. The square root of  $\langle TRE^2(\mathbf{r}) \rangle$ , or the  $rms(TRE)$ ,

serves as our estimate of registration accuracy at the position  $\mathbf{r}$ .

For all 34 possible locations of the contacts on the two sides of the skull,  $rms(TRE)$  is approximately 0.15 mm in every case.

#### 2.2.4.2 Mutual information based rigid body local image registration

The point-based rigid body registration is guaranteed to provide a globally well registered image. However, our specific aim is to have good registration around each inner ear, which might be better obtained by local registration algorithms. Thus, we have tested an intensity-based local registration method in this work. All the images are first rigidly registered to  $V_{ref}$  using a mutual information (MI) [55, 56] based image transformation, followed by localized rigid MI registration centered in a region of interest (RoI) of approximately  $35 \times 35 \times 35 \text{ mm}^3$  around the inner ear. Once registered, the respective arrays are referred to with a subscript of  $(i, ref)$ , indicating registration of image  $i$  to  $V_{ref}$ .

Figure 2.5 provides a visual verification of the quality of this registration step. The difference image calculated between the point registered image and the reference image slice [Fig. 2.5c] shows larger areas of intensity disagreements (regions in shades of gray and white) compared to the difference image calculated between the locally registered image and the reference image slice [Fig. 2.5e]. The single large bright spot at the middle of the top half of Fig. 2.5e corresponds to an electrode in the image and is present in the difference image [Fig. 2.5c] as well. Even with a highly accurate registration, an electrode will have high intensity in a difference image because  $V_{ref}$  is an extended HU image and assigns much higher values of intensity to the metallic electrodes than the limited HU image  $V_4$ . In Fig. 2.5f, the locally registered array agrees more closely with the ground truth than the array obtained from point registration. It is visually evident that the local image registration yields better results than the global registration, and therefore, this is our choice of registration method. A disadvantage of using intensity-based methods is that there is no way to calculate TRE, which we must estimate to determine the effects of registration in

our subsequent error analyses. Therefore, we will use the TRE estimates of Sec. 2.2.4.1 as an error bound to judge the quality of our intensity-based registration. Because our local image registration is more accurate than the point-based registration, the estimate of  $rms(TRE) = 0.15$  mm obtained from Sec. 2.2.4.1 serves as an upper bound on our current registration error.

### 2.2.5 Electrode Localization Errors

The distance between an electrode localized in an image and its corresponding ground truth localization in the registered reference image  $V_{ref}$  defines what we call the “image-based” localization error for the electrode. Even though we calculate this distance on the basis of manual localizations, we use multiple averages from the manual results of different experts to virtually negate the procedural errors, so that the “image-based” localization error only reflects the error intrinsically due to image quality. The overall image-based localization errors are defined as the array of distances between each of the electrodes registered to the space of  $V_{ref}$  and the corresponding ground truth electrodes defined in  $V_{ref}$ . The array of distances is defined as  $\{\Delta_{m(i,j)}^s\}_{(j=1)}^N$ , where the distance for each electrode  $j$  in array  $s$  in an image  $i$  is

$$\Delta_{m(i,j)}^s = \|\text{Image}^s(j)_{(i,ref)} - \text{Truth}^s(j)_{(ref,ref)}\| \quad (2.3)$$

The subscript  $m$  in the equation is used to differentiate this measure of image-based localization error from the automatic algorithm localization errors that will be discussed below in Sec. 2.3.1. For each scan, the errors can be considered to be drawn from a population that follows a continuous normal distribution with zero mean. Informal analysis of the correlations between the  $x$ ,  $y$ , and  $z$  components of the errors of each electrode with other electrodes in the array confirmed the errors at each electrode are independent and statistical analysis can be carried out assuming independence accordingly. This also

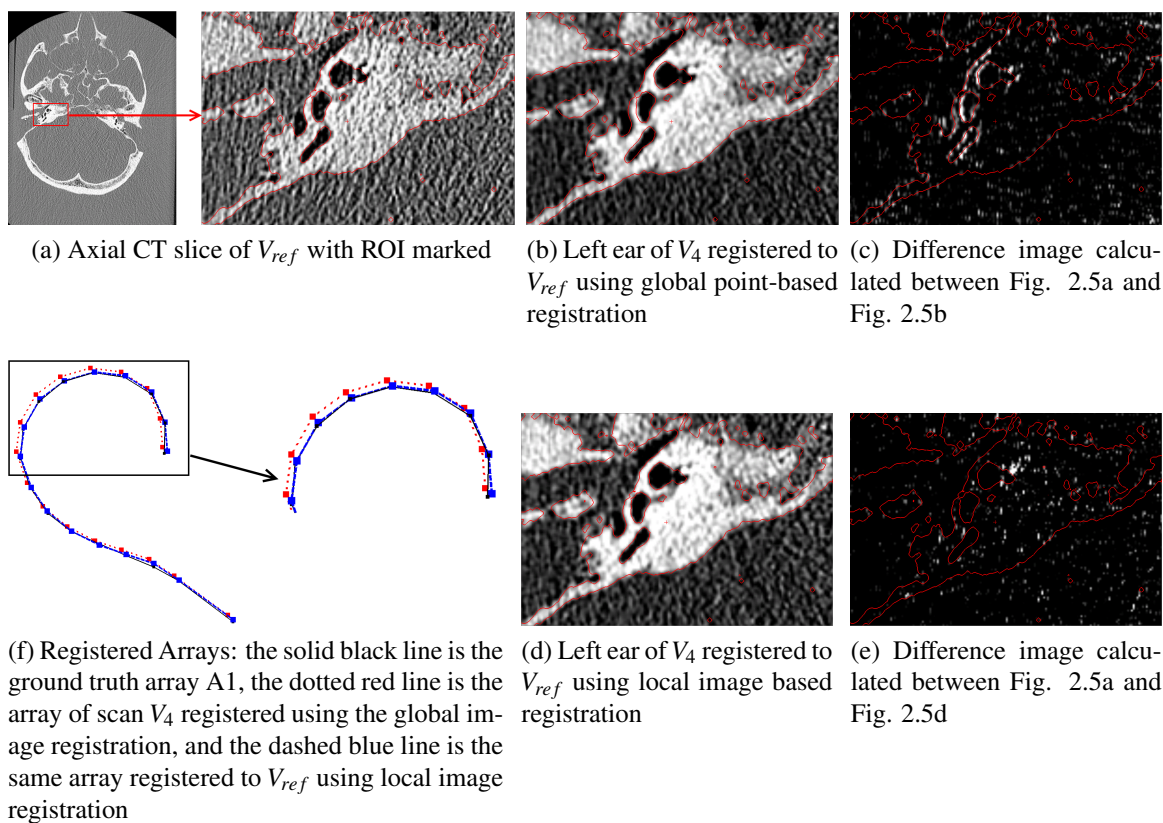


Figure 2.5: Visual verification of registration accuracy in a representative scan ( $V_4$ ). (a–e) The red isocontours were generated on the reference image (a) and indicate the edges of the bones in that panel. The isocontours were projected to the other panels to show that the locally registered version [(d) and (e)] closely matches (a), while the point registered image [(b) and (c)] has a slight but significant difference from the reference image. (a) Axial CT slice of  $V_{ref}$  with ROI marked. (b) Left ear of  $V_4$  registered to  $V_{ref}$  using global point-based registration. (c) Difference image calculated between images (a) and (b). (d) Left ear of  $V_4$  registered to  $V_{ref}$  using local image based registration. (e) Difference image calculated between images (a) and (d). (f) Registered arrays: the solid black line is the ground truth array A1, the dotted red line is the array of scan  $V_4$  registered using the point-based registration, and the dashed blue line is the same array registered to  $V_{ref}$  using local image registration.

suggests that registration errors are negligible at the scale of the localization errors, since we expect that significant registration errors would have led to correlated directional errors. We conclude that bias due to the registration errors in measurement of localization errors is thereby not an issue here.

### 2.3 Results

Image-based localization errors averaged across all electrodes for both A1 and A2 for each CT image are shown in Fig. 2.6. The errors for  $V_2^{(E)}$  are zero since it is the chosen reference image. In order to estimate the statistical significance of the effects of specific acquisition parameters on the image-based localization accuracy of the CI arrays, we carried out a series of statistical tests on these errors. We used two sample Welch’s t-tests [57] and one way analysis of variance [58], accounting for unequal variances. Along with the statistical significance of the effects, the effect sizes for each test are also reported in terms of the Cohen’s d values [59] of the tests, which are the ratio of the difference of group means to the pooled standard deviation, to be better able to compare how much each parameter affects the localization accuracy.

The errors are grouped by the values of the three major acquisition parameters of the original scans – exposure, voxel diagonal lengths, and whether the reconstruction was carried out using an extended or a limited HU range – using the ranges of values in Sec. 2.2.2. Each of the test groups is designed in such a way that the only variable that changes between the chosen scans is the acquisition parameter whose effect we are testing for. This section exclusively deals with the outcomes of the tests on the image-based localization errors, with the results listed in the “image-based” section of Table 2.7. Later, in Sec. 2.3.1, we will look at the effects of the same acquisition parameters on the arrays localized by two automatic electrode localization algorithms, and the results are discussed in the “Auto I” and “Auto II” sections of Table 2.7. Any “–” in Table 2.7 signifies that sufficient data are not present to carry out the comparison. The null hypothesis is that the means of the

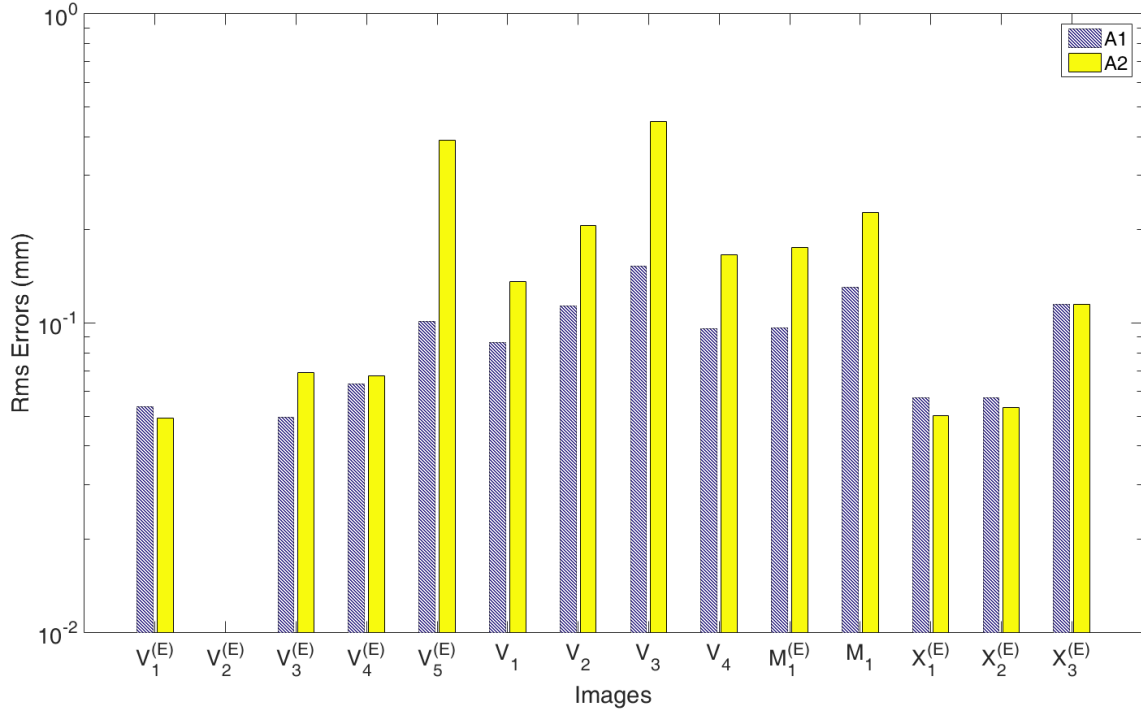


Figure 2.6: Image-Based Localization Errors across A1 and A2

different groups do not vary to within the significance level of 0.05. All the calculations are carried out in MATLAB (Mathworks, Natick, Massachusetts). Calculation of confidence intervals for measures of effect size was carried out using the measures of effect size [60] MATLAB toolbox.

**Effect of Spacing between Electrodes:** In order to estimate the effect of electrode spacing, Bonferroni corrected t-tests were performed on the image-based localization errors, which showed that there is a significant effect of the array model on the accuracy of image-based localization (“image-based” column of Table 2.2). We can conclude from a one-tailed corrected t-test that the errors for array A2 are significantly worse than the errors for array A1. As shown in parentheses in the “image-based” column of Table 2.2, the mean of the errors for array A2 is around twice that of A1. This result is intuitive because the closer electrode spacing for A2 provides less image contrast between electrodes than A1.

**HU Range of Reconstruction:** Changing the HU range was found to affect determination of the correct CI electrode locations for both A1 and A2 (Table 2.3). The group mean of errors for a limited HU image is nearly twice that of extended HU for A1 and more than twice for A2 at the same high dose and mid resolution.

**Orientation:** Images  $V_1^{(E)}$ ,  $V_2^{(E)}$ , and  $V_3^{(E)}$  were acquired with identical parameters but with different orientations of the phantom skull in the scanner. Orientation controls the severity of the beam hardening artifacts around the electrodes depending on whether dense structures like teeth or receiver coils lie in the path of the CT beams before striking the electrodes — severe beam hardening artifacts might form that could make it harder to localize the electrodes. We found a significant localization error change only for A2 due to orientation, shown in Table 2.4, but this is a relatively small change in terms of actual group means.

**Resolution:** The length of a voxel diagonal in a CT acquisition is a direct measure of the resolution of an image. In most of the images in our dataset, an electrode is physically smaller in volume than one voxel and generally appears to occupy no more than a few voxels in any image. Poor resolutions cause partial volume effects to dominate, leading to distortions in how the arrays are visualized in the final image. Statistical tests (Table 2.5 showed that lower resolution is associated with poorer accuracy for localizing both the A1 and A2 arrays under all conditions except one (A1 for limited HU, mid dose reconstructions). However, limited HU range can have somewhat similar effects on image quality as poor resolution. It is possible that in the case where change of resolution was not read as significantly affecting the localization accuracy, the stronger effects of a limited HU range occluded any effects due to low resolution.

**Dose:** We use exposure values as indicative of the radiation dose since all images were acquired at similar tube voltages. A lower CT dose can lead to higher image noise,

which in turn could introduce spurious noisy voxels that appear like electrodes and reduce the accuracy of localization. Tests showed that the effect of dose on the image-based localization accuracy of A1 and A2 is found to be significant in only one case out of six (Table 2.6), and even then, it does not change the mean errors as much as resolution. It is likely that the dose is not measured as having a significant effect in the first case because the poorer accuracy in that test can also be driven by the effects of limited HU. In the third case, the t values show that the effect of dose was sizeable but not enough to be significant at our sample sizes.

Table 2.2: Effect of electrode spacing on localization errors.

Factor	Test Conditions	Image-based	Auto I	Auto II
Spacing between electrodes (A1, A2)	All resolution, dose and HU ranges	(0.0835, 0.1442)	No	No

The error subgroups being compared are mentioned in parentheses under the column 'Factor'. If a statistically significant effect ( $p < 0.05$ ) is present, the group means are specified in mm, while 'No' indicates the absence of a statistical effect.

Table 2.3: Effect of HU range during reconstruction. Significant p-values are in bold text.

Factor	Test Conditions	Localization Method	Array Type	t-statistic	p-value	Group means	Cohen's d
HU range (Ext HU, Lim HU)	High Dose, Mid Res	Image-based	A1	t(22.31) = -3.87	<b>&lt;0.001</b>	(0.048, 0.081)	1.341
			A2	t(19.01) = -4.62	<b>&lt;0.001</b>	(0.054, 0.123)	1.745

Figure 2.7 maps the effect sizes in terms of Cohen's d values of the different factors on image-based localization along with their 95% confidence intervals. The horizontal axis denotes each of the different tests carried out as listed in Table 2.7. It can be concluded that while all factors affect localization errors to some degree, resolution and HU range have more impact in general than the other two factors.

### 2.3.1 Evaluation of Automatic Cochlear Implant Array Localization Using the Phantom

As an example of the phantom's use as a validation tool, we compare the performance of two automatic electrode localization techniques on the same image set. The first method

Table 2.4: Effect of Orientation. The '—' imply no single Cohen's d value could be calculated since the test was an ANOVA between three groups. Significant p-values are in bold text.

Factor	Test Conditions	Localization Method	Array Type	t-statistic or F-statistic	p-value	Group means	Cohen's d
Orientation	Ext HU, High Dose, Mid Res	Image-based	A1	t(31.91) = 0.58	0.57	(0.050, 0.046)	-0.198
			A2	t(31.93) = -2.78	<b>0.009</b>	(0.044, 0.065)	0.954
		Auto I	A1	F(2, 48) = 0.01	0.99	(0.147, 0.149, 0.150)	—
			A2	F(2, 48) = 0.87	0.43	(0.181, 0.217, 0.157)	—
		Auto II	A1	F(2, 48) = 1.60	0.21	(0.134, 0.176, 0.149)	—
			A2	F(2, 48) = 0.84	0.44	(0.121, 0.148, 0.134)	—

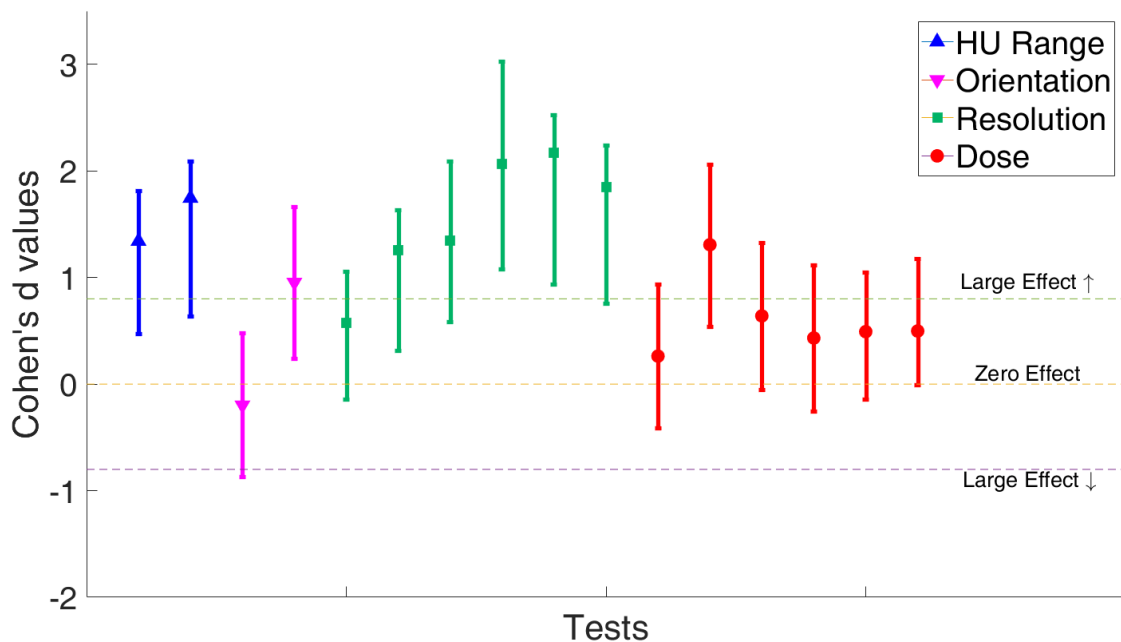


Figure 2.7: Effect size values for image-based localization errors across A1 and A2

Table 2.5: Effect of Resolution. Incomplete data has been marked as '—', implying that no test can be performed. Significant p-values are in bold text.

Factor	Test Conditions	Localization Method	Array Type	t-statistic	p-value	Group means	Cohen's d
Resolution (Mid res, Low res)	Lim HU, Mid dose	Image-based	A1	t(19.36) = -1.54	0.139	(0.098, 0.131)	0.577
			A2	t(18.82) = -3.30	<b>0.004</b>	(0.154, 0.371)	1.252
		Auto I	A1	t(24.75) = -41.54	<b>&lt;0.001</b>	(0.176, 4.357)	14.250
			A2	—	—	—	—
		Auto II	A1	—	—	—	—
			A2	—	—	—	—
Resolution (Mid res, Low res)	Ext HU, Mid dose	Image-based	A1	t(30.79) = -3.92	<b>&lt;0.001</b>	(0.058, 0.096)	1.344
			A2	t(16.21) = -6.02	<b>&lt;0.001</b>	(0.066, 0.344)	2.067
		Auto I	A1	t(19.72) = -1.28	0.22	(0.142, 0.186)	0.438
			A2	t(30.37) = -2.34	<b>0.03</b>	(0.147, 0.215)	0.806
		Auto II	A1	t(18.77) = -4.90	<b>&lt;0.001</b>	(0.125, 0.276)	1.679
			A2	t(20.07) = -2.75	<b>0.01</b>	(0.128, 0.230)	0.942
Resolution (High res, Very Low res)	Ext HU, Low dose	Image-based	A1	t(19.56) = -5.84	<b>&lt;0.001</b>	(0.055, 0.109)	2.171
			A2	t(20.26) = -5.07	<b>&lt;0.001</b>	(0.046, 0.106)	1.848
		Auto I	A1	t(24.69) = -0.50	0.62	(0.090, 0.098)	0.164
			A2	t(48.97) = -0.76	0.45	(0.126, 0.144)	0.184
		Auto II	A1	t(43.67) = 0.90	0.37	(0.094, 0.084)	-0.238
			A2	t(21.64) = -3.01	<b>&lt;0.001</b>	(0.079, 0.129)	1.057

Table 2.6: Effect of Dose. Incomplete data has been marked as '—', implying that no test can be performed. Significant p-values are in bold text.

Factor	Test Conditions	Localization Method	Array Type	t-statistic	p-value	Group means	Cohen's d
Dose (High Dose, Mid Dose)	Lim HU, Mid res	Image-based	A1	t(29.46) = -1.86	0.07	(0.081, 0.105)	0.639
			A2	t(22.59) = -1.26	0.22	(0.123, 0.166)	0.432
	Auto I	A1	A1	—	—	—	—
			A2	—	—	—	—
	Auto II	A1	A1	—	—	—	—
			A2	—	—	—	—
Dose (High Dose, Mid Dose)	Ext HU, Low res	Image-based	A1	t(29.04) = -0.76	0.45	(0.087, 0.096)	0.262
			A2	t(24.94) = -3.81	<b>0.001</b>	(0.143, 0.344)	1.307
	Auto I	A1	A1	t(29.26) = 0.71	0.48	(0.225, 0.186)	-0.242
			A2	t(21.18) = 1.47	0.16	(0.305, 0.215)	-0.504
	Auto II	A1	A1	t(21.86) = -5.39	<b>&lt;0.001</b>	(0.102, 0.276)	1.848
			A2	t(27.14) = -1.70	0.1	(0.160, 0.230)	0.580
Dose (High Dose, Mid Dose)	Ext HU, Mid res	Image-based	A1	t(26.21) = -1.53	0.14	(0.048, 0.058)	0.492
			A2	t(47.03) = -1.96	0.06	(0.054, 0.066)	0.498
	Auto I	A1	A1	t(31.76) = 0.49	0.63	(0.149, 0.142)	-0.127
			A2	t(49.43) = 1.47	0.15	(0.185, 0.147)	-0.316
	Auto II	A1	A1	t(54.29) = 2.15	<b>0.04</b>	(0.153, 0.125)	-0.444
			A2	t(31.08) = 0.38	0.70	(0.134, 0.128)	-0.1

Table 2.7: Summary of effects of CT parameters on localization accuracy. The error subgroups being compared are mentioned in parentheses under the column 'Factor'. Incomplete data has been marked as '—'; implying that no test can be performed. If a statistically significant effect ( $p < 0.05$ ) is present, the group means are specified in mm, while 'X' indicates the absence of a statistical effect.

Factor	Test Conditions		A1		A2	
	Image-based	Auto I	Auto II	Image-based	Auto I	Auto II
<b>HU range</b> (Ext HU, Lim HU)						
	High Dose, Mid Res	(0.048, 0.081)	—	(0.054, 0.123)	—	—
<b>Orientation</b>	High Dose, Mid Res	X	X	(0.044, 0.065)	X	X
<b>Resolution</b> (Mid res, Low res)	Lim HU, Mid Dose	X	(0.176, 4.357)	(0.154, 0.371)	—	—
	Ext HU, Mid Dose	(0.058, 0.096)	X	(0.066, 0.344)	(0.147, 0.215)	(0.128, 0.230)
<b>Resolution</b> (High res, Very low res)	Ext HU, Low Dose	(0.055, 0.109)	X	(0.046, 0.106)	X	(0.079, 0.129)
<b>Dose</b> (High dose, Mid dose)	Lim HU, Mid Res	X	—	X	—	—
	Ext HU, Low Res	X	X	(0.102, 0.276)	X	X
	Ext HU, Mid Res	X	X	(0.153, 0.125)	X	X

(Auto I) is a graph-based technique [45], whereas the second (Auto II) is a preliminary extension to this approach under development. It fine-tunes the processing steps and optimization cost functions and is currently under evaluation. More detailed discussion of these two techniques would be out of scope for this paper since our aim is to develop the phantom as a generalized validation tool irrespective of how a particular image analysis technique actually works. In every CT scan, the electrode arrays were automatically localized using these two techniques. On average, it takes only about 10 seconds to automatically localize an array with either method. Also, automatic techniques can be executed without human intervention on large-scale datasets.

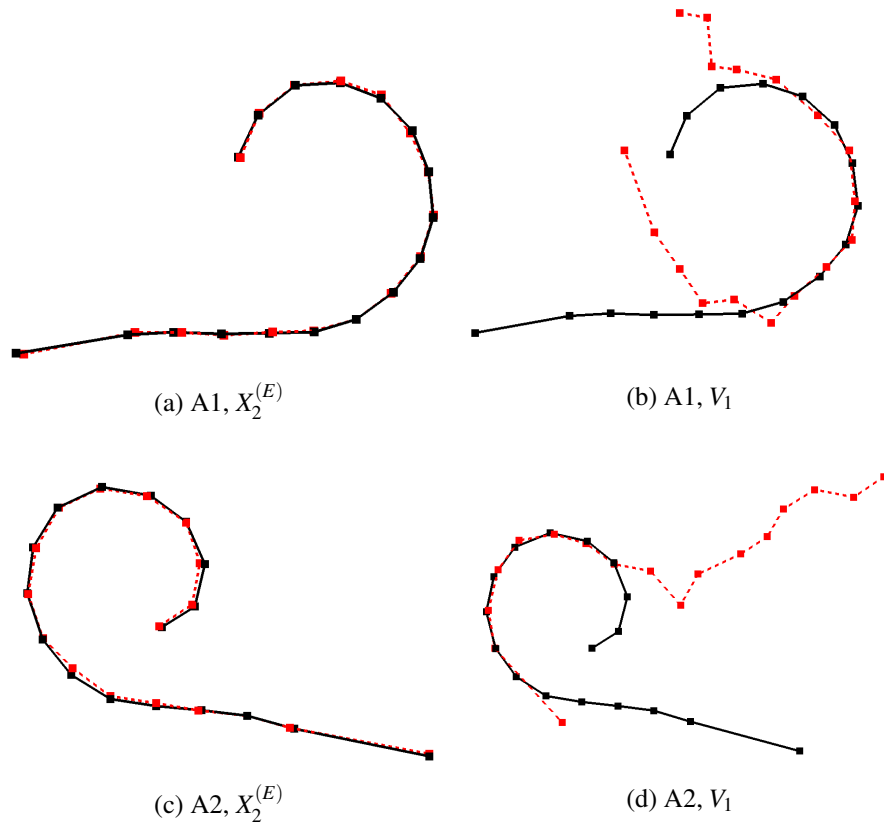


Figure 2.8: Good Results (a and c) vs Failed Results (b and d). The solid black line is the ground truth array of  $V_{ref}$ , while the dashed red line is the automatically localized array registered to  $V_{ref}$ .

Thus, the automatic methods are substantially faster and require much less effort than

a manual segmentation approach. The designs of Auto I and II are such that they expect the electrodes to be brighter than bone and thus, they work best with extended HU images. Of the 28 images of the CI arrays, Auto I failed to produce any result only in one limited HU case (A2 of  $V_2$ ). There were four other cases where the results were considered as “failures” by expert raters (A1 of  $V_1$  and  $V_2$ ; A2 of  $V_1$  and  $V_4$ ). Auto II failed on all limited HU images ( $V_1 — V_4, M_1$ ), though this is unsurprising since this algorithm was fine-tuned for extended HU images and needs modification to handle limited HU images. Examples of results considered “good” and “failed” are demonstrated in Fig. 2.8. The failed results are not used in subsequent analyses. Overall, we obtain 23 automatic localization results from Auto I and 18 from Auto II.

The error of automatic localization method  $a$  for every electrode  $j$  in each array  $s$  in scan  $i$  was defined similarly as for image-based localization errors:

$$\Delta_{a(i,j)}^s = \|Automatic^s(j)_{(i,ref)} - Truth^s(j)_{(ref,ref)}\| \quad (2.4)$$

Since image-based localization errors measure the error in the average of multiple expert localizations, they define the electrode localization error due to the imaging technique alone, whereas the automatic localization error also includes errors made by the algorithmic electrode localization process.

### 2.3.1.1 Automatic localization errors

Figures 2.9a and 2.9b show the rms errors over all electrodes for A1 and A2, respectively, in each image. Unsurprisingly, Bonferroni corrected one-tailed t-tests statistically confirm that the automatic localization techniques add error to the image-based localization error. This error, contributed by the localization procedure, increases the net error in almost every case. The exceptions are the A2 array in the images  $V_5^{(E)}$  and  $M_1$ , where the random errors in the automatic localization tended to cancel out some of the image-based localiza-

tion errors. However, the automatic methods provide very good results on the extended HU images, as rated by experts.

### 2.3.1.2 Effect of acquisition parameters

Figures 2.10a and 2.10b show the errors of localization on the two types of arrays using the two methods, respectively. The effects of electrode spacing on automatic localization errors (using Bonferroni corrected t-tests) are shown in Table 2.2. We found no effect of electrode spacing on the automatic localization errors. This allows us to group the errors from the two types of electrodes together.

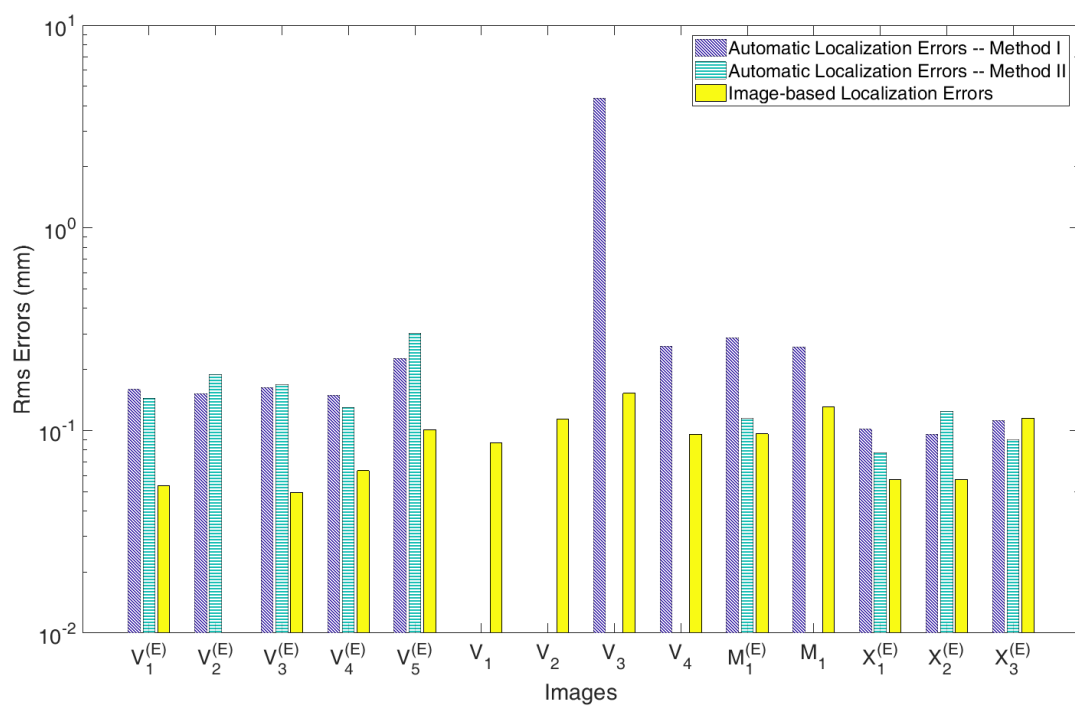
**HU range of reconstruction:** It is not possible to test the effects of the HU range of reconstruction on automatic localization techniques since the methods used did not work on enough limited HU images.

**Orientation:** There was no significant effect of orientation on localization errors from either algorithm.

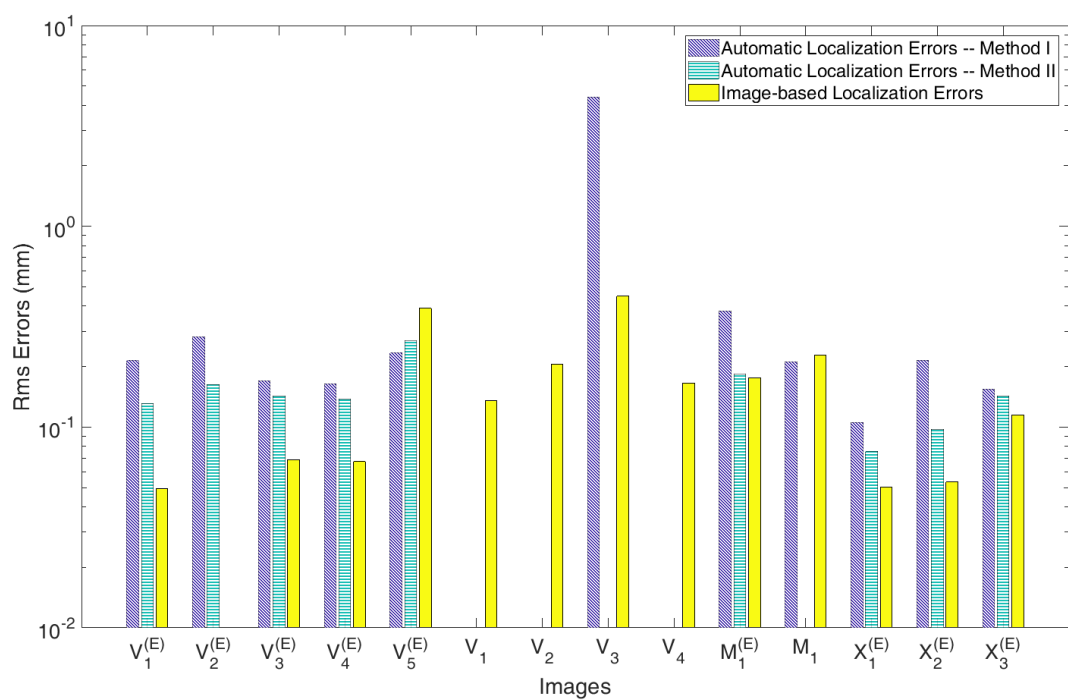
**Resolution:** T-tests on  $\Delta_{a(i,j)}^s$  for Auto I show statistically significant effects of change of resolution on only two out of five of the conditions tested for, and three out of four test groups exhibited significant effects of resolution change for Auto II, with the lower resolution images producing the worse results in every case (Table 2.7).

**Dose:** Two t-tests on  $\Delta_{a(i,j)}^s$  from both Auto I and Auto II show a significant effect of change of dose only for array A1 localized by Auto II. In every other case, the automatic localization results were unaffected by the dose changes tested (Table 2.7).

Figures 2.11 and 2.12 map the effect sizes of the tests on automatic localization errors in terms of their Cohen's d values and the 95% confidence intervals. The horizontal axis marks each of the different tests carried out as listed in Table 2.7. The effect size of the first test on resolution in Fig. 2.11 is a clear outlier, which is obtained from the test of errors

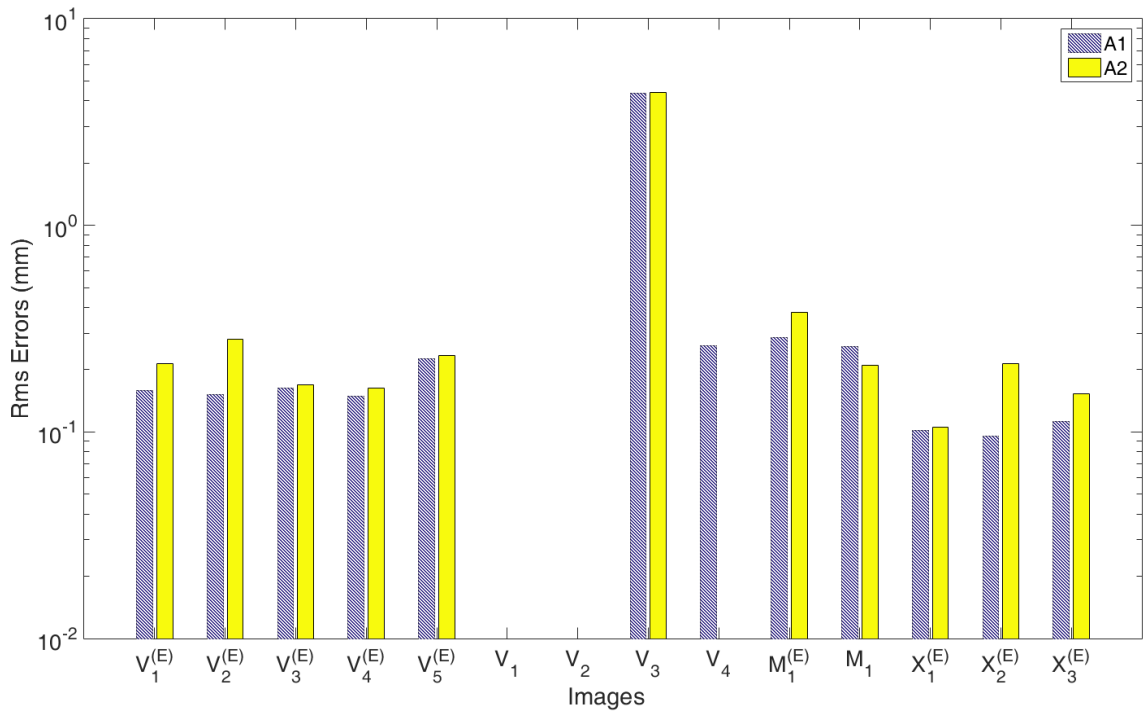


(a)  $\Delta_{a(i,j)}^s$  and  $\Delta_{m(i,j)}^s$  on A1

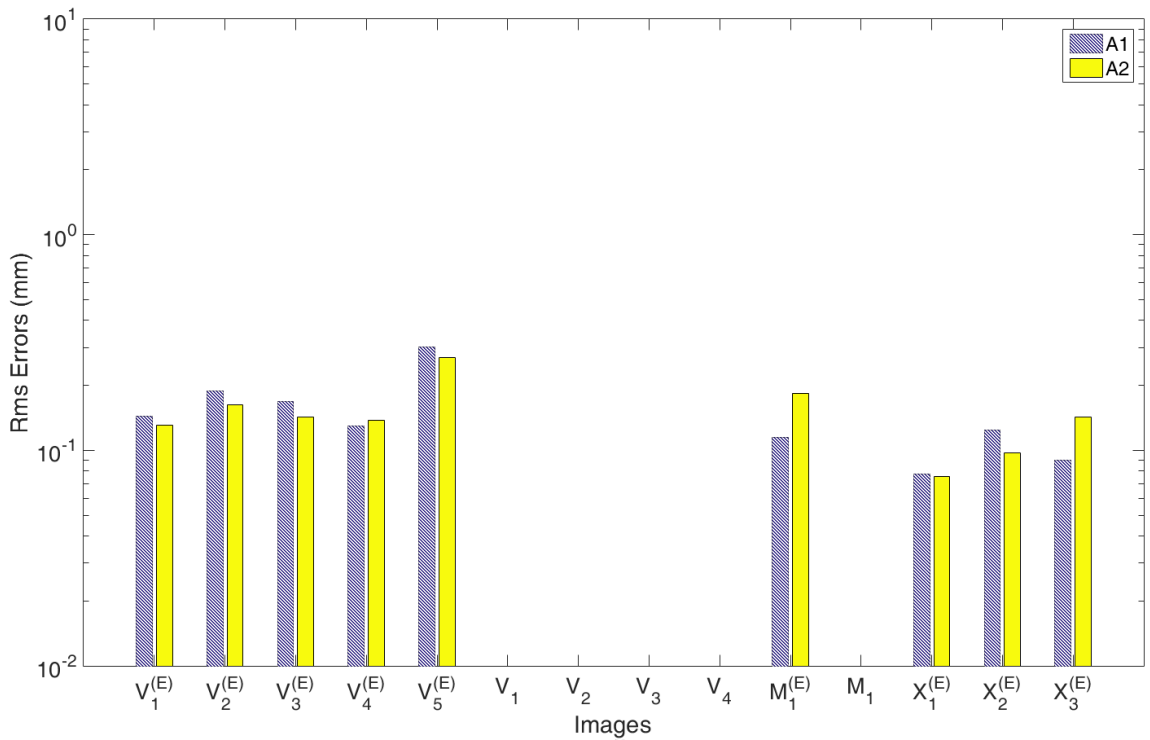


(b)  $\Delta_{a(i,j)}^s$  and  $\Delta_{m(i,j)}^s$  on A2

Figure 2.9: Automatic and Image-Based Localization Errors



(a) Automatic Localization Errors for A1 and A2 (Auto I)



(b) Automatic Localization Errors for A1 and A2 (Auto II)

Figure 2.10: Automatic Localization Errors

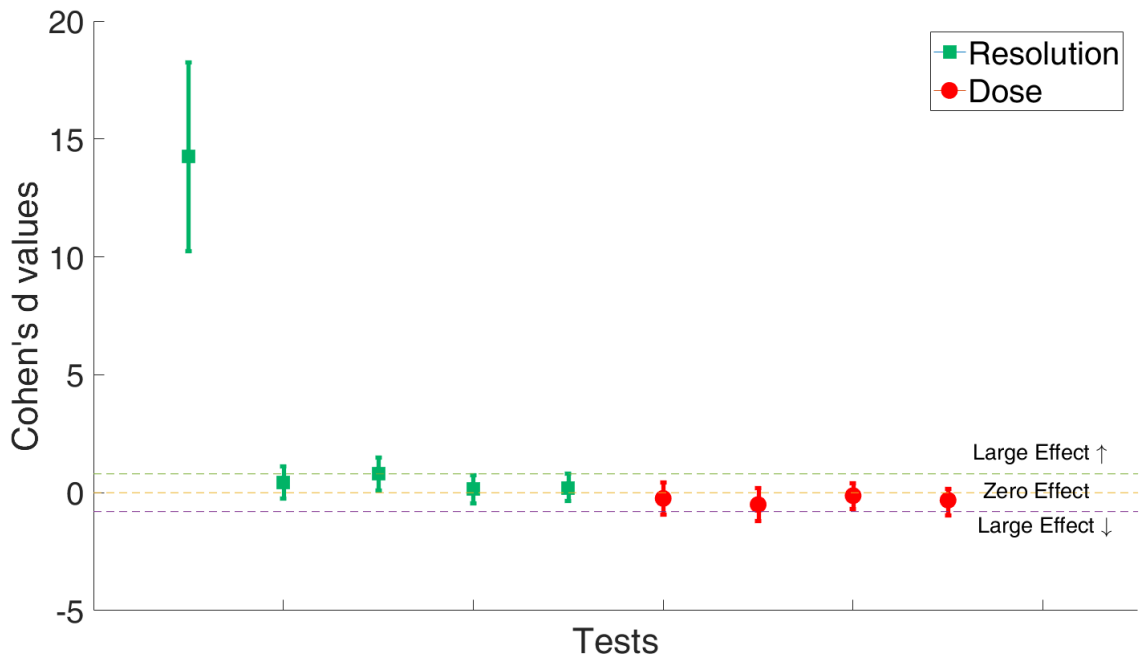


Figure 2.11: Effect size values for automatic localization errors across A1 and A2 (Auto I)

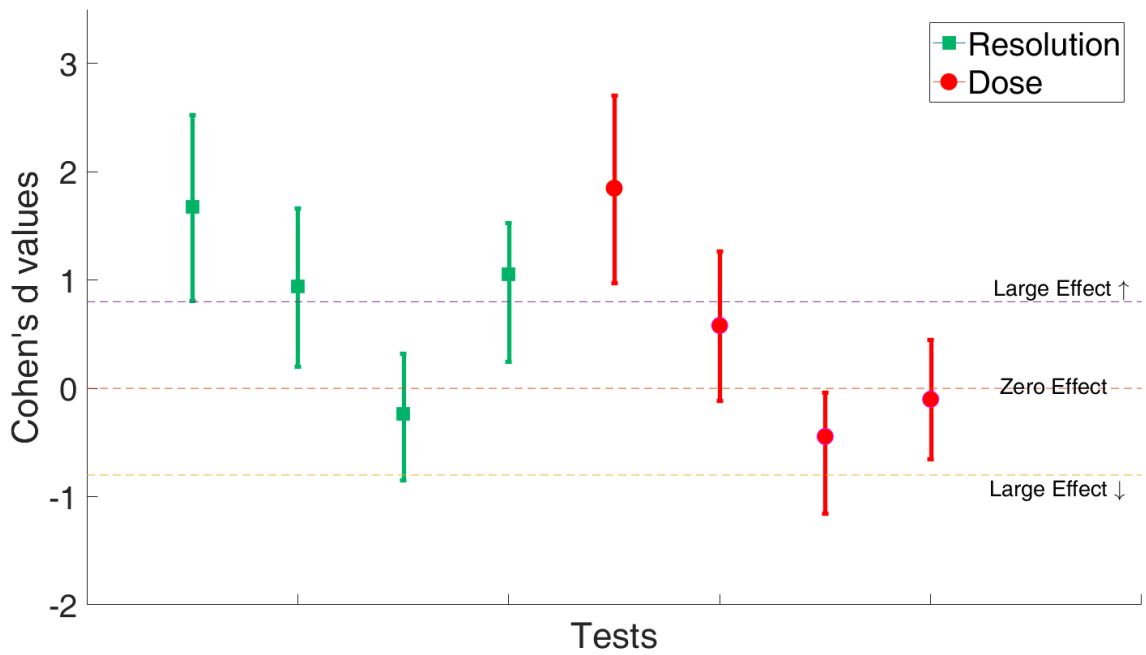


Figure 2.12: Effect size values for automatic localization errors across A1 and A2 (Auto II)

from Auto I on limited HU, mid dose images (Table 2.7). This was possibly due to quite a poor result on the limited HU low res image  $V_4$ , which was nevertheless included because it was not a complete failure. Although this was to be expected since Auto I was not designed to work for limited HU images, this effect of poor localization increases the apparent effect of resolution in this one test group. Even without counting this particular outlier, resolution has a large and significant effect in at least one set of images for Auto I, whereas dose has no significant effect at all. In case of Auto II, the effect of resolution is much more pronounced, with three out of four test groups exhibiting large and significant effects. By comparison, only in one case, dose does have a large effect. We can thereby conclude that Auto I is, in general, robust to changes of dose and resolution, and the localization accuracy of Auto II is significantly affected by image resolution.

This method has also later been used to validate an advanced version of Auto II [61].

### 2.3.2 Modeling Expected Errors based on Image Quality

After isolating the effects of the image acquisition parameters, we can now use a linear regression model to estimate localization error based on the image quality. This is a simple model that nevertheless gives us a good idea of how much error we can expect based on the CT acquisition parameters. Table 2.8 lists the estimated values of the intercept and coefficients for the significant factors when fitting a linear regression model to our average error data of the form

$$\text{error} = \alpha + \beta * \text{resolution} + \gamma * \text{dose} + \delta * [\text{HU}]. \quad (2.5)$$

In this model, “resolution” and “dose” are numerical variables, “HU” is a Boolean indicator,  $\alpha$  is the estimated intercept, and  $\beta$ ,  $\gamma$  and  $\delta$  are the estimated model coefficients. According to our fit, if we aim to only use images where the image-based localization error of array A1 is 0.1 mm or less, and the image is a limited HU image with a midrange dose

Table 2.8: Standard Linear Model fit with intercept of average localization error values.

Variables	Estimated Values of Coefficients			
	Image-based (A1)	Image-based (A2)	Auto I	Auto II
(Intercept)	-0.00048	-0.1301	-3.6367	-0.036273
Resolution	0.23973	1.040524	11.079	0.49949
Dose	—	-0.0004	—	-0.000099
HU	-0.058276	-1.7414	-2.122	—

of 350 mAs, the resolution must not exceed 0.42 mm in voxel diagonal length, whereas the resolution limit for an array A2 in a similar image would be 0.35 mm. Such a model can define a range of image parameters that are good enough for the purpose of limiting the error arising out of image quality.

Standard linear regression models can be fitted to the observed errors for both Auto I and Auto II. Unlike in the case of image-based errors, the automatic localization errors from arrays A1 and A2 can be pooled together because there is no significant effect of the array model on the errors. Auto I has the same model specifications as the image-based errors, whereas Auto II is fitted without the HU indicator. The coefficients are listed in Table 2.8, and we can determine acceptable ranges of parameters to limit the expected localization errors from either of these localization methods. For example, if we want to select images which would have no more than 0.2 mm localization error from method Auto I, we would only accept extended HU images of resolution 0.54 mm or better and limited HU images of resolution 0.35 mm or better.

## 2.4 Conclusions

In this paper, we have described the development of and initial results from what is to the best of our knowledge the first CI phantom for evaluating the sensitivity of image analysis techniques to acquisition parameters. Using a dataset obtained by imaging the phantom in different scanners, we have determined the limit to how accurately electrodes can be localized in images with various acquisition parameters. The summary of our tests

shown in Table 2.7 shows that changes of the HU range and resolution of reconstruction always affect the determination of the correct CI array locations. Dose and orientation affects localization accuracy as well, but their effects are not as strong (Fig. 2.7). On our tested images, image-based localization of A1 is insensitive to changes of orientation (for high dose, mid resolution, and extended HU reconstructions), but this factor significantly affects the localization of A2. Dose has only a minimal effect, with only the errors for array A2 being affected in one out of three test groups.

One limitation of the current work is that the accuracy of the chosen ground truth is determined by the precision of the reference CT volume. Without a better option for a ground truth, we used the best electrode position that we could define by repeated measurements on our best CT image. A potentially better approach would be to use a micro-CT to define the ground truth[62]. Size limitations of scanners that are currently available do not allow us to micro-CT something as large as our phantom. Once micro-CT technology that allows for imaging of larger samples becomes more widely available, such images could provide a better gold standard for electrode position in the phantom.

Even with high-resolution CT, critical small-scale intracochlear structures are still invisible, and thus, measuring electrode position in the context of the cochlea remains difficult. The most accurate approach has been to use statistical shape models of the cochlea, which rely on the visible external walls of the cochlea as a landmark to estimate the location of invisible intracochlear structures[63, 64]. Thus, in future work, we will also use the phantom to evaluate how accurately intracochlear anatomy structures can be localized when using different image acquisition parameters.

## **2.5 Acknowledgements**

This research has been supported in part by grants R01DC014037, R01DC008408, and R01DC014462 from the National Institute on Deafness and other communication disorders. The content is solely the responsibility of the authors and does not necessarily repre-

sent the official views of these institutes. The authors would also like to thank Advanced Bionics for providing the CI devices for this study, and the Biostatistics Clinics hosted by the Department of Biostatistics, Vanderbilt University for methodological guidance regarding the statistical calculations.

## Chapter 3

### FURTHER EVIDENCE OF THE RELATIONSHIP BETWEEN COCHLEAR IMPLANT ELECTRODE POSITIONING AND HEARING OUTCOMES

Srijata Chakravorti<sup>†1</sup>, Jack H. Noble<sup>†1,2,3</sup>, René H. Gifford<sup>2</sup>, Benoit M. Dawant<sup>1</sup>, Brendan  
P. O’Connell<sup>3</sup>, Jianing Wang<sup>1</sup>, and Robert F. Labadie<sup>3</sup>

† co-first authors

<sup>1</sup> Department of Electrical Engineering and Computer Science, Vanderbilt University

<sup>2</sup> Vanderbilt Bill Wilkerson Center, Department of Hearing and Speech Sciences,  
Vanderbilt University Medical Center

<sup>3</sup> Department of Otolaryngology-Head and Neck Surgery, Vanderbilt University Medical  
Center

---

This chapter is a non-final version of an article published in final form as “Further Evidence of the Relationship Between Cochlear Implant Electrode Positioning and Hearing Outcomes”, *Otology & Neurotology*, 40(5), 617–624. This chapter has been reproduced with the permission of the publisher and all co-authors: <https://doi.org/10.1097/MAO.0000000000002204>

### 3.1 Introduction

Cochlear implants (CI) are neuroprosthetics that have been adopted as standard of care treatment for patients with at least a moderate sloping to profound sensorineural hearing loss. Average speech recognition scores in quiet are approximately 60% correct for Consonant-Nucleus-Consonant (CNC) monosyllabic word scores and 70% for AzBio sentence recognition tests in quiet [4–7]. However, despite the remarkable effectiveness of CIs in the general population, there is a considerable degree of unexplained variability in patient outcomes [8]. It is important to know exactly how demographic and surgical factors affect outcomes, so that both patient counseling and surgical practices can be better tailored to the specific conditions of each individual patient.

Many studies have been undertaken by different groups to determine the causes of CI performance outcome variability for adult recipients. Certain factors have been consistently found to be significant. The duration of deafness before CI implantation has been repeatedly found to be strongly and negatively correlated with outcome for postlingually deafened CI users [8–14]. A longer duration of untreated deafness can reduce cell survival in the cochlea and affect residual speech processing capabilities. The length of use of the implant is defined as the duration between the surgical implantation and the testing date, which reflects familiarity with the device and hence improved acclimatization. A longer length of use generally has a strong positive effect on outcomes [9, 15–17]. Age at implantation and the age at the onset of deafness have a noteworthy effect in the adult population only after age 60 [9, 12]. Age at CI implantation is less strongly correlated with outcomes, although it should be noted that across studies, the definition of "younger" and "older" users is not consistent. Holden et al. [8] found a significant difference in mean CNC word scores between users less than and more than 65 years of age.

Preimplantation cognitive factors are also thought to affect CI outcomes since they reflect cognitive adaptability of patients. However, these factors have not been routinely studied in CI recipients, and different measures used across studies make conclusions dif-

difficult. The general consensus is that better performance in certain cognitive functions, like visuo-spatial processing tasks and verbal learning measures, is correlated with better word recognition; however, there is no evidence that general intellectual capacity is linked to better outcomes [65–67]. The etiology of hearing loss is another important factor that can indicate the degree of neuronal survival, which is thought to directly affect hearing performance. Some studies [68, 69] demonstrated a strong correlation between the causes of hearing loss with preserved spiral ganglion cell count. Patients who have hearing loss due to toxicity or sudden idiopathic deafness likely have more residual nerve cells in the cochlea, and can thus be expected to have a better performance with CIs, compared with patients with labyrinthitis ossificans, congenital, or genetic causes of hearing loss. Blamey et al. [9] found similar results in terms of poorer performance of patients affected by labyrinthitis, but did not find any direct correlation of surviving ganglion cell numbers and performance. More recently, electrophysiological responses measured either at extracochlear [70] or intracochlear [71] locations have been used as a surrogate for neural survival and/or health, and better outcomes are found to be correlated with better electrophysiological responses.

Recently, studies have shown that the final CI position also has a significant association with hearing outcomes. Specifically, studies have consistently established that a scalar translocation of the array across the basilar membrane from scala tympani (ST) to scala vestibuli (SV) is strongly associated with poorer hearing outcomes [8, 18–22]. Some studies report no correlation between outcomes and positioning of the array in ST [23, 24], but they agree that small sample sizes might have made it difficult to find a significant correlation. On the other hand, findings conflict regarding depth of insertion of the CI array into the cochlea. While a number of studies [19, 21, 25, 26] conclude that monosyllabic word scores were positively correlated with insertion depth of the most basal electrode, Khan et al. [27] and Lee et al. [28] did not find any significant correlation of insertion depth. Finley et al. [20] and Holden et al. [8], on the other hand, found a negative correlation of depth with outcomes. Possible reasons for this variability are that the effect differs for straight

versus precurved arrays and that the relationship may not be monotonic, i.e., insertions that are too deep and ones that are too shallow both have negative effects on outcomes.

One other factor of electrode positioning that has not been extensively studied is the distance of the electrode array to the modiolus. Until recently, there were no tools available to automatically and accurately measure this distance on a large scale, which explains why this factor has not been included in many studies. Modiolar proximity is expected to lead to improved hearing outcomes since the spiral ganglion cells are housed in the modiolus, and reducing the distance leads to lower charge requirement for upper stimulation levels [72], which can, in turn, reduce spread of excitation and channel interaction [73]. Holden et al. [8] measured the modiolar proximity in terms of a unitless “wrapping factor” and concluded that a closely wrapped array, i.e., an array that is positioned closer to the modiolus, leads to significantly higher word recognition scores. On a set of 25 ears with MedEL (ME) (Innsbruck, Austria) implants, Esquia-Medina et al. [24] confirmed that hearing outcomes and average electrode to modiolus proximity were strongly and positively correlated 6 months after implantation. However, this correlation does not hold at 12 months, possibly due to the effects of training and acclimatization in the long term. Further investigation is required to evaluate the role of modiolar distance in affecting hearing outcomes over time.

The objective of our current study is to model the variance in audiological scores as a function of electrode position, specifically modiolar distance, scalar location, and insertion depth. A potential drawback of most of the large sample studies in this field is that they are multicenter studies with inconsistent definitions of similar measures. Our study is based on data curated from a single center (seven full time equivalent audiologists practicing at a single physical site and seven surgeons who perform cochlear implantation at adjacent adult and pediatric hospitals) which has consistent metrics and CI programming techniques. Based on the literature discussed above, we hypothesized a priori that full ST insertion and closer modiolar proximity would be strongly and positively correlated with audiological outcomes.

### 3.2 Materials and Methods

Data on 220 CI ears were obtained from an Institutional Review Board-approved database of adult CI users who underwent postoperative Computed Tomography (CT) scanning. A wide variety of implants, both straight and precurved, are represented in our dataset (see Table 3.1), from manufacturers Advanced Bionics (AB) (Valencia, CA), Cochlear (CO) (Sydney, New South Wales, Australia), and MedEL (ME) (Innsbruck, Austria). To segment the cochlear anatomy, we used a non-rigid shape model of intracochlear structures defined using high resolution  $\mu$ CTs of 10 cochlea specimens. Automated algorithms were used to nonrigidly register the model to new patient CT images to localize intracochlear structures with mean errors of approximately 0.2mm [63, 74, 75]. Since our automated image analysis techniques require normal cochlear anatomy, we ensured that there were no malformed cochleae in our dataset. The CI electrodes were localized on postoperative CTs using automated algorithms as well, with mean localization errors of approximately 0.13mm [44, 45]. First, a set of candidate points for the electrodes were found in the CT based on intensity and shape features, and then a path joining the most viable candidate points is found representing the electrode array. Rigid coregistration of the preoperative and the postoperative images provided us with the locations of the implanted electrodes with reference to the intracochlear structures. Specifically, we measure one continuous modiolar proximity variable (mean distance from intracochlear electrodes to the modiolus), one categorical scalar location variable (whether the implant is fully positioned in the ST with no apparent basilar membrane (BM) damage or translocation to the SV), and two continuous insertion depth variables (angular depth of the tip of the array and depth of the most basal electrode as a linear distance from the opening of the cochlea). These positional measurements relate the postsurgical electrode position to the intracochlear structures and are independent of the actual number of electrodes or inter-electrode spacing of the arrays so that they can be generically applied across array types. These measurements are illustrated in Figure 3.1. Besides positional factors, we also controlled for demographic factors including age at

implantation, sex, prelingual onset of deafness, and length of use of the device. Audiological outcome measures used were the CNC monosyllabic word scores, measured in terms of percent correct [76], and Bamford-Kowal-Bench Sentences in Noise (BKB-SIN) scores [77], measured in terms of the signal-to-noise ratio (SNR) in dB at which sentences could be recognized with 50% accuracy. Speech recognition at lower SNR corresponds to better hearing in noise, and thus a lower BKB-SIN score indicates better performance. The factors are summarized in Table 3.2. It should be noted that not every patient had both CNC and BKB-SIN scores. As is evident from the numbers in Table 3.2, only a subset of patient ears used in the CNC model was used in fitting the BKB-SIN model.

Table 3.1: Straight and precurved arrays included in the study

Manufacturer	Total arrays	Straight arrays	Precurved arrays
AB	50	Hifocus 1J (29)	MidScala (21)
CO	120	CO-422 (20), CO-ST (11)	Contour Advance (89)
ME	50	ME-24 (3), ME-28 (22), ME-MD (1), ME-ST (24)	–

To analyze how each of the factors is associated with hearing outcome, stepwise multiple regression was conducted with backward elimination of the weakly correlated factors (Pearson correlation coefficients of all factors with outcomes are listed in Table 3.3). Since our dataset does not have data for all factors from every patient ear, missing data were excluded at every step of the fitting process based on the factors present in the model at the current step. Factors with  $p$  value above the critical  $p$ -value of 0.15 were eliminated in steps until all remaining factors were below the critical value and resulted in an overall significant model assessed by an F-test ( $p \leq 0.05$ ). This generalized linear model (GLM) is the simplest linear model that provides the best explanation of the variability of postoperative audiological scores. No interaction terms were included, assuming additivity of all factors. All computations were conducted in MATLAB (Mathworks, Natick, MA).

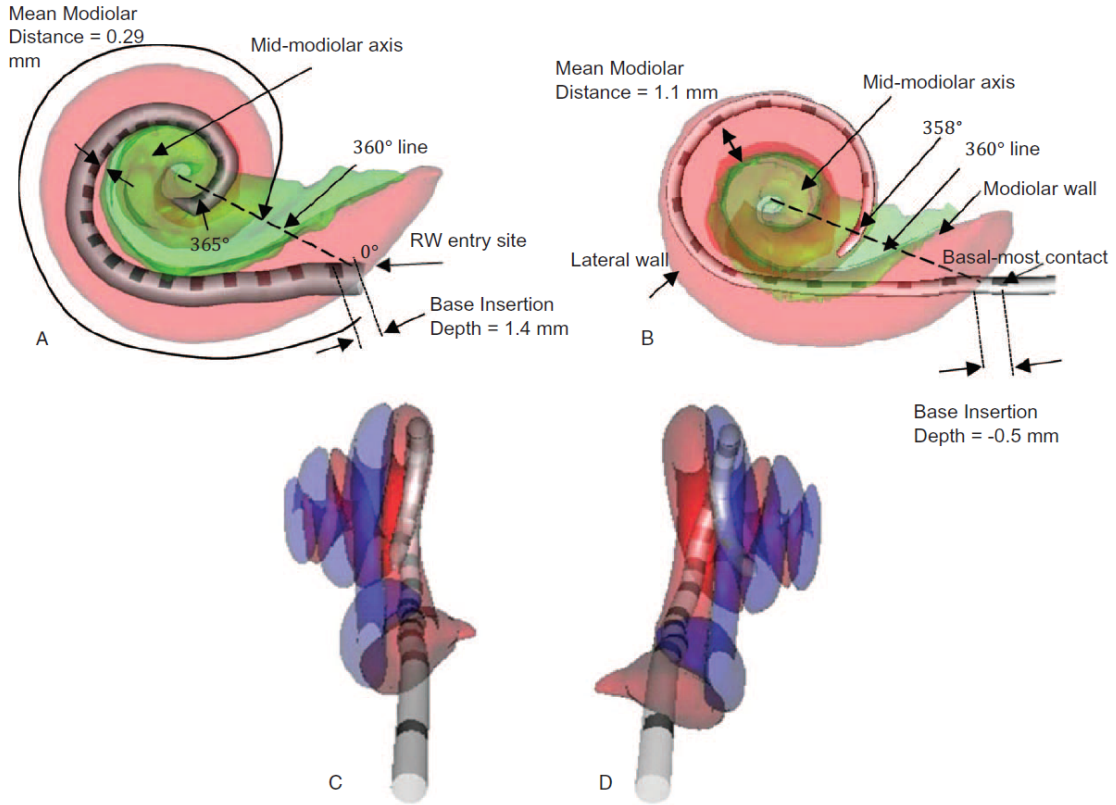


Figure 3.1: (A) Perimodiolar-positioned, precurved array and (B) lateral wall-positioned, straight array. Tip insertion depth of the array is measured in angle around the mid-modiolar axis to the most distal contact and is 365 degrees in (A) and 358 degrees in (B). In (C) and (D), examples of (C) full ST positioning and (D) scalar translocation of a CI array are shown. The structure in red is the scala tympani, and the structure in blue is the scala vestibuli. In (C), the array is completely positioned in the scala tympani. In (D), the apical part of the array has translocated into the scala vestibuli, which causes trauma to the intracochlear structures. CI indicates cochlear implants; ST, scala tympani.

### 3.3 Results

A GLM was built for CNC word recognition, in percent correct, for precurved arrays using data from a total of 92 patients with CI experience in the range of 6 months to 13 years (mean  $\pm$  sd = 2.75  $\pm$  2.42 yr). The significant factors predictive of better CNC performance in the least-fit GLM were full ST insertion, closer distance of the electrodes to the modiolus, male sex, and shallower base insertion depth (Table 3.4). For BKB-SIN sentence recognition, available for 85 precurved arrays, we observed similar significant

Table 3.2: Summary of factors included in each GLM

	Precurved Arrays		Straight Arrays	
	CNC words (%), n = 92	BKB-SIN (dB), n = 85	CNC Words (%), n = 91	BKB-SIN (dB), n = 89
<b>Scores</b>	[0, 98] 52.41 ± 24.97	[2.5, 23.5] 13.51 ± 6.05	[0, 100] 43.81 ± 25.49	[1.5, 23.5] 14.79 ± 5.62
<b>Full scala tympani insertion</b>	47 fully in ST, 45 partly or wholly in SV	42 fully in ST, 43 partly or wholly in SV	77 fully in ST, 11 partly or wholly in SV	72 fully in ST, 11 partly or wholly in SV
<b>Mean modiolar distance (mm)</b>	[0.16, 0.92] 0.48 ± 0.15	[0.16, 0.82] 0.47 ± 0.15	[0.44, 1.63] 1.16 ± 0.16	[0.44, 1.63] 1.16 ± 0.16
<b>Base insertion depth (mm)</b>	[-3.01, 6.30] 2.32 ± 1.16	[-3.01, 4.25] 2.26 ± 1.06	[-9.57, 4.60] 1.42 ± 2.41	[-9.57, 4.60] 1.36 ± 2.43
<b>Tip insertion depth (degrees)</b>	[114.86, 679.46] 376.42 ± 68.22	[114.86, 584.04] 371.45 ± 61.66	[217.47, 716.76] 453.86 ± 128.33	[217.47, 716.76] 454.32 ± 129.89
<b>Age at implantation (yr)</b>	[12.25, 89.23] 57.10 ± std 16.91	[12.25, 89.23] 57.92 ± 16.93	[7.05, 85.95] 56.14 ± 18.01	[7.05, 85.95] 55.96 ± 18.03
<b>Gender</b>	52 Males, 40 Females	50 Males, 35 Females	53 Males, 38 Females	51 Males, 38 Females
<b>Prelingually deafened</b>	13 Prelingually Deafened, 79 Postlingually Deafened	13 Prelingually Deafened, 72 Postlingually Deafened	18 Prelingually Deafened, 73 Postlingually Deafened	18 Prelingually Deafened, 71 Postlingually Deafened
<b>Length of CI use (yr)</b>	[0.53, 12.92] 2.75 ± 2.42	[0.53, 12.92] 2.80 ± 2.46	[0.18, 16.55] 2.87 ± 3.57	[0.18, 16.55] 2.89 ± 3.63

For numeric variables, ranges are shown in square brackets followed by mean ± 1 standard deviation. BKB-SIN indicates Bamford-Kowal-Bench Sentences in Noise; CNC, Consonant-Nucleus-Consonant; ST, scala tympani; SV, scala vestibuli.

factors – full ST insertion and lower (i.e., closer) average modiolar distance of the array, along with younger age at implantation and postlingual onset of deafness.

For straight arrays, the significant predictors of better CNC word scores for 91 cases that had between 2 months and 16 years of use (mean ± sd = 2.87 ± 3.57 yr) were deeper insertion depth, postlingual onset of deafness, and longer duration of CI experience (Table 3.5). Better BKB-SIN values (obtained from 89 cases) for straight arrays were significantly modeled by deeper insertion depth, younger age at implantation, and postlingual onset of deafness.

Table 3.3: Pearson correlation coefficients between factors and audiological scores

	Precurved Arrays				Straight Arrays			
	CNC words (N = 92)		BKB-SIN (N = 85)		CNC Words (N = 91)		BKB-SIN (N = 89)	
	R	<i>p</i>	R	<i>p</i>	R	<i>p</i>	R	<i>p</i>
<b>Full scala tympani insertion</b>	<b>0.27</b>	<b>0.009</b>	<b>-0.3</b>	<b>0.004</b>	-0.02	0.854	0.03	0.752
<b>Mean modiolar distance</b>	<b>-0.27</b>	<b>0.006</b>	<b>0.27</b>	<b>0.008</b>	0.15	0.14	-0.07	0.472
<b>Base insertion depth</b>	<b>-0.14</b>	<b>0.178</b>	0.01	0.926	<b>0.31</b>	<b>0.002</b>	<b>-0.28</b>	<b>0.007</b>
<b>Tip insertion depth</b>	0.08	0.45	-0.11	0.301	0.19	0.073	-0.12	0.241
<b>Age at implantation</b>	-0.22	0.022	<b>0.29</b>	<b>0.004</b>	-0.06	0.566	<b>0.12</b>	<b>0.227</b>
<b>Gender</b>	<b>-0.09</b>	<b>0.361</b>	0.12	0.231	-0.09	0.335	0.09	0.345
<b>Prelingually deafened</b>	-0.04	0.659	<b>0</b>	<b>0.988</b>	<b>-0.26</b>	<b>0.005</b>	<b>0.24</b>	<b>0.014</b>
<b>Length of CI use</b>	0.26	0.006	-0.19	0.053	<b>0.12</b>	<b>0.231</b>	-0.03	0.778
<b>GLM</b>	<b>0.43</b>	<b>&lt;0.001</b>	<b>0.51</b>	<b>&lt;0.001</b>	<b>0.47</b>	<b>&lt;0.001</b>	<b>0.47</b>	<b>&lt;0.001</b>

BKB-SIN indicates Bamford-Kowal-Bench Sentences in Noise; CI, cochlear implants; CNC, Consonant-Nucleus-Consonant; GLM, generalized linear models; ST, scala tympani; SV, scala vestibuli. Numbers in bold indicate factors that are significant in GLM.

Table 3.4: Model specifications for precurved arrays

	Precurved Arrays			
	CNC words (n = 92)		BKB-SIN (n = 85)	
	Estimate	<i>p</i>	Estimate	<i>p</i>
<b>Intercept</b>	79.58%	<0.001	2.04 dB	0.523
<b>Full Scala Tympani Insertion</b>	10.28%	0.041	-3.25 dB	0.006
<b>Gender</b>	-8.49%	0.088	-	-
<b>Age At Implantation</b>	-	-	0.12 dB/year	0.001
<b>Prelingually Deafened</b>	-	-	3.84 dB	0.031
<b>Mean Modiolar Distance</b>	-43.30 %/mm	0.008	11.50 dB/mm	0.005
<b>Base Insertion Depth</b>	-3.49 %/mm	0.107	-	-
<b>F statistic vs constant model</b>	<b>F = 4.8, p = 0.002</b>		<b>F = 8.41, p &lt;0.001</b>	

Any “-” indicates that the factor was not significant in the final GLM for the respective outcome measure. BKB-SIN indicates Bamford-Kowal-Bench Sentences in Noise; CNC, Consonant-Nucleus-Consonant.

Table 3.5: Model specifications for straight arrays

	Straight Arrays			
	CNC words (n = 91)		BKB-SIN (n = 89)	
	Estimate	<i>p</i>	Estimate	<i>p</i>
<b>Intercept</b>	38.66%	<0.001	8.77 dB	<0.001
<b>Age at Implantation</b>	–	–	0.10 dB/yr	0.003
<b>Prelingually Deafened</b>	-23.17%	<0.001	5.37 dB	0.001
<b>Length of CI use</b>	1.73%/yr	0.018	–	–
<b>Base Insertion Depth</b>	3.35%/mm	0.001	-0.67 dB/mm	0.004
<b>F statistic vs constant model</b>	<b>F = 7.12, <i>p</i> &lt; 0.001</b>		<b>F = 7.82, <i>p</i> &lt; 0.001</b>	

Any “–” indicates that the factor was not significant in the final GLM for the respective outcome measure. BKB-SIN indicates Bamford-Kowal-Bench Sentences in Noise; CNC, Consonant-Nucleus-Consonant.

### 3.4 Discussion

#### 3.4.1 Precurved (a.k.a. Perimodiolar) Electrodes

For precurved arrays, variables associated with higher potential for CNC word recognition include sex (men > women), full ST placement, lower (i.e., closer) average modiolar distance, and shallower insertion depth. BKB-SIN scores were also significantly affected by ST scalar positioning and mean modiolar distance, but not by insertion depth. Although the aim of the implantation is to place the CI array fully into ST, a number of factors—such as electrode design, surgical approach, and patient-specific cochlea shape—can lead one or more of the electrodes to break through the basilar and Reissner’s membranes and pass into SV. Figure 3.1 shows an example of a full ST placement (Fig. 3.1C) and a translocation into SV (Fig. 3.1D). Note that even a direct SV insertion is more traumatic than an ST insertion [78]. In our linear model, we define a CI array as being a “full ST insertion” if no electrodes are located in SV. It has been well established that positioning the electrode array entirely in the ST limits trauma to the intracochlear structures and improves hearing outcomes [22]. The findings herein corroborate this notion, with an estimated difference of 10.28-percentage points in CNC word scores and 3.25 dB in BKB-SIN SNR-50 scores between a full ST insertion and an insertion with translocation into SV. Of note here is that

the 3.25 dB difference for BKB-SIN SNR-50 is clinically significant given that the 95% confidence interval data for this measure places the critical difference at 3.1 dB for adult CI users administered two paired lists [76]. Independently, scalar location accounts for 7 and 9% of the variability of the CNC word scores and BKB-SIN scores, respectively (Table 3.3).

The variability in the outcomes explained by the modiolar distance was 7% for both CNC words and BKB-SIN scores (Table 3.3). Since precurved arrays are designed to be positioned close to the modiolus, it is intuitive that deviations from this ideal position would significantly affect hearing outcomes. Based on our model estimates, positioning the array by an average of 0.5mm away from the modiolus can decrease CNC scores by 21.65-percentage points and BKB-SIN values by 5.75 dB. This agrees with the correlations reported in literature, specifically that reported by Holden et al. [8].

The other positional factor that has a significant but negative effect is the base insertion depth, with a coefficient of determination of 0.02. This is not entirely surprising because deeper insertions that push the array towards the lateral wall might make modiolar stimulations less effective for precurved arrays. For every 1mm of additional insertion, the CNC word recognition decreases by 3.49-percentage points.

The other factors which are significant in the models are age at implantation, sex of the patient, and the indicator for prelingual deafness. The BKB-SIN performance in general is poorer with increasing age at implantation by about 1.2 dB for every 10 years of age difference at surgery, while prelingual deafness is associated with 3.84 dB poorer scores with all other factors constant. Our model suggests that CNC values were about 8.5-percentage points better in men than in women, which indicates that there might be some independent factor of electrode placement correlated with sex that we did not control for in the model, e.g., it is well known that male cochleae are larger on average than female cochleae [79]. Further, since

- 1) prelingual deafness is found to be significant for straight arrays for both CNC and

BKB-SIN scores and BKB-SIN scores for precurved arrays; and

- 2) there is a significant correlation between sex and prelingual deafness ( $|R| = 0.25, p \leq 0.05$ ) in our dataset

it is possible that the sex variable is actually capturing the effect of prelingual deafness on CNC values for the precurved group. In total, these three demographic factors, along with the descriptors of electrode position, account for 18% of the variability of CNC scores and 26% of the variability of BKB-SIN scores (Table 3.3).

### **3.4.2 Implications for Precurved (a.k.a. Perimodiolar) Electrodes**

The implications of this GLM are better understood with how expected hearing outcomes change with electrode position. Consider the demographic of postlingually deafened men who were implanted with a precurved array at 35 years of age and have 5 years of CI experience. According to our GLM, if a precurved array was ideally implanted with a full ST insertion, a mean modiolar distance of 0.18 mm, which is two standard deviations better than average, and at a base insertion depth of 0 mm, which is two standard deviations shallower than average, the expected CNC score and confidence interval are 82% [66%, 98%] for such patients. In contrast, population average positioning (modiolar distance = 0.48 mm, insertion depth = 2.32mm) leads to an expected CNC score of 61% [53%, 69%] with a full ST placement or 51% [43%, 59%] with a scalar translocation. Finally, with a poor positioning of a scalar translocation, 0.78mm mean modiolar distance, which is two standard deviations worse than average, and at a depth of 4.64 mm, which is two standard deviations deeper than average, the expected CNC score is 30% [15%,45%]. Between an ideal electrode position (full ST insertion) and 0.18mm modiolar distance to a poor placement of partial ST insertion and 0.78mm modiolar distance, the expected score changes by over 50-percentage points with no overlap in confidence intervals. This is a considerable change in predicted outcome, and illustrates the remarkable influence of the surgical

process on user experience.

### **3.4.3 Lateral Wall (a.k.a. Straight) Electrodes**

The positional factor primarily predictive of better expected performance on CNC word tests with straight arrays is greater base insertion depth. It accounts for 10 and 8% of the variability in CNC word scores and BKB-SIN scores, respectively. An insertion that is deeper by one standard deviation of our sample, i.e., 2.4 mm, is associated with an improvement of 8.04-percentage points on the CNC score and 1.61 dB on the BKB-SIN score. This agrees with the strong positive correlation between basal insertion depth and audiological outcomes reported previously [19, 21, 25, 26].

The significant biographic factors were similar to those found for precurved arrays—better BKB-SIN scores were associated with younger age at implantation and postlingual onset of deafness; and better CNC word scores were associated with longer duration of CI experience and postlingual onset of deafness. The effects of these factors agree with findings in previous studies – experience with the device is associated with better outcomes, while prelingual deafness and later age at implantation are associated with poorer outcomes, independent of electrode position. In total, the positional and demographic factors account for 22% of the variability of both CNC and BKB-SIN scores.

### **3.4.4 Implications for Lateral Wall (a.k.a. Straight) Electrodes**

To understand the impact of electrode position on CNC scores for lateral wall arrays, consider a demographic of postlingually deafened male or female individuals implanted with a straight array at 35 years of age and with 5 years of CI use when the audiological testing occurred. Our model predicts that if the implant was inserted to a depth of  $-3.4$  mm, which is two standard deviations shallower than average, the expected CNC score would be 36% [25%, 47%]. If the array was inserted to a population average 1.42 mm, the expected CNC score would be 52% [46%, 59%]. If the array were inserted further to 6.24 mm, which

is two standard deviations deeper than average, the expected score would be 68% [56%, 80%]. Our GLM predicts that deeper insertions are associated with significantly better expected outcomes. However, beyond the range of insertion depths in our dataset, there likely are rapidly diminishing benefits to deeper insertions given the increased likelihood of trauma to the apical walls of the cochlea and failure to achieve proper basal stimulation [20].

### **3.4.5 Implications for Surgical Procedures**

We found using our GLM analysis for 35-year old male patients with 5 years of CI use that if using a precurved electrode array, the expected outcome as a function of excellent, average with full ST positioning, average with scalar translocation, and poor electrode position are CNC scores of 82, 61, 51, and 30% for mean  $\pm 2$  sd in electrode positioning. On the other hand, the expected outcome when using a straight electrode array as a function of deep, average, and shallow electrode depth are CNC scores of 68, 52, and 36% for mean  $\pm 2$  sd in electrode base insertion depth. What is the clinical impact of these predictions? For straight arrays, the likely cause for shallow insertions in our retrospective dataset is that the surgeon perceived resistance and wisely chose to stop the insertion procedure without further advancement to avoid potentially causing additional intracochlear trauma. This retrospective study does not show that further advancement of the array in such cases where resistance is felt would result in improved outcomes, and it is quite possible to have the opposite effect due to increased intracochlear trauma. Similarly, it is also possible that the deeper insertions in our dataset were obtained when resistance was never perceived and less trauma occurred, in which case the direct cause for better outcomes could be reduced trauma, rather than increased depth. In this context, we can conclude that any advances to surgical techniques and array devices that permit deeper atraumatic insertion of the array should lead to improved outcomes. This could include techniques for patient customized selection of arrays that are appropriately sized for the patient's cochlea [80].

For precurved arrays, advances to surgical technique and devices that permit reducing scalar translocations and obtaining more perimodiolar positioning of the array should lead to improved outcomes. For example, techniques for patient-customized electrode insertion procedure planning have shown promise for improving the modiolar positioning and scalar location of precurved arrays [81, 82].

### **3.4.6 Limitations**

Limitations of the current study include the demographic factors that were not modeled, including length of deafness, daily CI wear time, etiology, and cognitive factors, which will be explored in future work. As more data are collected, it will be possible in future analyses to further categorize results according to device type, as it is well known that cochlear implant design has an important impact on outcomes. After controlling for base insertion depth, tip insertion depth isn't a significant predictor of outcomes; however, the two are highly correlated. It is also of note that the relationship between insertion depth and outcomes is likely not monotonic. If the insertion is too shallow the outcomes are poor due to extracochlear electrodes and lack of low frequency stimulation; too deep and trauma could outweigh the benefits of a more complete frequency map. Supplemental online data from Rivas and Cakir et al. [80] with MedEl arrays show a trend of better outcomes with increased insertion depth for arrays inserted up to around 500 degrees, and beyond that point outcomes no longer improve with increasing depth. Thus, the use of linear modeling to capture this relationship is likely sub-optimal. Another potential confound for insertion depth due to the retrospective nature of our dataset is that it is likely that most shallow insertions in our dataset occurred because the surgeon perceived resistance and deliberately concluded the insertion procedure at a shallow depth. The perception of resistance suggests trauma could have occurred, which could impact hearing outcomes.

### **3.5 Conclusions**

Our results using 220 patient ears confirm the significant association between electrode positioning and audiological outcomes. Controlling for biographic factors like age at implantation, sex of patient, linguistic capabilities at the onset of deafness, and length of device use, the most significant predictors of outcome for precurved arrays were full ST insertion and the modiolar distance, while for the lateral wall arrays the depth of insertion was the most significant factor. We demonstrate how to use our linear model to determine the expected hearing outcome as a function of patient demographics and electrode position. A comprehensive knowledge of how each of these positional factors affects hearing outcomes for different demographics is critical in guiding patient counseling. These data also hold implications for future electrode design and support the importance of development of improved methods for patient-customized surgical planning and guidance techniques [81, 82] and postoperative mapping techniques [52, 83, 84].

### **3.6 Acknowledgements**

This work was supported in part by grants R01DC014462, R01DC008408, and R01DC014037, from the National Institute for Deafness and Communication Disorders and by the grant UL1TR000445 from the National Center for Advancing Translational Sciences. The content is solely the responsibility of the authors and does not necessarily represent the official views of these institutes.

## Chapter 4

### EFFECTS OF PRECURVED COCHLEAR IMPLANT POSITION ON OPEN-SET WORD RECOGNITION OUTCOMES

Srijata Chakravorti<sup>1</sup>, Benoit M. Dawant<sup>1</sup>, René H. Gifford<sup>2</sup>, Linsey Sunderhaus<sup>2</sup>, Robert  
F. Labadie<sup>3</sup> and Jack H. Noble<sup>1</sup>

<sup>1</sup> Department of Electrical Engineering and Computer Science, Vanderbilt University

<sup>2</sup> Vanderbilt Bill Wilkerson Center, Department of Hearing and Speech Sciences,  
Vanderbilt University Medical Center

<sup>3</sup> Department of Otolaryngology-Head and Neck Surgery, Vanderbilt University Medical  
Center

## 4.1 Introduction

Cochlear implants (CIs) are standard-of-care neuroprosthetics for moderate to profound sensory hearing loss used by over 324,200 people around the world [2]. They are among the most successful medical prosthetics in use, producing consistently high average speech recognition around 60% correct for Consonant-Nucleus-Consonant (CNC) monosyllabic word scores and 70% for AzBio sentence recognition tests in quiet. Despite their success in a majority of the implanted population, occasional cases of poor performance lead to considerable unexplained variance in the hearing outcomes. Research into causes of outcome variability has repeatedly found certain factors to be correlated with the outcomes. Postlingual hearing loss has generally been associated with better outcomes compared to prelingual onset of hearing loss [85], possibly owing to differences in early speech development. The length of experience using the CI also improves hearing outcomes [9, 15–17], since longer duration of use leads to greater acclimatization and is associated with more training.

Duration of hearing loss has been a consistent indicator, with longer durations associated with poorer hearing outcomes with CIs [8–14, 86, 87], although other studies [28, 88] found no such association. Age at implantation has also been identified as an important predictor, but only in certain cases – for example, some studies find it significant only after age 60 [8, 9, 12], and others have found its contribution to be important only when the duration of hearing loss is less than 10 years [86]. Both of these factors are possibly affected by the same underlying changes in neuronal survival with age, especially with the absence of auditory stimulation during untreated hearing loss.

Increasingly, studies also find that positioning affects outcomes after controlling for demographics. It is interesting to note that there are several contradictory conclusions about individual factors. Several studies indicate that full insertion into the scala tympani (ST) is associated with better outcomes compared to cases where the array translocates across the basilar membrane into the scala vestibuli (SV) [8, 18–22]. While some studies

did not find this correlation [23, 24], the sample sizes are small which could have prevented a conclusion of significant correlation. Closer proximity to the modiolus has been reported to improve outcomes [8, 89–92], which can be explained by the fact that the spiral ganglion cells are located in the modiolus, and closer proximity limits the spread of excitation and reduces channel interaction [73]. Other studies note that this is an effect that is no longer significant with increase in CI experience, possibly due to training and acclimatization [24].

The effect of the depth of CI array insertion has had the most conflicting conclusions in the literature. While many studies note a positive correlation of insertion depth with outcomes [19, 21, 25, 26, 93], others have found no significant association [27, 28], while yet others report a negative correlation of insertion depth with outcomes [8, 20]. Several of these studies include both straight and precurved arrays in the same cohort even though they might have different associations with insertion depth, which is one possible reason for the lack of consensus. Nevertheless, this is a factor that merits further careful study since its effect is possibly non-monotonic, and both very shallow and very deep insertions might be detrimental to hearing outcomes.

To be able to modify electrode design and improve surgical techniques for better hearing outcomes, there is a need to conclusively identify exactly which positioning factors are associated with better outcomes while accounting for the effects of demographics. Many of the studies cited here relied on relatively small sample sizes, which makes it difficult to control for multiple relevant confounds and reach conclusions about statistical significance. In Chapter 3, we analyzed the effect of four positioning factors on hearing outcomes in a dataset of 220 CI recipients with mixed straight and precurved arrays. A unique feature of our approach was separately modeling straight and precurved arrays, since their optimal positions are different – precurved arrays curve onto the inner wall of the cochlea, while straight arrays rest along the outer wall. Using supervised automatic feature selection to construct general linear models, we demonstrated how the final positions of the different CI arrays influence outcomes. For precurved arrays, based on 92 ears, we found that the

significant positional features were linear base insertion depth, mean modiolar distance and full ST insertion.

However, there were some interactions between the positioning factors that could not be fully explained. Especially for precurved arrays, preliminary results showed nonlinear interactions between insertion depth and modiolar distance, which complicates the interpretation of the general linear model (GLM) results since both were significant features in the GLM. Additionally, confounds like cochlea size and duration of hearing loss must be considered to better clarify the role of position, which requires a larger dataset for the necessary statistical power to find true statistical significance among these multiple factors. In this current work, we expand our dataset of precurved arrays with the aim to rigorously explore the relationship between position and outcomes. We select appropriate image processing algorithms to extract position features, and analyze the linear correlation between these features and outcomes after controlling for demographics.

## **4.2 Material and Methods**

### **4.2.1 Dataset**

We obtained data for 277 ears from an Institutional Review Board (IRB) approved database of 242 adult CI users who were either scanned at Vanderbilt or were registered in the Image-guided Cochlear Implant Programming clinical trial at Vanderbilt (NCT03306082). All of them were implanted with precurved arrays with no follow up revision surgery. Implants included devices from both manufacturers Advanced Bionics (Valencia, CA, USA) and Cochlear (Sydney, New South Wales, Australia). Specifically, we extracted the data for the duration of hearing loss (HL), the age of the patient at implantation, and the number of years the patient has used the device. The outcome measure of interest is the Consonant-Nucleus-Consonant (CNC) monosyllabic word scores[76] at last follow up for patients who have been implanted for at least 3 months. This test measures hearing capabilities in a

quiet environment based on the correct recognition of 50 spoken words. The demographics data are described in Table 4.1.

#### **4.2.2 Features Computed from CT Images**

The cochlear anatomy was identified from the preoperative computed tomography (CT) images using a non-rigid shape model of intracochlear structures defined on  $\mu$ CTs of 10 cochlear specimens, which was nonrigidly registered to new patient CT images with an approximate mean error of 0.2 mm [63, 74, 75]. The CI position was localized from the postoperative images [44, 45] with an approximate mean localization error of 0.13 mm. We rigidly coregistered the preoperative and postoperative images so that we can calculate features to describe the position of the electrode array relative to the intracochlear anatomy. We described the insertion depth of the electrode array with two continuous variables – the base insertion depth, which is the linear distance of the most basal active electrode from the opening of the cochlea, and the tip insertion depth, which is the angular depth of the most apical electrode. The proximity to the modiolus was described by the average distance of the intracochlear electrodes to the modiolus surface. A categorical variable was created to denote if the array was fully inserted in the ST or not. We also calculated the cochlear duct length from our cochlear mesh segmentation [80] as a measure of cochlear size. Table 4.1 lists the features of interest collected from medical records as well as the generated features.

To ensure that our dataset had no outliers in terms of anatomy, insertion, and external confounds, we examined all the processed ears in the dataset for any tip foldovers, shallow insertions (less than two electrodes in the cochlea) and trends that indicate possible device malfunction. Two ears associated with the same patient were removed due to concerns of overall health decline, and one ear from a unilaterally implanted patient was removed due to concerns of device failure when the test was performed. Our final dataset has 274 ears implanted with precurved arrays, and the classification of device types are documented in

Table 4.1: Patient demographics, position features, and outcomes

		Mean $\pm$ St. Dev.	Range
Outcomes:	CNC at last follow up	52.66 $\pm$ 25.32	(0, 98)
Demographics:	Duration of Hearing Loss (yr)	26.60 $\pm$ 17.51	(0.4, 79.3)
	Age at Implantation (yr)	62 $\pm$ 15	(23, 89)
	Length of Use (yr)	2.01 $\pm$ 1.77	(0.06, 12.52)
		<b>n</b>	<b>%</b>
	Gender: Female	134	47.86
	Prelingual Hearing Loss	21	7.53
Position:	Cochlear Duct Length (mm)	33.19 $\pm$ 1.40	(29.66, 38.29)
	Mean Modiolar Distance (mm)	0.47 $\pm$ 0.18	(0.07, 1.14)
	Apical Mean Modiolar Distance (mm)	0.33 $\pm$ 0.25	(0.03, 1.42)
	Basal Mean Modiolar Distance (mm)	0.55 $\pm$ 0.29	(0.04, 1.26)
	Tip Insertion Depth (degrees)	376.93 $\pm$ 46.92	(229.74, 515.59)
	Base Insertion Depth (mm)	1.93 $\pm$ 1.13	(-1.28, 5.54)
		<b>n</b>	<b>%</b>
	Full Scala Tympani Insertion	219	71.57

Table 4.2.

Table 4.2: Precurved arrays included in the study

Manufacturer	Device Type	Number
Advanced Bionics	Mid Scala	82
Cochlear	Contour Advance	98
Cochlear	532/632	94

### 4.2.3 Analysis

Our aim is to identify the electrode location factors that contribute to variability in outcomes. Following an exploratory correlation analysis of the data, we analyze the effect of the features on the outcome and on each other. Our hypothesis follows from our previous studies: that deeper insertion and lower modiolar distance are necessary for good outcomes, as long as that positioning does not cause trauma. All data analysis was carried out in Python 3.6.

## 4.3 Results

### 4.3.1 Relationship between features and outcome

We explored the relationship of outcomes with each of the continuous features for all 274 ears. To ascertain if a feature significantly affected the outcome, Pearson's correlation coefficient was calculated for each feature and outcome pair. If the  $p$ -value was lower than the significance level of 0.05, it is considered a significant effect on outcome and the corresponding feature is plotted in red. In Figure 4.1, despite the high noise levels in the data, it is clear from the correlation value that all continuous demographic features are significantly linearly correlated to the outcome. Of the positional features in Figure 4.2, mean modiolar distance and tip insertion depth were significantly correlated to the outcomes.

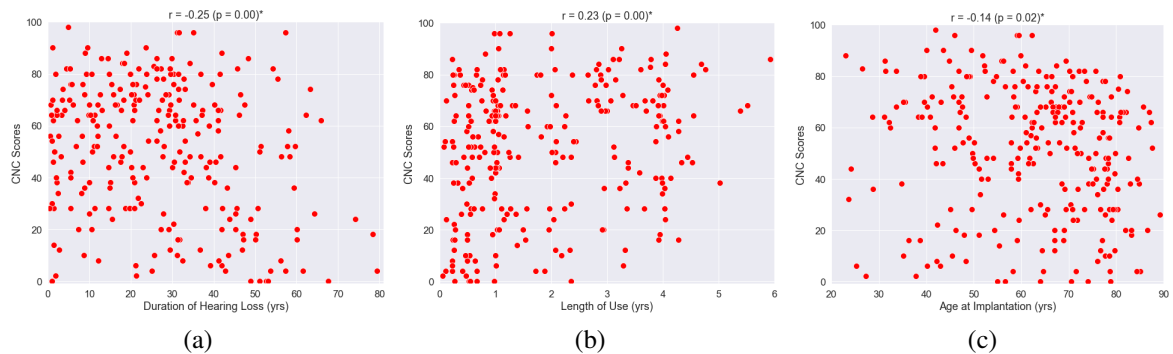


Figure 4.1: Correlation of Continuous Demographic Features with CNC scores

To analyze the effect of the three categorical variables – gender, prelingual onset of hearing loss and scalar translocation – we use a t-test to evaluate the difference of group means between the different levels of the variables. Figure 4.3 shows the boxplot and the results of the t-test in the titles. Gender does not affect the group outcomes, but both prelingual onset of hearing loss and scalar translocation do. In the following sections, we will delve further into the position variables that significantly affect the outcome.

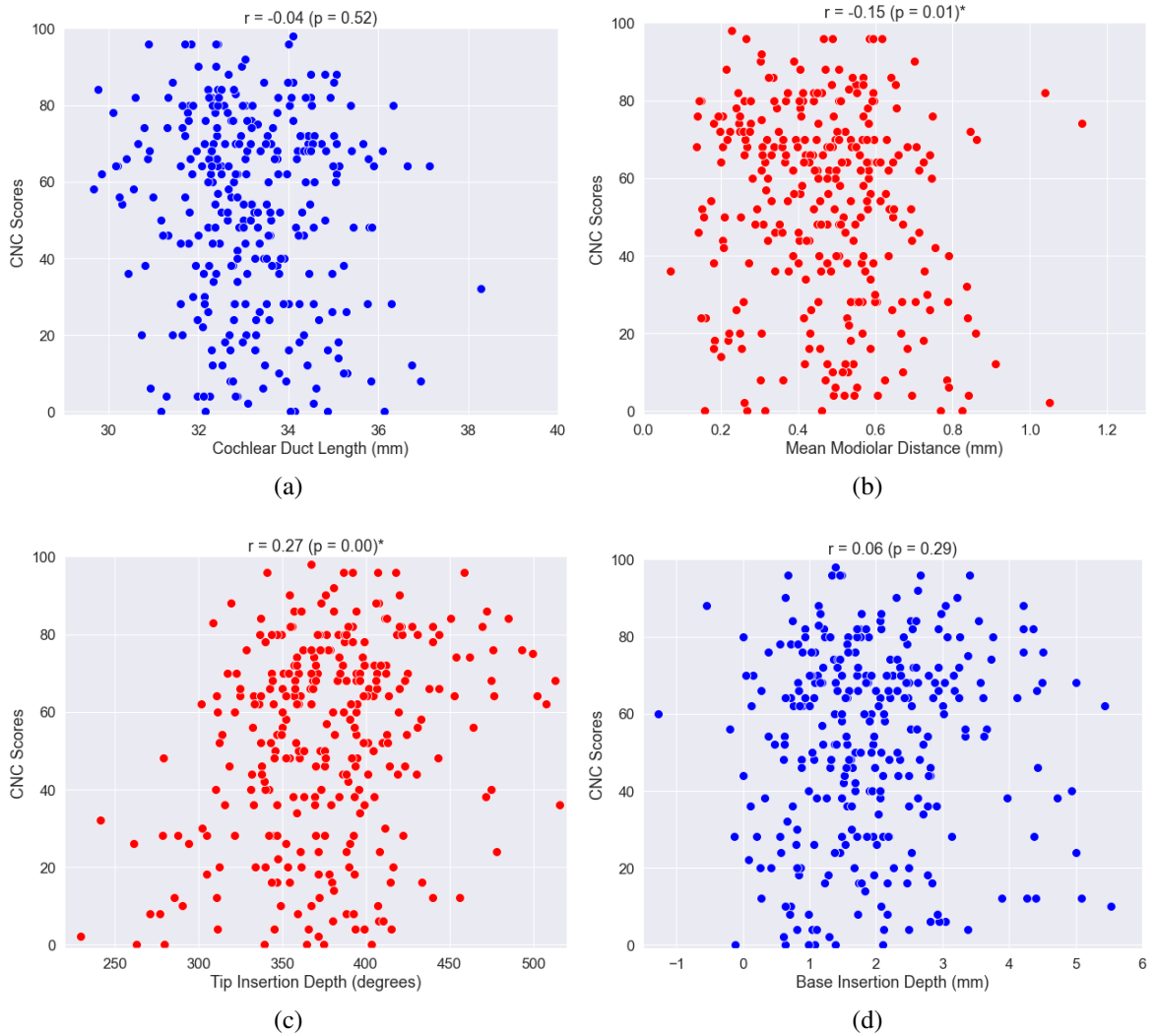


Figure 4.2: Correlation of Continuous Position Features with CNC scores

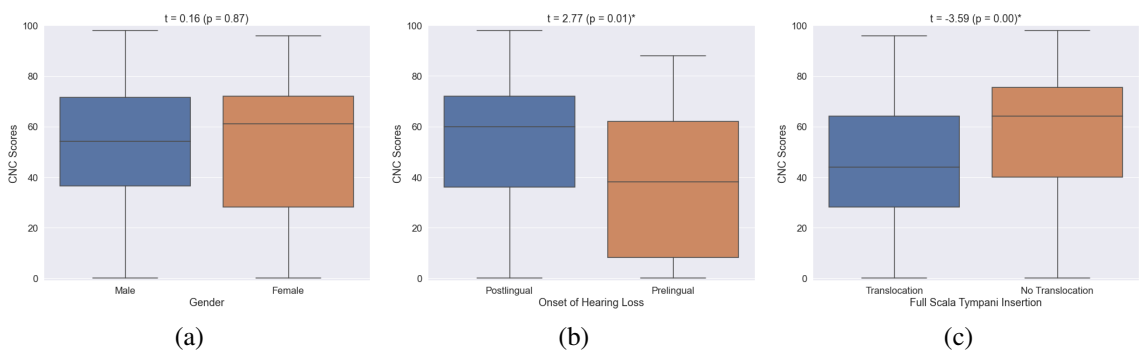


Figure 4.3: Effect of Categorical Position Features on CNC scores

### 4.3.2 Analyzing modiolar distance

Mean modiolar distance is significantly negatively correlated to the outcomes in our dataset. However, physiologically, we know that there is a bony section at the basal part of the cochlea which might impede electric stimulation of spiral ganglia nerves by the basal electrodes. To analyze if there is any differential effect on the correlation to outcome between the basal and apical parts, we calculated two separate measures – a basal mean modiolar distance to capture the average distance to the modiolus for all electrodes shallower than 240 degrees; and an apical mean modiolar distance, capturing the mean distance for the electrodes lying 240 degrees and deeper. Figure 4.4 shows that it is indeed the apical mean modiolar distance that is significantly linearly correlated, and the basal mean modiolar distance is not correlated to the outcome.

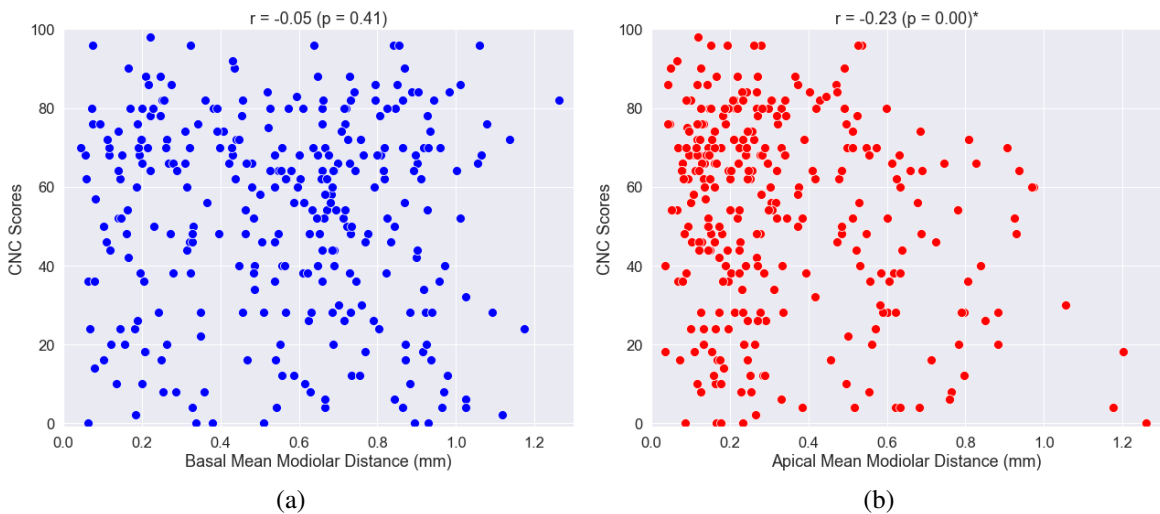


Figure 4.4: Correlation of Different Modiolar Distance Features with CNC scores

### 4.3.3 Tip Insertion Depth and Apical Mean Modiolar Distance

Focusing only on position features relating to the apical part of the cochlea, both tip insertion depth and apical mean modiolar distance are significantly correlated with the

outcomes. Figure 4.5 plots these two features against each other, and they are colored differentially based on the outcome quartile. Pearson's correlation coefficient shows that these two features are also significantly linearly correlated to each other.

The facts that these two features are correlated in opposing ways to the outcome – tip insertion depth is positively correlated while apical mean modiolar distance is negatively correlated, with comparable  $r$  values – and are also correlated with each other, raises the question of whether both are indeed independently influential for the outcome. The trend in Figure 4.5 reveals that all the highest quartile ears (green) are clustered towards lower apical mean modiolar distance and higher tip insertion depth. To verify numerically, we split the figure into four quadrants using thresholds of apical mean modiolar distance = 0.6 mm and tip insertion depth = 300 degrees, isolating the highest outcome datapoints to the fourth quadrant. We calculate the group means of datapoints in all of these four quadrants and carry out a one-way ANOVA followed by multiple comparisons test (Tukey Honest Significant Difference test) between the group means. The results in Figure 4.6 show that (a) the group mean of quadrant 4 is significantly higher than all the others, (b) the group means of quadrants 1 and 3 are not significantly different from each other, and (c) the group mean of quadrant 2 is significantly lower than quadrant 4, and lower than the other two groups, although not significantly.

#### **4.3.4 Linear Regression**

To gauge the relative importance of each of the features towards the outcome, we use multiple linear regression to fit a model with all the significantly correlated features. Figure 4.7a demonstrates the absolute coefficient values standardized by the standard deviations of the continuous variables, and unchanged for the categorical variables. This means that with all other variables constant, the corresponding length of the bar would be the change in outcome for 1 standard deviation change for the continuous variables, and for a change between categories for the categorical variables. The color of the bar is red if the coefficient

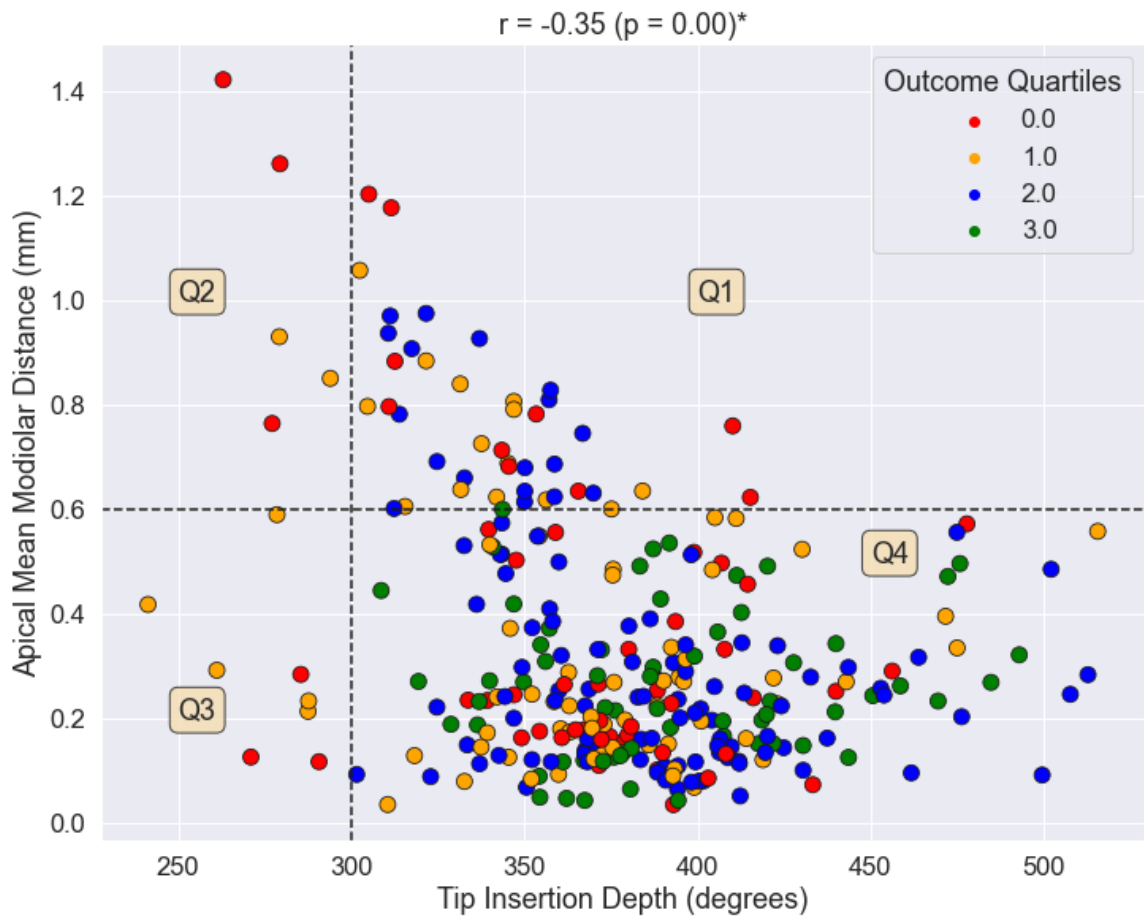


Figure 4.5: Correlation of Tip Insertion Depth with Apical Mean Modiolar Distance. The datapoints are colored based on the outcome quartile, i.e. red if the CNC score was (0–25), orange if CNC score was (25–50), blue if CNC score was (50–75), and green if CNC score was (75–100)

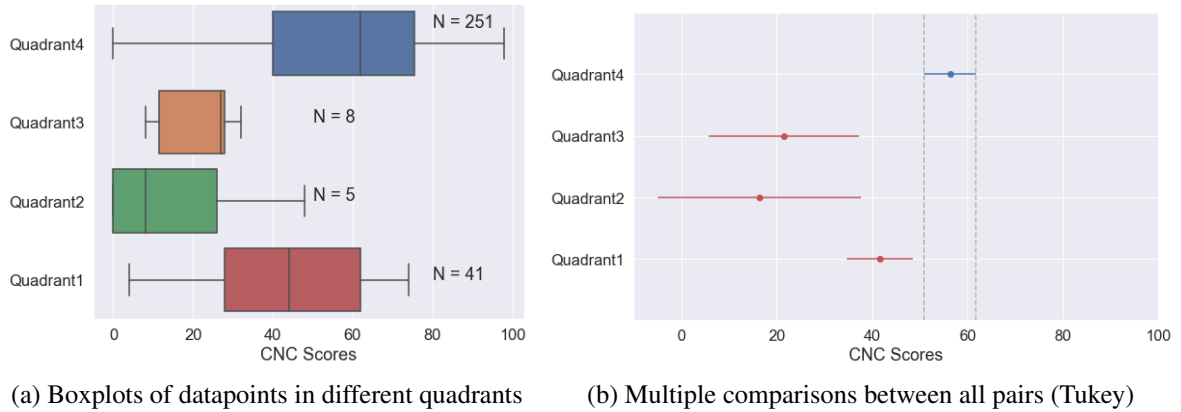


Figure 4.6: Analysis of relative importance of tip insertion depth and apical mean modiolar distance using group means

$p$ -value is less than the significance level of 0.05, and blue otherwise. All of the correlated features were significant in the regression model except apical mean modiolar distance. The predictive power of this model is tested in a leave-one-out validation in Figure 4.7b and produces a mean absolute error of 17.77 percentage points.

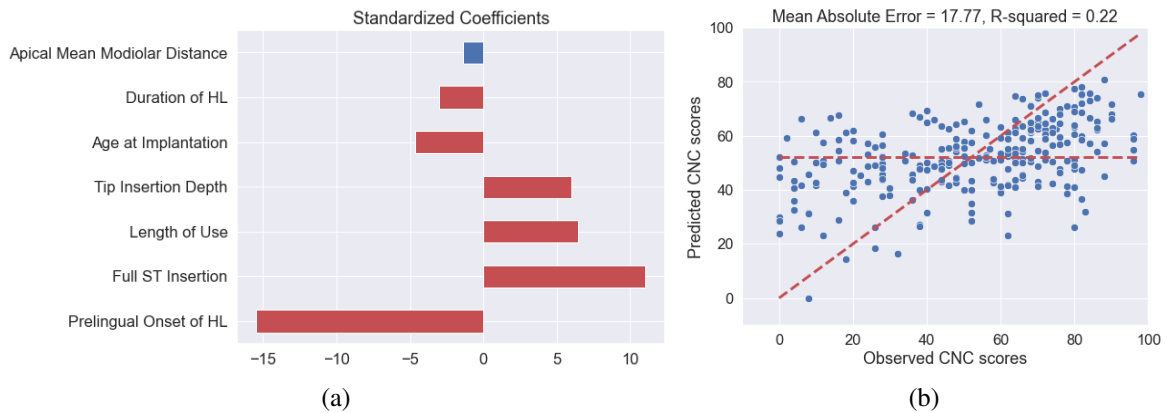


Figure 4.7: Multiple Linear Regression Model

## 4.4 Discussion

### 4.4.1 Effects of Demographics

Patients with postlingual onset of hearing loss as a group perform better than patients with prelingual onset of hearing loss in our dataset, which supports the existing conclusions in the literature [8–14]. This feature has the single greatest impact on outcomes. The other relevant demographics features – duration of HL, age at implantation, and length of use – were all significantly linearly correlated with the outcome. A closer look at Figure 4.1a shows that the association of duration of HL with CNC scores is piecewise linear. That is, up to approximately 35 years of hearing loss, the effects are scattered but the group average outcome is good and there is no significant decrease with age (mean =  $56.6 \pm 22.8\%$ ;  $r = 0.07$ ,  $p = 0.3$ ). An implantation age beyond 35 or more years of hearing loss, however, has much lower chance of producing good outcomes (mean =  $40.6 \pm 27.5\%$ ) and outcomes worsen with age ( $r = -0.26$ ,  $p \leq 0.05$ ), possibly due to gradual degeneration of spiral ganglia nerves. Similarly, in Figure 4.1b, up to approximately 1.5 years of use, the results are scattered and there are both very good and very bad outcomes which increases with experience (mean =  $48.2 \pm 25.8\%$ ;  $r = 0.22$ ,  $p \leq 0.05$ ). Beyond that level of experience, the outcomes still linearly improve with increasing length of use but have a greater group average and lower variance about the mean (mean =  $56.6 \pm 23.7\%$ ;  $r = 0.19$ ,  $p \leq 0.05$ ).

The association of the age at implantation to the outcomes is generally negative. After about 66 years of age, for example, implantation produces significantly lower ( $p \leq 0.05$ ) outcomes (mean =  $48.9 \pm 23.7\%$ ) which worsens with age ( $r = -0.26$ ,  $p \leq 0.05$ ) than implantation prior to that age (mean =  $55.0 \pm 26.2\%$ ;  $r=0.02$ ,  $p = 0.85$ ). It should also be noted that the duration of hearing loss and age at implantation are significantly associated with an  $r$  value of 0.13 ( $p \leq 0.05$ ), and the underlying reason for poorer outcomes at older ages is possibly the same – nervous degeneration.

#### 4.4.2 Effect of Position

Full ST insertion significantly improves group outcome in our dataset (Figure 4.3c), which correspond to other well-established findings in literature [8, 18–22]. It is possible that the trauma that occurs when the array punctures the basilar membrane significantly reduces the benefits from an otherwise good positioning. Another contributing factor could be that electrodes in the SV are more distant from the spiral ganglion than those in ST, especially in the more apical regions, and this causes inefficient stimulation and worse effects of channel overlap once the array translocates into the SV.

Among the continuous features, tip insertion depth is most strongly correlated to the outcomes and has the greatest unit effect on the outcomes (Figure 4.7a). Base insertion depth was not significantly correlated to the outcomes. While the two insertion depths are strongly correlated and describe similar features, base insertion depth cannot sufficiently describe how deeply the whole array was inserted due to the presence of variable slack, and tip insertion depth can better describe the position of the array relative to the spiral ganglia, especially in the apical parts. The size of the cochlea, measured by the cochlear duct length, did not significantly affect outcomes either.

Mean modiolar distance was also found to be associated with outcomes (Figure 4.2b), although this is a more significant effect in the deeper, apical parts of the cochlea (Figure 4.4). This reinforces the idea that good placement in the deeper parts of the cochlea is the discriminative factor between good and bad outcomes.

The two apical position descriptors, tip insertion depth and apical mean modiolar distance, are also significantly correlated with each other, which makes interpretation of their individual effects harder. From Figures 4.5 and 4.6, it seems that both a good tip insertion depth and a good mean modiolar distance (Q4) are necessary for good outcomes. The marginal groups where we only had one good factor (Q1 and Q3) produced statistically similar group means that were significantly lower than with both the features well positioned. The group with bad positioning with respect to both factors (Q2) had a lower group mean

than all the others. However, the good and bad classes are unbalanced, and the arbitrary definition of "good" and "bad" ranges of the features definitely affects the interpretation. At the same time, the standardized coefficient of apical mean modiolar distance is not significant in Figure 4.7a, which would indicate that after controlling for tip insertion depth and full ST insertion, modiolar distance is not a significant factor for the outcome. Ultimately, a larger sample size is required to conclude whether modiolar proximity is independently significant for the outcomes.

The surgical implication of these findings is that techniques that result in a deeper insertion with low modiolar distance at the tip, without causing the trauma of rupturing the basilar membrane, should be prioritized as they are necessary factors for good outcomes. However, it should be noted that due to the retrospective nature of this study, it is possible that many insertions were concluded at shallower depths because the surgeon encountered resistance, which means that trauma had already occurred. Therefore, the perceived effect of shallower insertions being associated with poorer outcomes might be driven by intra-cochlear trauma worsening hearing outcomes.

#### **4.4.3 Simulation**

Let us consider a demographic of CI candidates with statistically good demographic features – implanted at age 30 after 20 years of postlingual hearing loss, and a 5 year experience with the CI before being tested. Assuming an apical mean modiolar distance of 0.3 mm, which is the average for the whole population, the predicted change in average CNC outcomes with different tip insertion depths according to our linear regression model is demonstrated in Figure 4.8a both with and without full ST insertion. Similarly, assuming a population average tip insertion depth of 377 degrees, the predicted change of average outcomes with the different apical mean modiolar distance is shown in Figure 4.8b. This serves to illustrate the statistical effects of the positional features over the population; this linear model does not have the accuracy to produce patient-specific predictions.

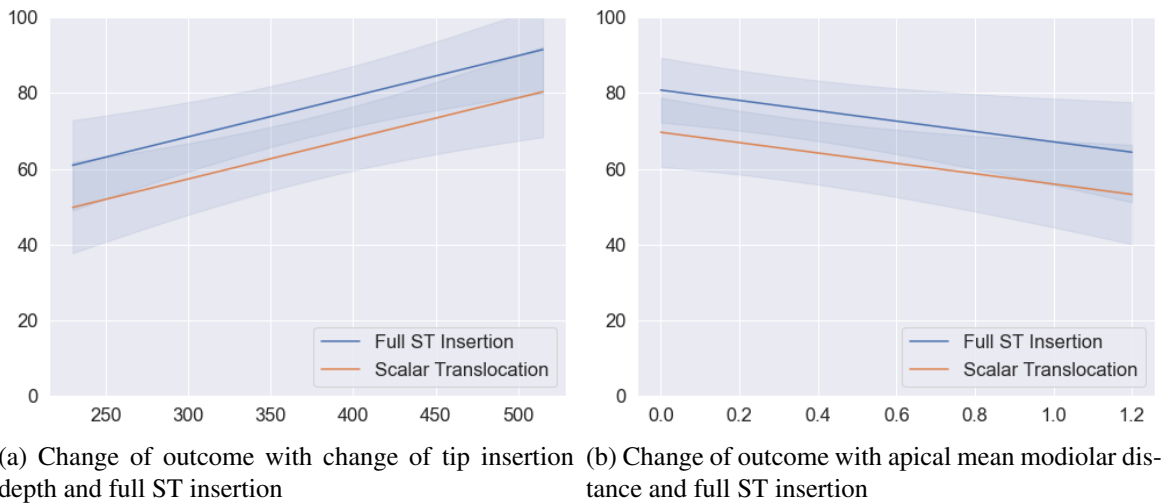


Figure 4.8: Variation of mean predicted outcome with the change of the important position factors

#### 4.5 Conclusions

In this work, using an expanded dataset of 274 precurved arrays, we analyzed different positional variables to identify the necessary configuration for good hearing outcomes. After controlling for the significant demographic variables, like duration of hearing loss, age of implantation and length of use, we found that full ST insertion and tip insertion depth are significant features influencing the outcome. Apical mean modiolar distance was significantly correlated with the outcomes, but results indicate that it does not have a significant effect on outcomes after controlling for other factors. A larger dataset is required to establish if it indeed has a significant independent effect on outcomes. Overall, our results indicate that deeper insertion depth and closer apical positioning to the modiulus without scalar translocation are necessary if we want to produce good outcomes.

Current limitations of the study generally relate to sparsity of the reported medical data. For example, there is evidence that hearing preservation in the implanted ear affects hearing outcomes [94], which we could not model due to data constraints. Both in literature [9, 68–71] and in a subset of our data, we found indication that etiology is also a potent

demographic factor – if the underlying cause of hearing loss does not typically cause neural degeneration, the CI outcomes are likely to be better. Similarly, there are reports of the correlation between cognitive test scores and CI outcomes [65–67]. Controlling for all of these known confounds can help identify the effects of positioning factors more accurately, and a comprehensive understanding of these positional associations can greatly help guide patient counseling and surgical techniques. In our future work, we aim to improve data collection and aggregate these additional key demographics features into our dataset and appropriate predictive models.

#### **4.6 Acknowledgments**

This work was supported in part by grants R01DC014462, R01DC008408, and R01DC014037, from the National Institute for Deafness and Communication Disorders and by grant UL1TR000445 from the National Center for Advancing Translational Sciences. The content is solely the responsibility of the authors and does not necessarily represent the official views of these institutes.

## Chapter 5

### IDENTIFYING EFFECTS OF SURGICAL TARGETING IN LASER INTERSTITIAL THERMAL THERAPY FOR MESIAL TEMPORAL LOBE EPILEPSY

This chapter includes materials published in the following publications and has been reproduced with the permission of the publishers and all co-authors:

Wu, C.<sup>†</sup>, Jermakowicz, W. J.<sup>†</sup>, **Chakravorti, S.**<sup>†</sup>, Cajigas, I., Sharan, A. D., Jagid, J. R.,..., D’Haese, P.-F. (2019). *Effects of surgical targeting in laser interstitial thermal therapy for mesial temporal lobe epilepsy : A multicenter study of 234 patients*. *Epilepsia*, 60(6), 1171–1183. <https://doi.org/10.1111/epi.15565>

(<sup>†</sup> co-first authors)

and

**Chakravorti, S.**, Jermakowicz, W. J., Wu, C., Li, R., Wirz Gonzalez, R., Dawant, B. M., & D’Haese, P.-F. (2019). *Evaluation of nonrigid registration around the hippocampus for the construction of statistical maps in a multicenter dataset of epilepsy laser ablation patients*. In Proc. of SPIE Vol. 10951. <https://doi.org/10.1117/12.2512587>

## 5.1 Introduction

Mesial temporal epilepsy (mTLE) affects the majority of surgical drug-resistant epilepsy (DRE) candidates[95]. Although more efficacious than medical therapy alone for DRE, epilepsy surgery remains highly underutilized, in part due to concerns of the morbidity associated with traditional craniotomies[96]. Although anterior temporal lobectomy (ATL) remains the “gold standard” for the treatment of drug-resistant mTLE, newer therapies such as laser interstitial thermal therapy (LITT) have emerged. As a minimally invasive procedure with shorter hospitalizations and lower morbidity, including less impairment to cognitive function, LITT has the potential to gain wider acceptance [33, 36, 38, 97, 98]. To date, single-institution series of LITT have demonstrated 38%-78% seizure freedom with at least 1 year of follow-up, with upward of 60%-89% seizure freedom in patients with radiographic evidence of hippocampal sclerosis (rHS) [32, 33, 36, 38, 39, 97, 99–101].

Although no studies have identified any significant correlation between ablation volumes and seizure outcomes [36, 38, 39], laser catheter placement is thought to play a role [38–40]. As such, we must consider potential differences in surgical technique. Unfortunately, no study has specifically studied the optimal region of ablation for LITT in mTLE. Given the novelty of LITT, no protocol for targeting exists and no single center has the experience to define optimal laser catheter placement. The only study to specifically address this issue revealed that greater mesial hippocampal head ablation correlates with improved seizure outcome [38]. Ultimately, the lack of robust methods capable of incorporating the inherent variability of patient anatomy and the variability of the ablated volumes with clinical outcomes have hindered three-dimensional quantitative analysis of surgical targeting and its impact on the likelihood of seizure freedom. As such, specific three-dimensional characteristics of an optimal LITT ablation for mTLE remain unknown. We therefore aimed to investigate both patient and surgical factors associated with seizure outcome from LITT for mTLE in a large multicenter cohort in order to better understand patient selection, surgical technique, and overall outcome for this procedure.

## **5.2 Methods**

### **5.2.1 Study design**

This multicenter, retrospective cohort study included 234 patients who underwent amygdalohippocampal complex (AHC) LITT for treatment of mTLE across 11 centers in the United States between December 2011 and August 2017. Each participating institution obtained their own institutional review board (IRB) approval for collecting the data and sharing deidentified versions of this data. Given the retrospective nature and the use of only deidentified data for this study, no patient consents were required.

Aggregation, deidentification, normalization, and comparison of data were accomplished with the CranialCloud platform (Neurotargeting LLC) and algorithms developed at Vanderbilt University [102, 103]. The CranialCloud architecture addresses issues of patient privacy by allowing sharing of encrypted and deidentified data between institutions, while retaining potential patient identifiers within each institution, according to respective IRB policies.

### **5.2.2 Participants**

Patients who underwent LITT for mTLE with at least 1-year follow-up were included in this study. A total of 274 patients had undergone local multidisciplinary evaluation for DRE, at which time each institution's epilepsy program had agreed on the diagnosis of mTLE and determined the appropriateness of AHC LITT. The operative procedure has been described previously and involves stereotactic placement of a laser fiber and magnetic resonance imaging (MRI) thermometry for real-time feedback of the ablation [33, 38, 40]. Given the retrospective nature of this study, each institution performed the procedure according to its own practices, with no effort to standardize across institutions. At least 1 year of clinical follow-up was available for 234 patients. To critically assess ablation location, patients were required to have a preoperative volumetric 1-mm<sup>3</sup> voxel-size T1-

weighted MRI of the brain; as well as postoperative volumetric 1-mm<sup>3</sup> voxel-size T1-weighted gadolinium-enhanced MRI of the brain, in which the ablation cavity could be clearly identified. A total of 175 MRI pairs were analyzed after excluding patients with insufficient imaging (Figure 5.1).

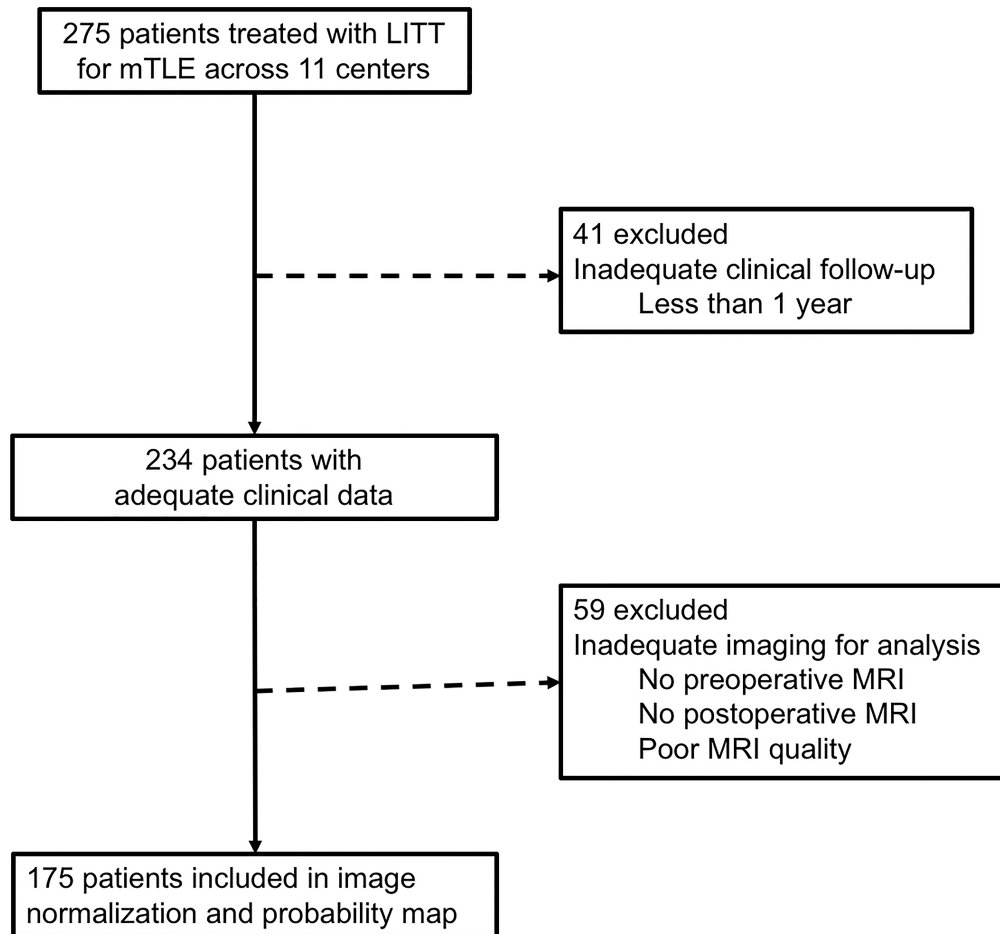


Figure 5.1: Flowchart of subject selection for analysis of clinical outcomes and calculation of the Engel I outcomes probability map in normalized atlas space

### 5.2.3 Data collection

For 234 subjects, clinical data were obtained retrospectively from each participating institution. Demographic data consisted of sex and handedness. Clinical variables consisted of laterality of mTLE, presence of rHS on MRI, presence of a lesion aside from

rHS on MRI (dual pathology), concordant positron emission tomography (PET) temporal hypometabolism, seizure type (focal aware seizures (FAS), focal impaired awareness seizures (FIAS), focal to bilateral tonic-clonic (FTC) seizures), concordance of video-electroencephalography (EEG), and use of intracranial EEG (iEEG) monitoring prior to LITT. Radiographic interpretations regarding the presence of rHS or dual pathology were initially performed by a neuroradiologist and confirmed by a consensus decision at each institution's multidisciplinary surgical epilepsy conference. Similarly, to define the region of seizure onset, the interpretation of long-term video-EEG was agreed upon during this same conference. Clinical outcomes consisted of seizure outcomes (Engel score) at 6-month intervals until the most recent follow-up, the presence of intracranial hemorrhage on postoperative imaging, and reported postoperative complications. The retrospective nature of this study and the variability in neuropsychological panels performed at each institution prevented collection of standardized quantitative cognitive and mood assessments across the cohort.

#### **5.2.4 Ablation cavity quantification**

All ablation cavities were manually traced by an investigator blinded to seizure outcomes. By convention, the ring of gadolinium enhancement was included within the segmented ablation volume, as this enhancement represents blood-brain barrier breakdown. Because this postoperative sequence is acquired immediately after completion of ablation, there is no time-dependent variability in the radiographic appearance of the ablation between patients [40].

#### **5.2.5 Image Normalization and Segmentation**

To compare the specific location of the ablation across patients, specifically relative to the hippocampus and amygdala, we considered a subset of 106 patients from 8 institutions with high-resolution contrasted preoperative T1 images. Of them, 71 were rHS and 35

were non-rHS subjects. The reference for image normalization was a 3T T1w image (1 mm isotropic) of a healthy non-rHS volunteer at Vanderbilt University Medical Center. We described and validated this method in [103]. We briefly explain the steps in this section.

A neurosurgeon (WJ) blinded to seizure outcomes manually traced the hippocampi in all 106 images according to European Alzheimers Disease Consortiums (EADC) HarP guidelines [104, 105]. After an initial affine alignment of the images [55, 56], adaptive bases algorithm (ABA) was used for intensity-based non-rigid image registration [106]. ABA was chosen as a representative method because previous studies have established that it provides accurate non-rigid registration for regions of the brain that have low T1-contrast [107, 108]. To evaluate the correspondence quality, the patient hippocampi were compared to the hippocampi of the atlas in atlas space. The error at a certain node of the atlas hippocampus surface ( $H_0$ ) is defined as the distance between that node and the closest point on each patient hippocampus surface ( $H_1$ ) after it has been transformed to atlas space. The average node error (ANE) at a node consists of all such errors averaged over the subjects, and is used to assess the local quality of registration. This overall error is a combination of the errors associated with the manual tracings as well as the registration error.

The local correspondence errors after segmentation and registration are displayed by coloring the right hippocampus in the atlas with the absolute ANE at every node (Figure 5.2). Only the right side is demonstrated here since the left hippocampus shares a similar node error distribution. The green regions of the hippocampus are the areas where the absolute ANE is low (within 1 mm) while the red regions denote larger deviations of the surface from the atlas hippocampus (see colorbar on the right). A lower surface error implies that the registration method has achieved good local agreement between the patient and atlas images. It is apparent that the majority of the body of the hippocampus corresponds well to the atlas hippocampus after registration, while small regions at the anterior and posterior extremities of the head and the tail suffer from higher surface errors. In fact, 90% of

the mean errors for non-rHS patients are less than 2.02 mm, and within 2.15 mm for rHS patients (table 5.1).

A potential concern of using a non-rHS atlas image for rHS patients was that the registration might not be accurate around the hippocampal region due to differences in expected volume. While on the right side, the average node errors are significantly higher ( $p < 0.05$ ) for rHS patients than for non-rHS patients (figure 5.2), the difference is not significant for the left hippocampus. For both sides, the group means and medians are within an acceptable range (table 5.1) and we qualitatively verified that the registration was as close and accurate for all the rHS images as in the non-rHS images around the hippocampal body (figure 5.2).

EADC's HarP guidelines lead to good reproducibility on comparable high quality images. However, there is a considerable variance in the image quality in our dataset, leaving a possibility of segmentation errors compounding the registration error. We therefore carried out a qualitative blind review of the segmentations between two raters (CW and WJ) to analyze which regions were contributing the most to segmentation error. Both raters noted that even when the overall tracing is acceptable, the most common regions of disagreement were the head and tail boundaries which were difficult to make out. This indicates that the high error regions in figure 5.2 are largely caused by segmentation difficulties, which most commonly occurs due to low quality images in the dataset where the anatomy is not clearly visible.

We can thus conclude that our scheme of normalizing all patient images to the atlas is highly accurate around the hippocampus due to the  $< 1$  mm surface error, and can be reliably used for registering the postoperative images to the atlas. It is difficult to conclude anything regarding the registration accuracy at the boundaries of the head and the tail due to the segmentation errors. Due to the smoothness constraints of ABA during registration and low contrast near the hippocampus, we can reasonably assume that the overall registration error is of the same order as the high confidence regions, and the spikes in the Average

Surface Error (ASE) (figure 5.2) were due to segmentation problems near the extremities. We acknowledge the approximate error of registration at 1.34 mm ( $\sim 1$  voxel) and we are cautious about any population based inferences made around these anatomic locations at this scale. We also use this registration method to carry out an automatic atlas based segmentation of the hippocampus and amygdala on the other 69 pre-operative images in our dataset.

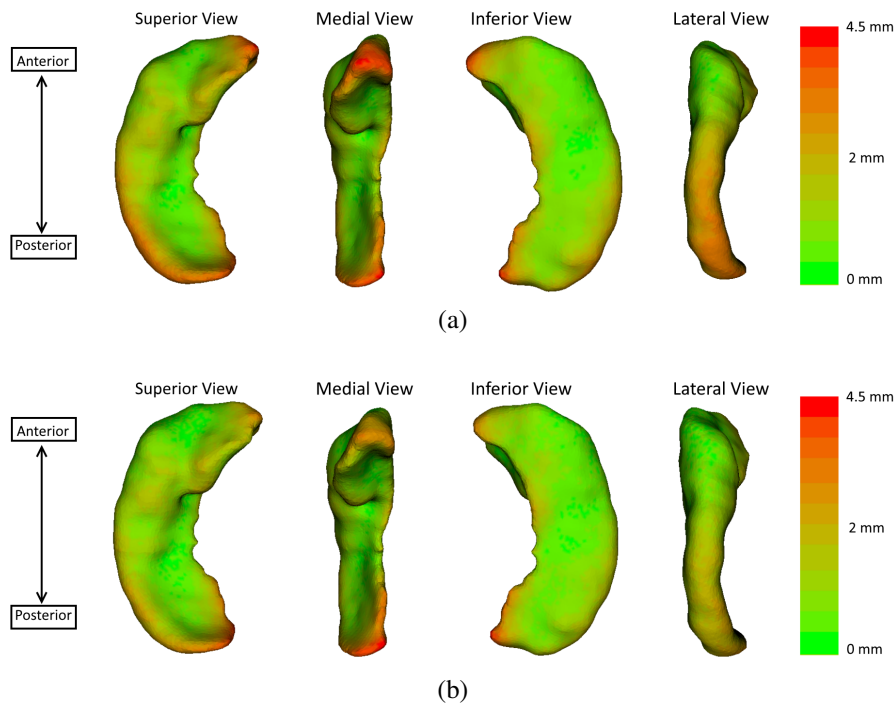


Figure 5.2: Accuracy of nonrigid registration at predicting hippocampal borders from pre-operative MRI. Absolute values of average node errors (ANE) demonstrated here for predicting the right hippocampus in patients (a) with rHS and (b) without rHS shown from superior, medial, inferior and lateral views.

### 5.2.6 Volume of ablation

The extent to which the amygdala and hippocampus were ablated was calculated for each subject in common atlas space. Once normalized, the manually segmented ablation cavity was superimposed over anatomical structures, which allowed for the calculation of

Table 5.1: Mean, median and 90th percentile of the average node errors, separated for rHS and non-rHS patients.

Patient rHS diagnosis	Side	Mean $\pm$ std (mm)	Median (mm)	90th percentile (mm)
rHS	Left	$1.34 \pm 0.54$	1.22	2.07
	Right	$1.33 \pm 0.74$	1.15	2.15
Non-rHS	Left	$1.27 \pm 0.65$	1.11	2.02
	Right	$1.05 \pm 0.67$	0.91	1.94

the percentage of amygdala and hippocampus ablated (Figure 5.3).

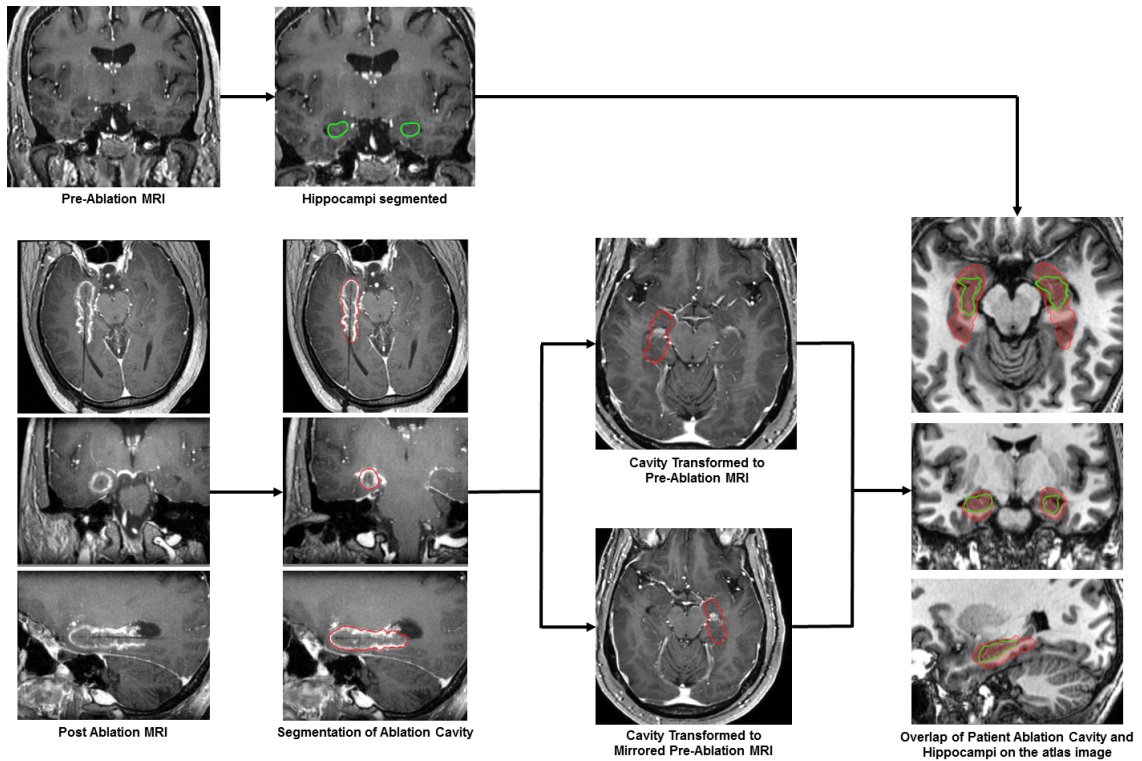


Figure 5.3: Work flow for image-processing. For each patient, the ablation cavity was manually segmented according to previously described methods [40]. Preoperative and postoperative images along with the manually segmented ablation cavity were normalized to a common reference space [103]. Once completed for the entire cohort, a critical population-based analysis of ablation volumes and locations could be performed

### **5.2.7 Statistical analysis of clinical variables**

Two binary indicator variables were derived to identify whether a patient had (a) an Engel I outcome or (b) either Engel I or II outcomes at 6, 12, 18, 24 months, and at last follow-up. Univariate logistic regression was performed using the aforementioned demographic variables, clinical variables, and complications as independent variables. Missing data were removed prior to performing the regressions. Odds ratios (ORs) were used to estimate the effect of candidate independent variables on either freedom from disabling seizures or being almost seizure-free ( $p < 0.05$ ). Multivariate logistic regression was subsequently performed.

### **5.2.8 Statistical analysis of ablation location**

Each ablation cavity was duplicated and mirrored to the contralateral side such that regardless of the side of ablation, each patient would contribute to ablation locations over an AHC in atlas space (Figure 5.3). The reliability of the mirrored image is possible only through the utilization of our validated nonlinear image normalization algorithm. An aggregate ablation map was first generated corresponding to the frequency that each voxel was ablated across the entire cohort.

To analyze the role of the ablation location in seizure outcome, a positive predictive value (PPV) map (association between Engel I outcomes and the ablation of a voxel) and a negative predictive value (NPV) map (association between Engel class II-IV outcomes and not ablating a voxel) were calculated. The details of this statistical analysis are delineated in Appendix S1 in 5.7; but in short, Bayesian models were generated for each ablated voxel to quantify the probability of Engel I outcome at last follow-up. Each voxel was treated independently because generation of models with dependencies on either patient or outcome groups would not only be exceedingly complex to generate, but also difficult to clearly interpret.

Finally, to translate these findings, a theoretical favorable ablation zone with the dimensions of a typical ablation cavity was generated. Because the highest NPVs represent voxels associated with the most significant chance of persistent seizures if not ablated, all values greater than 50% were included in this theoretical zone. This zone was then translated anteriorly and medially as to maximize inclusion of the highest PPVs. Although multiple theoretical unfavorable ablation zones may exist, such a zone was generated by excluding all NPVs less than 80% and minimizing inclusion of the highest PPVs.

Table 5.2: Patient demographics and characteristics relative to seizure outcomes

	Entire cohort		Association with Engel I outcome				Association with Engel I or II outcome			
	n = 234		P value				P value			
	$\mu \pm \sigma$	Range	6 mo	12 mo	18 mo	24 mo	6 mo	12 mo	18 mo	24 mo
Age (y)	42 ± 15	(7-82)	<b>0.005</b>	0.213	0.477	0.652	<b>0.020</b>	<b>0.001</b>	0.053	0.093
Follow-up (mo)	30 ± 14	(12-75)								
	n	%								
Gender										
Female	124	53.0	0.984	0.636	0.185	0.534	0.340	0.210	0.729	0.643
Handedness <sup>a</sup>										
Right	161	83.4								
Left	29	15.0	0.533	0.218	0.324	0.438	0.611	0.656	0.929	0.679
Ambidextrous	3	1.6								
Side of LITT										
Left	136	58.1	0.604	0.732	0.719	0.953	0.804	0.691	0.690	0.440
rHS on MRI										
Yes	172	73.5	<b>0.048</b>	0.289	0.225	0.613	0.232	0.587	0.751	0.969
Dual pathology on MRI <sup>a</sup>										
Yes	49	21.1	0.504	0.454	<b>0.043</b>	0.171	0.322	0.933	0.206	0.537
PET <sup>a</sup>										
Ipsilateral	139	73.5	0.749	0.423	0.140	0.262	0.879	0.670	0.660	0.924
Negative	29	15.3								
Bilateral	16	8.5								
Contralateral	3	1.6								
Seizure type <sup>b</sup>										
FIAS	223	95.3	0.311	0.392	0.506	0.158	0.800	0.701	0.369	1.000
FTC	107	45.7	0.841	0.506	0.490	0.106	<b>0.016</b>	<b>0.007</b>	0.109	<b>0.030</b>
FAS	38	16.2	0.684	0.708	0.327	0.870	0.206	0.074	0.078	0.346
EEG localization <sup>a</sup>										
Ipsilateral	180	83.7	0.427	0.175	0.302	0.069	0.630	0.379	0.551	0.618
Bitemporal	20	9.3								
Multifocal	5	2.3								
Nonlocalized	6	2.8								
Ipsilateral extratemporal	3	1.4								
Contralateral temporal	1	0.5								
Invasive monitoring										
Yes	48	20.5	0.978	0.959	0.475	0.942	0.749	0.696	0.564	0.950

Reported are P values for the univariate analysis between each variable and seizure outcome. Significant values ( $p < 0.05$ ) are denoted by bold font. Abbreviations: EEG, electroencephalography; FAS, focal aware seizures; FIAS, focal impaired awareness seizures; FTC, focal to bilateral tonic-clonic seizures; LITT, laser interstitial thermal therapy; PET, positron-emission tomography; rHS, radiographic hippocampal sclerosis.

<sup>a</sup>Variables with missing data. The numbers and percentages reported reflect the number of patients missing data.

<sup>b</sup>Because patients may have more than one seizure type, each patient could belong to multiple seizure type categories. For this reason, the total percentage of patients for this variable is greater than 100%.

## 5.3 Results

### 5.3.1 Seizure outcomes

At 1 year postoperatively, 134 of 231 patients (58.0%) achieved Engel class I outcomes, and 178 patients (77.1%) achieved either Engel I or II outcomes. At 18 months, 82 of 161 patients (50.9%) achieved Engel I outcomes, and 118 patients (73.3%) achieved either Engel I or II outcomes. At 2 years, 96 of 167 patients (57.5%) achieved Engel I outcomes, and 134 patients (80.2%) achieved either Engel I or II outcomes. At last follow-up of at least 1 year ( $30 \pm 14$  months, 12-75 months), 134 of 234 patients (58.0%) achieved Engel I outcomes, and 180 patients (76.9%) achieved either Engel I or II outcomes.

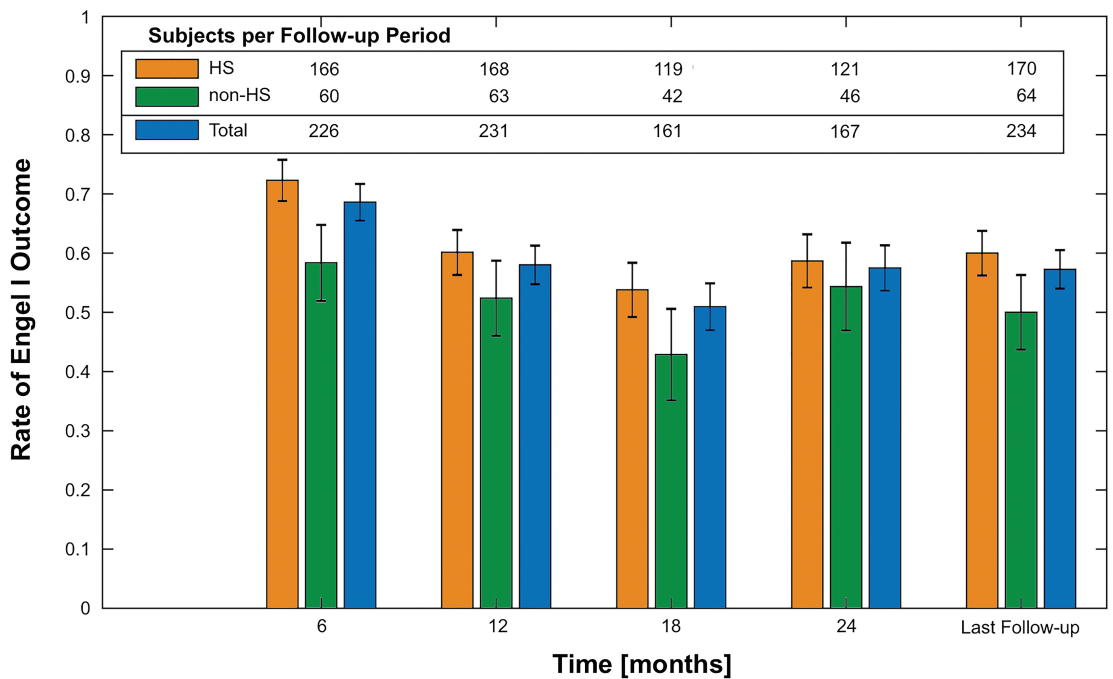


Figure 5.4: Rates of Engel I outcome at 6-month epochs for the entire cohort, the radio-graphic hippocampal sclerosis (rHS) subgroup, and the non-rHS subgroup. Error bars represent the standard error. Univariate regression demonstrated no significant difference in the 95% confidence intervals between the rHS and non-rHS subgroups. Seizure outcomes were durable between 12 months after laser interstitial thermal therapy and at last follow-up

Given the retrospective nature of this study, seizure outcomes were not available at all

time intervals for all patients. In combination with limited follow-up in some patients, this limitation resulted in different cohort sizes at each time point. Statistical analyses of demographic information and clinical details relative to seizure outcomes are summarized in Table 5.2.

There were no significant differences in seizure outcomes between the rHS and non-rHS subgroups after 6 months of follow-up (Figure 5.4). Even after excluding patients with dual pathology from this rHS subgroup, no significant difference was seen at any time point ( $p \geq 0.078$ ). Implementation of iEEG was not associated with seizure outcome ( $p \geq 0.475$ ), but since iEEG monitoring in patients without rHS may confirm isolated mesial onset and the use of iEEG was disproportionately high in the non-rHS group ( $n = 33$ ,  $p \leq 0.001$ ), further analysis was performed by combining non-rHS patients who underwent iEEG with the rHS subgroup. This cohort of rHS patients plus non-rHS patients with iEEG confirmation of mesial onset did not experience greater rates of Engel I outcomes either ( $p \geq 0.239$ ).

Patients with a history of FTC were less likely to demonstrate Engel I outcomes at last follow-up (odds ratio [OR] = 0.52, 95% confidence interval [CI] = 0.27-0.98,  $p \leq 0.042$ ) and either Engel I or II outcomes at 6 months, 12 months, and last followup (OR = 0.31-0.38, 95% CI = 0.14-0.83,  $p \leq 0.014$ ).

Age was not associated with long-term Engel I or II outcomes. At no time point was sex, handedness, side of ablation, side of mTLE, dual pathology, ablation of the dominant hemisphere, concordant PET hypometabolism, or concordance of video-EEG significantly associated with seizure outcomes.

### **5.3.2 Complications**

Postoperative hemorrhage was identified in three patients (1.3%), of which one was associated with clinical symptoms (transient double vision). A total of 42 complications were recorded for 35 patients (15.0%), of which 8 were transient neurologic deficits and 34 were

persistent at last follow-up. Visual disturbances were most common (5.1%), followed by worsening of a preexisting affective disorder (4.3%). Given the retrospective nature of the study, details regarding the severity of symptoms were not consistently available. Similarly, language and memory deficits could not be quantified and are likely underestimated. The one death in this cohort was attributed to sudden unexplained death in epilepsy (SUDEP) occurring 12 months postoperatively. Recorded complications are detailed in Table 5.3. The presence of a postoperative complication was associated with a lower chance of Engel I outcomes at 24 months and at last follow-up (OR = 0.18-0.26, 95% CI = 0.04-0.86,  $p \leq 0.026$ ).

Table 5.3: Reported complications based on retrospective chart review

	<b>Transient</b>	<b>Persistent at Last Follow-up</b>
	<b>n (%)</b>	<b>n (%)</b>
<b>Worsening baseline affective disorder</b>	0 (0.00%)	10 (-4.27%)
<b>Visual Field Deficit</b>	2 (-0.85%)	9 (-3.85%)
<b>Language or Memory Deficit</b>	1 (-0.43%)	6 (-2.56%)
<b>New onset affective disorder</b>	1 (-0.43%)	4 (-1.71%)
<b>Double Vision</b>	2 (-0.85%)	3 (-1.28%)
<b>Chronic Headache</b>	0 (0.00%)	1 (-0.43%)
<b>Sensory loss</b>	1 (-0.43%)	1 (-0.43%)
<b>Motor deficit</b>	1 (-0.43%)	0 (0.00%)

Affective disorders and visual symptoms were the most common complications. Unfortunately, given the retrospective nature of the study, details regarding the severity of symptoms were not consistently available. Similarly, language and memory deficits could not be quantified and are likely underestimated. The one death occurred approximately 1-year after surgery and was attributed to SUDEP.

### 5.3.3 Volume of ablation for mesial structures

Multivariate regression analysis demonstrated that more extensive amygdalar ablation was associated with Engel I outcomes at 6, 12, and 18 months, and at last followup (OR = 1.60-1.77 per additional percent ablated,  $p \leq 0.040$ ); and increasing hippocampal ablation was associated with a decreased chance of Engel I outcomes at 6, 18, and 24 months (OR

= 0.04 per additional percent ablated,  $p \leq 0.040$ ).

### 5.3.4 Ablation location

The aggregate ablation map for 175 patients illustrates that all ablations were centered around the long axis of the AHC (Figure 5.5). The overall diameter of the ellipsoid representing all possible ablated voxels measures approximately 30 mm in the coronal plane. Because the ablation is roughly centered around the laser catheter and has an average diameter of 15 mm, we can estimate a maximal difference in implanted probe position of approximately 15 mm. This finding highlights the degree of variability that currently exists in AHC targeting for LITT.

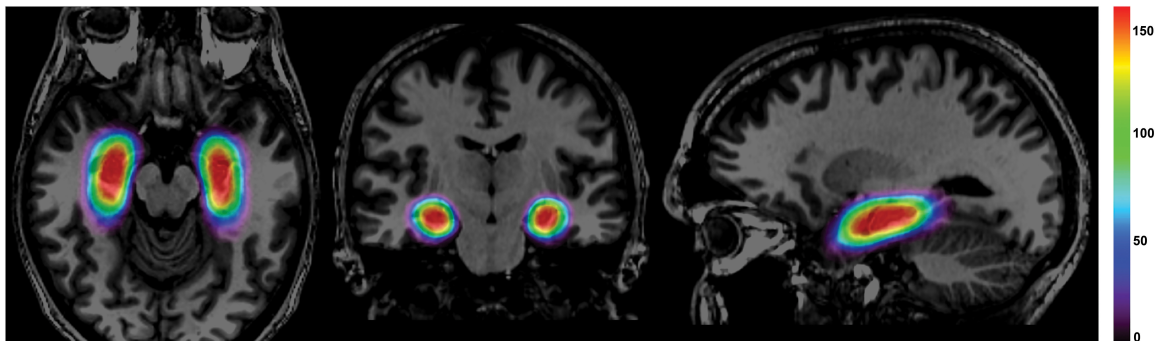


Figure 5.5: Heat map of the distribution of ablations in 175 patients treated across 11 comprehensive epilepsy centers. Effectively all ablations (red) were centered around the long axis of the AHC and extended posteriorly to the level of the lateral mesencephalic sulcus. Variation in ablation location is represented by the less frequently ablated regions (green and blue) extending from this central core

The PPV and NPV maps for Engel I outcomes associated with each voxel are shown in Figure 5.6. The theoretical favorable and unfavorable ablations are delineated in Figure 5.7. Ablation of more mesial, anterior, and inferior structures of the temporal lobe—including the amygdala, hippocampal head, parahippocampal gyrus, entorhinal cortex, and perirhinal cortex—were associated with higher rates of Engel I outcomes. Excluding these structures from the ablation and focusing only around the hippocampal body and tail was associated with persistent seizures. Ablations extending posteriorly beyond the coronal plane in line

with the lateral mesencephalic sulcus were less likely to be associated with Engel I outcomes, and avoiding these posterior voxels was not associated with high rates of persistent seizures.

## **5.4 Discussion**

To date, small single-institution series have suggested that AHC LITT is a viable treatment for drug-resistant mTLE [32, 33, 36, 38, 39, 97, 99–101]. Unfortunately, without consideration of specific therapy location, which is subject to variability in patient anatomy and the surgery itself, these studies are limited in their ability to reliably report clinical outcomes. In this study, we have: (a) proposed a novel robust methodology using nonlinear normalization and statistical models to study complex brain therapies such as LITT for mTLE; (b) applied it to previously existing data in the largest and most comprehensive multicenter study to date; (c) demonstrated in 234 patients with at least 1-year follow-up that 58.0% achieved Engel I outcomes and 76.9% achieved either Engel I or II outcomes at the time of last follow-up; and (d) presented the first three-dimensional model of a favorable laser ablation zone.

### **5.4.1 Patient factors**

The presence of rHS on MRI has been associated with favorable surgical outcomes [97, 99, 101, 109]. Our findings, however, agree with recent studies, which have suggested that LITT is effective in properly selected patients with mTLE, regardless of isolated rHS [32, 110]. In truth, the presence of rHS should not be viewed as a singular epilepsy phenotype, but rather an attribute of distinct mTLE subtypes [111]. As such, the importance of a thorough preoperative assessment leveraging multiple modalities used to localize seizure onset emphasizes the need for LITT candidates to be evaluated at an experienced comprehensive epilepsy center.

In line with prior analyses of epilepsy surgery [112], FTC seizures were negatively

associated with seizure outcome. Particular caution should therefore be exercised when performing AHC LITT in patients with a history of FTC seizures, as they were 62% less likely to become almost seizure-free. This finding can be explained by the fact that patients with FTC are more likely to have lateral neocortical rather than mesial onset [113].

A shorter duration of epilepsy at the time of surgical intervention has also been described as a positive prognostic indicator [114, 115]. Unfortunately, given the retrospective nature of this study, such data were not reliably available from all participating centers and were therefore not included in our analysis.

#### **5.4.2 Surgical factors**

An appropriate surgical approach is critical to optimizing clinical outcomes in properly selected patients. The extent of surgical resection has remained controversial. Studies have emphasized the need for sufficient hippocampal resection to maximize chances of seizure freedom [116, 117]. At the same time, selective amygdalohippocampectomy has been shown to provide outcomes comparable to those of standard anterior temporal lobectomy [118, 119]; and the extent of hippocampal resection has been found to have no bearing on seizure freedom [119–121]. Prior studies of LITT for mTLE have demonstrated no relationship between the ablation volumes and seizure outcomes [36, 38, 39].

When considering these recommendations, one must acknowledge the considerable complexity of accurately measuring surgical resections. After a craniotomy, tissue manipulation, removal of brain tissue, loss of cerebrospinal fluid, gravity, and use of osmotic therapy distort patient anatomy on postoperative imaging [122]. As such, measurements on postoperative images remain challenging for procedures like a temporal lobectomy. The minimally invasive nature of LITT, however, results in minimal anatomic distortion and affords more accurate quantification of the intervention.

Multivariate regression analysis revealed that more extensive amygdalar ablation was associated with greater chances of Engel I outcomes at almost every time point. Although

more extensive hippocampal ablation was negatively associated with Engel I outcomes at almost every time point, this association was modest (OR = 0.04 per additional percent ablation) relative to those seen with volumes of amygdala ablated (OR = 1.60-1.77 per additional percent ablated). This finding may suggest that beyond some threshold volume of hippocampal ablation, further ablation may be counterproductive. To ablate greater volumes of the hippocampus, the laser trajectory would also have to involve the hippocampal body and tail posteriorly, thereby compromising ablation of the hippocampal head and amygdala. Further analysis is required to fully investigate this possibility.

Our investigation was therefore extended beyond ablation volumes with the goal of better understanding optimal targeting for LITT in mTLE. The requirement of cannulating the curved AHC with a straight laser catheter forces a compromise on ablation coverage. With a single laser trajectory, one must decide whether the amygdala and hippocampal head, entorhinal cortex, and parahippocampal gyrus versus the hippocampal tail should be prioritized. Few data exist currently to guide surgeons in their decision making, which is likely the reason that significantly different therapy locations exist between patients—we estimated a maximal targeting difference of approximately 15 mm (Figure 5.5).

Given their complementary nature, PPV and NPV maps must be considered along with the map of ablation distributions. Of note, caution must be exercised at the periphery of these maps, which may comprise of no more than half the cohort and is susceptible to extreme values. It is also important to remember that statistics were independently calculated for each voxel, resulting in artificial regional clusters with similar probability values. Given the capabilities of LITT and the consequent range of ablation volumes included in this analysis, we can only generalize our findings to ablations of comparable shapes and sizes. One cannot conclude that ablation of only high PPV or NPV regions in isolation will maximize chances of Engel I outcomes. Instead, as we have demonstrated in Figure 5.7, we can infer that inclusion of these regions within a typical ablation cavity will maximize chances of Engel I outcomes, while exclusion of these regions may be detrimental to chances of Engel

I outcomes.

We have demonstrated that patients have the greatest opportunity for Engel I outcomes when the ablation includes anteromesial temporal lobe structures including the amygdala, which coincides with our findings on amygdalar ablation volumes. Further examination of the maps highlights the importance of targeting the mesial hippocampus, parahippocampal gyrus, entorhinal cortex, and perirhinal cortex—as missing these structures frequently resulted in persistent seizures. The rhinal cortices are known to be highly epileptogenic and intensely interconnected within the limbic network [123], and Jermakowicz et al have previously described the importance of ablating the mesial hippocampal head [38].

Extending the ablation beyond the coronal plane in line with the lateral mesencephalic sulcus yields diminishing returns. More importantly, ablations that extend further posteriorly have been associated with damage to the optic radiations with resultant visual field deficits [124]. The lack of significant benefit with ablation of the hippocampal tail posteriorly may be related to the negative relationship between hippocampal ablation volumes and seizure outcome—as ablation of the hippocampal tail with a straight laser catheter necessitates a compromise of hippocampal head coverage.

Overall, this study sheds new light on previously published results by demonstrating the importance of therapy location in LITT. Specifically, the wide range of seizure-freedom rates published to date may stem not only from the fact that these studies may have been underpowered, but also from differences in ablation locations. To maximize the opportunity for seizure freedom, properly selected patients must undergo LITT of the appropriate mesial structures. Previously, variability in surgical targeting has not been consistently taken into consideration – an approach analogous to analyzing the efficacy of a new drug without factoring in drug serum levels or even the administered dosages. Ultimately, ablating the necessary anatomic structures is more important than the total amount of tissue ablated with LITT. That being said, a significant amount of work is still needed to further elucidate the nuances of ablation location and its impact on clinical outcomes. With strict

criteria of therapy delivery, LITT may be associated with higher rates of seizure control for appropriately selected patients with mTLE.

### **5.4.3 Complications**

The observed overall complication rate of 15.0% is comparable to existing has received on surgery for mTLE [125, 126]. The 1.3% rate of radiographic hemorrhage, 0.4% rate of symptomatic hemorrhage, and 0.4% rate of permanent deficit from hemorrhage is comparable to reported rates in stereotactic neurosurgical procedures [127]. The most common complications observed were affective disorders and visual disturbances. Comorbid mood disturbances in patients with epilepsy with worsening of symptoms after temporal lobe surgery have been described [128]. Unfortunately, the retrospective nature of this study limited our ability to quantify and critically evaluate neuropsychological changes in a large multicenter cohort. It is also unknown if these complications would resolve as patients are followed beyond the time constraints of this study. Visual disturbances such as diplopia and visual field loss have also been commonly described complications of temporal lobe surgery [100, 122, 129, 130]. Visual complications in 5.1% of this cohort are lower than what has been reported for both LITT and temporal lobe resections. Of interest, the presence of a postoperative complication was associated with poorer seizure outcome. Given the importance of ablation location on seizure outcomes, suboptimal ablation may result not only in a decreased opportunity for seizure freedom, but also in an increase in complications.

### **5.4.4 Limitations**

The retrospective nature of this study is its major limitation. Specific data points were obtained from each center through a chart review to develop a uniform data set for statistical analysis. As such, the analysis is subject to both recall and misclassification bias. Complications, in particular, may have been underreported, as minor complications not

documented in the medical record would have been missed. Similarly, the details of each complication were not consistently available, which limits a clear interpretation of its impact.

As previously noted, seizure outcome data were recorded in only 6-month epochs, rather than at every available time point. Furthermore, outcome data were not consistently available for all epochs, which explains the presence of larger numbers of subjects at later time points. As a result of such missing data, a formal Kaplan-Meier analysis could not be properly performed, as it would serve as a skewed representation of a small subgroup of the entire cohort. Instead, we have reported the proportion of patients with Engel I outcomes at each 6-month time point after LITT.

This study design also precluded critical assessment the effect of LITT on neuropsychological outcomes. Both the temporal pole and basal temporal regions have been associated with category-specific naming deficits and a more inferior ablation could lessen the described cognitive benefits of LITT [98, 131]. Further analysis of the specific effects of LITT location on cognitive and mood outcomes is necessary.

The image-based analysis depends entirely on the accuracy of the nonlinear registration algorithm. Although we chose to accept the mean error of 1.34 mm ( 1 voxel), this certainly serves as a potential source of error. Ultimately, we believe that this compromise does not significantly affect the overall results of the image-based analysis presented here.

Finally, it is again important to note that the calculation of PPV and NPV maps treated each voxel independently and did not group voxels by patients or outcomes. As delineated earlier, this limits the generalizability of our findings and mandates a degree of caution in the interpretation of the resulting probability maps.

## **5.5 Conclusion**

This work represents the first multicenter study of LITT for mTLE and the largest LITT series to date with long-term follow-up of seizure outcome. The Engel I outcome seen in

58% of the cohort is comparable to what has been published to date, and the persistence of this seizure outcome at 2 years demonstrates the durability of this therapy. Radiographic evidence of hippocampal sclerosis was not associated with seizure outcome. Patients presenting with a history of FTC are less likely to experience either Engel I or II outcomes. Consideration of surgical factors – with a focus on ablation location more so than ablation volumes alone – is imperative to the complete assessment of LITT. Our novel method of image analysis in this large multicenter cohort has revealed that ablations prioritizing the amygdala, but also including the hippocampal head, parahippocampal gyrus, and rhinal cortices, are associated with a greater chance of seizure freedom, while extending the ablation to the hippocampal tail yields diminishing returns. Although this serves as the first step toward standardizing targeting for LITT in mTLE, further work with the incorporation of more complete complications data is necessary to refine this analysis and define the minimal zone of ablation necessary to maximize seizure control and minimize associated morbidity.

## **5.6 Acknowledgements**

This study was funded by the National Institutes of Health (NIH; R01NS095291).

## **5.7 Supplementary Information: Calculation of Engel I Probability Maps**

To analyze the role of the ablation location in seizure outcome probability maps were calculated by incorporating seizure outcomes into the aggregated and normalized ablation maps.

First a positive predictive value (PPV) map was generated by calculating the association between seizure freedom (Engel I outcome) and the ablation of a particular voxel. For each voxel ablated, Bayes Theorem was used to estimate the probability of achieving an Engel I outcome by incorporating outcome data at last follow-up ( $> 1$  year). If we define  $P(b_i = 1)$  as the probability of voxel ( $i$ ) being ablated and define  $P(b_j = 1)$  as the probability of

voxel ( $j$ ) being ablated, then by assuming that the probability of an ablation of each pixel is independent of another:

$$P(b_i = 1 \& b_j = 1) = P(b_i = 1) * P(b_j = 1) \quad (5.1)$$

When considering seizure outcome, we have defined  $P(E_1)$  as the probability of a patient being seizure free and  $P(\bar{E}_1)$  as the probability of a patient not being seizure free, since  $\bar{x}$  denotes the complement of the event  $x$ . As such:

$$P(b_i = 1 | E_1) = \frac{\text{number of times voxel } b_i \text{ was ablated across all } E_1 \text{ patients}}{\Sigma(E_1 \text{ patients})} \quad (5.2)$$

and

$$P(b_i = 1 | \bar{E}_1) = \frac{\text{number of times voxel } b_i \text{ was ablated across all } \bar{E}_1 \text{ patients}}{\Sigma(\bar{E}_1 \text{ patients})} \quad (5.3)$$

According to the law of total probability, the probability that the  $i^{th}$  pixel is ablated regardless of outcome is:

$$P(b_i = 1) = P(b_i = 1 | E_1) * P(E_1) + P(b_i = 1 | \bar{E}_1) * P(\bar{E}_1) \quad (5.4)$$

The joint probability can always be related to the conditional probabilities as follows:

$$P(A \& B) = P(A | B) * P(B) \quad (5.5)$$

It then follows that the PPV of a particular voxel in terms of seizure freedom can be calculated as:

$$P(E_1|b_i = 1) = \frac{P(E_1 \& b_i = 1)}{P(b_i = 1)} \quad (5.6)$$

$$= \frac{P(b_i = 1|E_1) * P(E_1)}{P(b_i = 1)} \quad (5.7)$$

$$= \frac{P(b_i = 1|E_1) * P(E_1)}{P(b_i = 1|E_1) * P(E_1) + P(b_i = 1|\bar{E}_1) * P(\bar{E}_1)} \quad (5.8)$$

To visualize these probabilities in a three-dimensional map, we assigned each voxel a color based on the value between 0 and 1.

In a similar manner, we were able to generate a negative predictive value (NPV) map by calculating the association between persistent seizures (Engel II-IV outcome) and the absence of a particular voxel. If we define  $P(b_i = 0)$  as the probability of the voxel ( $i$ ) not being ablated, the NPV of a particular voxel in terms of seizure freedom can be calculated as:

$$P(\bar{E}_1|b_i = 0) = \frac{P(\bar{E}_1 \& b_i = 0)}{P(b_i = 0)} \quad (5.9)$$

$$= \frac{P(b_i = 0|\bar{E}_1) * P(\bar{E}_1)}{P(b_i = 0)} \quad (5.10)$$

$$= \frac{P(b_i = 0|\bar{E}_1) * P(E_1)}{P(b_i = 0|\bar{E}_1) * P(\bar{E}_1) + P(b_i = 0|E_1) * P(E_1)} \quad (5.11)$$

Once again, to visualize these probabilities in a three-dimensional map, we assigned each voxel a color based on the value between 0 and 1.

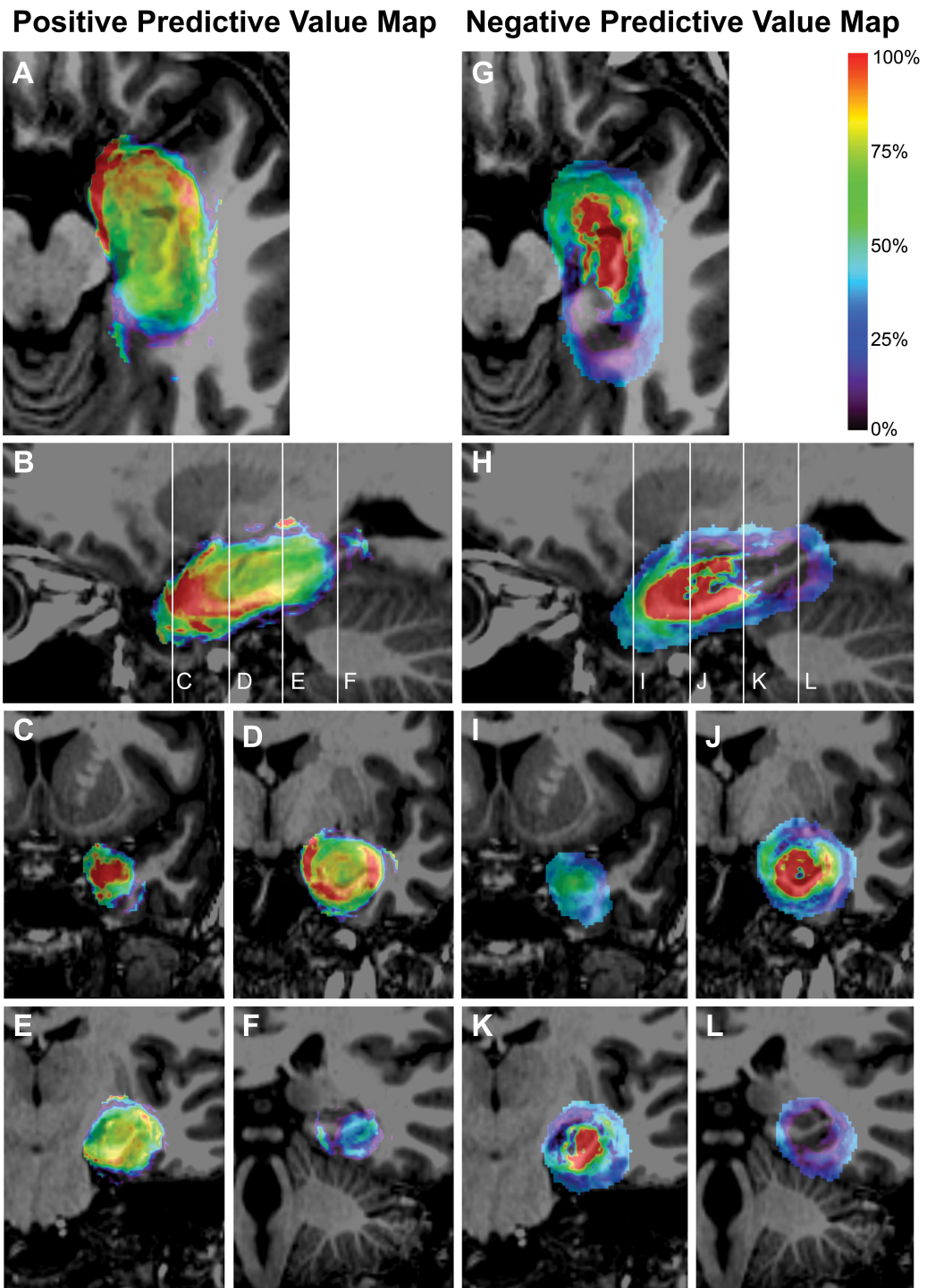


Figure 5.6: Maps representing the positive predictive value (PPV) (A-F) and negative predictive value (NPV) (G-L) of Engel I outcome associated with at least 1-year of follow-up for each voxel ablated in normalized atlas space for 175 patients. A, G, Represent axial views. B, H, Represent sagittal views.

Figure 5.6: C-F and I-L, Represent coronal views through the temporal pole, hippocampal head and posterior amygdala, hippocampal body, and hippocampal tail as represented by the reference lines on the sagittal image. Voxels were assigned a color if involved in the ablation of at least 4 patients. Each voxel was analyzed independently. Both maps demonstrate the importance of targeting the anterior, medial, and inferior structures in the mesial temporal lobe. Ablations extending posteriorly beyond the coronal plane in line with the lateral mesencephalic sulcus were less likely to be associated with Engel I outcomes

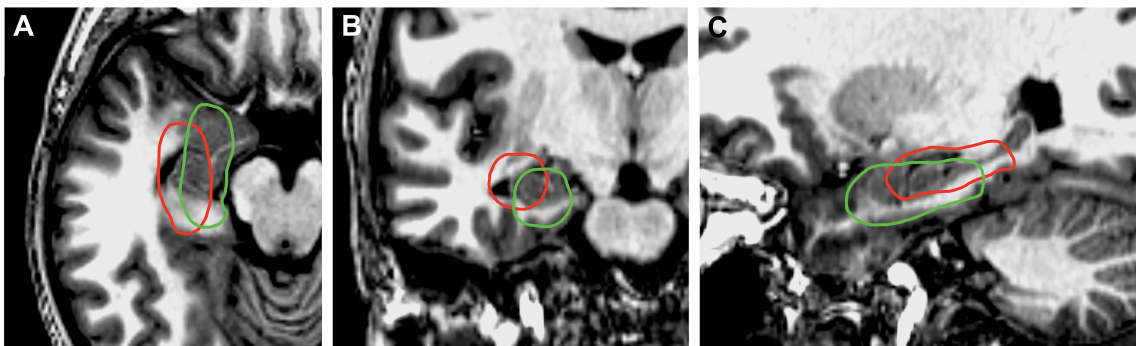


Figure 5.7: Theoretical favorable (green) and unfavorable (red) ablation locations based on the PPV and NPV maps. Both ablations are of roughly the same volume, but are located and oriented differently within the mesial temporal structures. The theoretical favorable ablation is located more anteriorly, medially, and inferiorly to cover the high probability voxels for both the PPV and NPV maps. This ablation covers the amygdala, hippocampus, parahippocampal gyrus, and rhinal cortices. The theoretical suboptimal ablation is located more posteriorly, laterally, and superiorly to exclude the high probability voxels for both the PPV and NPV maps. This ablation covers the posterolateral amygdala and hippocampus, but misses a large part of the amygdala, the mesial hippocampal head, parahippocampal gyrus, and rhinal cortices.

## Chapter 6

### SUMMARY AND FUTURE WORK

This dissertation describes methods to quantify patient outcomes by segmentation of medical images in two different domains of image guided surgery. We have demonstrated how to develop and use image processing and statistical tools to identify questions about patient performance, use appropriate analysis methods, and produce inferences that can help bridge the gap between optimal and actual outcomes. The major contributions are (1) development of a cochlear implant (CI) phantom that can be used to validate image segmentation methods on computed tomography (CT) images of implanted patients, as described in Chapter 2; (2) identification of significant position factors that affect hearing outcomes for both straight and precurved CI arrays in Chapters 3 and 4; and (3) identification of optimal targeting zone for laser interstitial thermal therapy (LITT) surgery for mesial temporal lobe epilepsy (mTLE) in Chapter 5. These are significant not just because of the resulting surgical recommendations described here, but also because they establish generalizable pipelines that could be used to analyze both thermo-ablative brain surgeries and electrode implantation methods.

In Chapter 2, we developed a CI phantom using a cadaveric skull filled with silicone, which, to the best of our knowledge, was the first CT phantom developed to analyze the sensitivity of image segmentation algorithms to CT image acquisition parameters. Having a method to define image parameters for image acquisition and to identify image processing errors was critical before we could investigate the correlation between automatically localized electrode positions and hearing outcomes. We scanned the phantom in different scanners using different acquisition protocols, rigidly registered all images to a selected base image, and investigated which parameters, when changed, caused significant changes in the baseline localization error associated with an image of a certain quality – defined as

the “image-based localization error”. We found that the Hounsfield Unit (HU) range and resolution of the CT reconstruction always significantly affect the image-based localization error, while CT dose and image orientation had weaker effects in limited cases. We also evaluated the robustness of several automatic electrode localization methods to changes in image acquisition protocols. Moreover, thanks to these sensitivity measures, we demonstrated how to determine the image acquisition protocol that should be used for a study if we want to limit localization errors to a certain value using a particular algorithm.

In Chapter 3, we used image segmentation algorithms, including the ones validated in Chapter 2, to identify the position of CI arrays relative to the patient anatomy for 220 implanted ears from patients scanned at Vanderbilt. We defined 4 variables to describe the CI position and collected data on 4 demographic covariates. The hearing outcomes of interest were percent correct CNC monosyllabic words and BKB-SIN scores. Using stepwise multiple linear regression with backward elimination of features above the critical  $p$ -value of 0.15, we created separate general linear models (GLM) for straight and precurved arrays. For straight arrays, after controlling for demographics, the basal depth of insertion was the only significant positioning factor; for precurved arrays, the significant features were the mean modiolar distance, base insertion depth and presence or absence of scalar translocation. This GLM also allowed us to estimate the expected population outcomes based on demographics and electrode position, which holds promising implications for future patient counseling, device choice and surgical planning.

In Chapter 4, we expanded on the question of CNC outcomes in precurved arrays, since there were certain features we could not investigate due to dataset limitations in the previous study. Multiple correlated position factors were found to be significant for precurved arrays in Chapter 3, and it was important to analyze if their significance in the final GLM were artifacts due to correlations between features. We added validated patient data to our dataset to increase it to almost three times the previous size (from 92 precurved arrays to 274), as well as increasing the types of demographic data we aggregated. Using linear correlation

analysis and multiple linear regression, we obtained a better idea of the importance and interactions between the three position factors that most affect outcomes – full ST insertion, insertion depth and modiolar distance. Our studies showed that the effects of insertion depth and modiolar distance were most significant at the apical part of the cochlea, and it is necessary that both of these features have good values for a good hearing outcome. These results add to increasing evidence in the literature that CI position affects outcomes, and deeper atraumatic insertions with lower apical distance to the modiolus are necessary for good outcomes for precurved arrays.

Finally in Chapter 5, we extended the use of segmentation and statistical analysis to LITT for mTLE. This was a different challenge in certain ways since the modality of brain images was magnetic resonance imaging (MRI), unlike CT in cochlear applications, and the image features of interest were irregular ablations instead of electrode arrays. The patient outcome was binary – whether the patients were completely free of seizures at last follow up or not – unlike the continuous range of performance testing with CIs. We aggregated a dataset of 234 patients who have had at least a 1-year postoperative follow up from 11 medical centers around the US, the largest LITT series at that point. We carried out a study with two raters to evaluate the quality of nonrigid registration between the patient images and the atlas. We were interested specifically in the errors around the hippocampus, which was the general target of ablation, and therefore we evaluated registration errors using the surface errors of the average segmented hippocampus after registration to the atlas. We found that our chosen registration method causes  $\approx 1$  mm surface error around the hippocampal region, and works relatively better for patients who did not have hippocampal sclerosis. Our raters also verified that the quality of registration was accurate for clinical purposes. Following this validation step, the raters manually segmented the ablation cavities in the postsurgical images, since their irregular and varied shapes made it difficult for existing segmentation algorithms to identify them with reasonable accuracy. Although this step was costly in terms of expert labor, it was much shorter than the time required to develop

and validate a new algorithm. We projected the cavities through the validated nonrigid registration pipeline onto a healthy subject atlas, and also mirrored them so that we had the same number of ablations reproduced on both left and right. The retrospective question of patient outcomes became: if we know that a certain point of the brain was ablated, what is the probability of a good outcome? We created three dimensional positive predictive value (PPV) and negative predictive value (NPV) maps on the healthy atlas brain by calculating the Bayesian conditional probability of seizure freedom. Our results showed that for better outcomes, it was necessary to target the anterior zones like the amygdala, while increased hippocampal ablation volume was associated with a decreased chance of good outcomes. Considering the problem of ablating a curved structure, the hippocampus, with a straight laser catheter, this means that ablation of the posterior hippocampus, up to the hippocampal tail, yielded diminishing returns. The main surgical takeaway was that laser ablations that prioritized the amygdala and included the hippocampal head, parahippocampal gyrus, and rhinal cortices had a greater chance of seizure freedom.

Building on the significant progress we made in answering the questions of how the positioning of interventions affect patient outcomes, we can outline several future steps to improve our inferences. The final results of all our applications are sensitive to the quality and quantity of our data. In developing our CT phantom in Chapter 2, we tried to address the problem of image data consistency by analyzing how much a difference in image quality can affect the same image processing algorithm. The analysis in Chapters 3 and 4 are limited by the size of the patient dataset, and we identified that the patient data was regrettably sparse when it came to demographic variables. Although we used statistical methods to identify trends underlying the noise, we ideally need significantly larger datasets to conclusively control for confounds and isolate the effects of position accurately.

Once we are satisfied that we have a large and complete dataset where we can identify most of the variation due to demographic confounds, we can explore the use of richer positioning data instead of the current summary variables. For example, the entire three-

dimensional positioning of the array with respect to the cochlear anatomy might reveal certain correlations to hearing outcomes that are not adequately captured by the use of insertion depth at a single point, or the average of the modiolar distance. Adding image features related to the anatomy surrounding the entire array might also explain patient specific factors contributing to the outcome that our current analysis cannot address. Finally, with enough longitudinal data, we can analyze the trend of outcomes instead of the hearing outcome at the last follow up, which varies for different patients. For this aim, however, we would need consistent and regular follow up testing, which links back to our first focus on improving consistency of data collection. With a larger dataset and exploration of more descriptive features, the final target step would be to produce accurate outcome prediction models. This could greatly aid patient counseling, device choice, and surgical guidance at a patient specific level.

The other major limitation of the studies in this dissertation is their retrospective nature. Collecting demographic data through chart review is subject to both recall and misclassification bias, especially for the data we collected from epilepsy patients. Additionally, at best we can only identify the necessary configuration for good outcomes – not the sufficient conditions. In the case of LITT ablation, while we identified the ablation necessary for seizure freedom, we do not have the data to predict if some or all of those regions have to be ablated to produce good outcomes in a new patient. The proposed next step would be a quasi-prospective study on how our 3D map can predict seizure freedom in a holdout set, which would provide conclusive outcomes on the sufficient extent of ablation for seizure freedom.

In case of CI insertions, we consistently found that shallower insertions are associated with poorer outcomes. But the current data cannot reveal if shallow insertions cause bad outcomes independently, or there was some trauma due to insertion, which caused both the poor outcomes as well as shallow insertion. Prospective studies that collect detailed notes on surgical choices is required to identify these causal relationships. Such studies can also

produce non-sparse datasets with consistent longitudinal follow up testing, which would also solve the problem of data quality.

Finally, the methods described in this dissertation could be easily applied to other surgical scenarios after appropriate validation. For example, the analysis of LITT patients can be extended to essential tremor (ET) patients who have undergone high frequency focused ultrasound (HIFU) ablation. This problem would be a natural extension, because from an analysis standpoint, it shares many similar characteristics with LITT for mTLE – it also involves correlating patient outcomes with varied irregular ablations on a well defined target zone in brain MRI. We could follow similar analysis methods to nonrigidly register images and create 3D maps that can identify the optimal target. Preliminary work done in this domain shows significant promise. We collected a small dataset of 10 patients treated with HIFU for ET on their left thalamus. All of them have preoperative and postoperative imaging as well as improvement of total Clinical Rating Scale for Tremor scores (CRST) as a measure of patient outcome. Using nonrigid registration to an atlas image, we can create probability maps that place the optimal target around the ventral posterior thalamus. A larger dataset and further studies are required to verify these findings.

In summary, this dissertation presents novel image processing and statistical analysis pipelines to analyze the correlation between patient outcomes and the anatomical position of intervention in Chapters 2, 3, 4 and 5. The inferences resulting from each study produced valuable insights for surgical planning as well as patient counseling. We acknowledge that by no means are these questions fully answered, and we have outlined several possible future directions to improve upon our findings in this chapter. However, we believe that the work described in this dissertation has made significant contributions towards identifying how good positioning can improve patient outcomes, and that the techniques described here will benefit future research in these areas.

## REFERENCES

- [1] NIDCD. How do we hear?, 2018. URL [https://www.nidcd.nih.gov/sites/default/files/Documents/health/images/howdowehear-\\_pdf\\_version.pdf](https://www.nidcd.nih.gov/sites/default/files/Documents/health/images/howdowehear-_pdf_version.pdf). Accessed: 2021-03-03.
- [2] NIDCD. Cochlear implants, 2017. URL <https://www.nidcd.nih.gov/health/cochlear-implants>. Accessed: 2021-03-03.
- [3] Blausen Medical. Medical gallery of blausen medical 2014. *WikiJournal of Medicine*, 1(2), 2014. ISSN 2002-4436. doi: <https://doi.org/10.15347/wjm/2014.010>.
- [4] Michael F Dorman, W Yost, BS Wilson, and René H Gifford. Speech perception and sound localization by adults with bilateral cochlear implants. *Seminars in Hearing*, 32:73–89, 2011. doi: 10.1055/s-0031-1271949.
- [5] Emily Buss, Harold C. Pillsbury, Craig A. Buchman, et al. Multicenter us bilateral med-el cochlear implantation study: Speech perception over the first year of use. *Ear and Hearing*, 29(1):20–32, 2008.
- [6] René H Gifford, Jon K Shallop, and Anna Mary Peterson. Speech recognition materials and ceiling effects: Considerations for cochlear implant programs. *Audiology and Neurotology*, 13(3):193–205, 2008.
- [7] Ruth Litovsky, Aaron Parkinson, Jennifer Arcaroli, and Carol Sammeth. Simultaneous bilateral cochlear implantation in adults: a multicenter clinical study. *Ear and hearing*, 27(6):714, 2006.
- [8] Laura K Holden, Charles C Finley, Jill B Firszt, Timothy A Holden, Christine Brenner, Lisa G Potts, Brenda D Gotter, Sallie S Vanderhoof, Karen Mispagel, Gitry Hey-

- debrand, et al. Factors affecting open-set word recognition in adults with cochlear implants. *Ear and hearing*, 34(3):342, 2013.
- [9] Peter Blamey, Patti Arndt, François Bergeron, Göran Bredberg, Judy Brimacombe, George Facer, Jan Larky, Bo Lindström, Julian Nedzelski, Ann Peterson, et al. Factors affecting auditory performance of postlinguistically deaf adults using cochlear implants. *Audiology and Neurotology*, 1(5):293–306, 1996.
- [10] JT Rubinstein, WS Parkinson, RS Tyler, and BJ Gantz. Residual speech recognition and cochlear implant performance: effects of implantation criteria. *The American journal of otology*, 20(4):445–452, 1999.
- [11] K. M. J. Green, Y. M. Bhatt, D. J. Mawman, M. P. O’Driscoll, S. R. Saeed, R. T. Ramsden, and M. W. Green. Predictors of Audiological Outcome Following Cochlear Implantation in Adults. *Cochlear implants ...*, 9(October):177–185, 2008. ISSN 1754-7628. doi: 10.1002/cii.326.
- [12] Janice Leung, Nae-Yuh Wang, Jennifer D Yeagle, Jill Chinnici, Stephen Bowditch, Howard W Francis, and John K Niparko. Predictive models for cochlear implantation in elderly candidates. *Archives of Otolaryngology–Head & Neck Surgery*, 131(12):1049–1054, 2005.
- [13] UK Cochlear Implant Study Group et al. Criteria of candidacy for unilateral cochlear implantation in postlingually deafened adults ii: cost-effectiveness analysis. *Ear and hearing*, 25(4):336–360, 2004.
- [14] David R Friedland, Holly S Venick, and John K Niparko. Choice of ear for cochlear implantation: the effect of history and residual hearing on predicted postoperative performance. *Otology & Neurotology*, 24(4):582–589, 2003.
- [15] Michael F Dorman, Maureen T Hannley, Korine Dankowski, Luke Smith, and Geary

- McCandless. Word recognition by 50 patients fitted with the symbion multichannel cochlear implant. *Ear and Hearing*, 10(1):44–49, 1989.
- [16] JB Millar, YC Tong, PJ Blamey, Graeme M Clark, RC Dowell, and PM Seligman. Speech processing for electrical stimulation of the auditory nerve. *Scientific publications, vol. 3, 1984-1986, no. 194*, 1986.
- [17] Richard C Dowell, Dianne J Mecklenburg, and Graeme M Clark. Speech recognition for 40 patients receiving multichannel cochlear implants. *Archives of Otolaryngology–Head & Neck Surgery*, 112(10):1054–1059, 1986.
- [18] Antje Aschendorff, Ralf Kubalek, Bernd Turowski, Friedhelm Zanella, Albrecht Hochmuth, Martin Schumacher, Thomas Klenzner, and Roland Laszig. Quality control after cochlear implant surgery by means of rotational tomography. *Otology and Neurotology*, 26(1):34–37, 2005.
- [19] Margaret W. Skinner, Timothy A. Holden, Bruce R. Whiting, Arne H. Voie, Barry Brunsden, J. Gail Neely, Eugene A. Saxon, Timothy E. Hullar, and Charles C. Finley. In vivo estimates of the position of advanced bionics electrode arrays in the human cochlea. *Annals of Otology, Rhinology and Laryngology*, 116(4):2–24, 2007.
- [20] Charles C Finley and Margaret W Skinner. Role of electrode placement as a contributor to variability in cochlear implant outcomes. *Otology & neurotology: official publication of the American Otological Society, American Neurotology Society [and] European Academy of Otology and Neurotology*, 29(7):920, 2008.
- [21] Brendan P O’Connell, Ahmet Cakir, Jacob B Hunter, David O Francis, Jack H Noble, Robert F Labadie, Geraldine Zuniga, Benoit M Dawant, Alejandro Rivas, and George B Wanna. Electrode location and angular insertion depth are predictors of audiologic outcomes in cochlear implantation. *Otology & neurotology: official pub-*

lication of the American Otological Society, American Neurotology Society [and] European Academy of Otology and Neurotology, 37(8):1016, 2016.

- [22] Brendan P O’Connell, Jacob B Hunter, and George B Wanna. The importance of electrode location in cochlear implantation. *Laryngoscope investigative otolaryngology*, 1(6):169–174, 2016.
- [23] George B. Wanna, Jack H. Noble, Theodore R. McRrackan, Benoit M. Dawant, Mary S. Dietrich, Linsey Watkins, Alejandro Rivas, Theodore A. Schuman, and Robert F. Labadie. Assessment of electrode placement and audiologic outcomes in bilateral cochlear implantation. *Otology and Neurotology*, 32(3):428–432, 2011.
- [24] Gonzalo N Esquia-Medina, Stéphanie Borel, Yann Nguyen, Emmanuèle Ambert-Dahan, Evelyne Ferrary, Olivier Sterkers, and Alexis Bozorg Grayeli. Is electrode-modiolus distance a prognostic factor for hearing performances after cochlear implant surgery? *Audiology and Neurotology*, 18(6):406–413, 2013.
- [25] Margaret W Skinner, Darlene R Ketten, Laura K Holden, Gary W Harding, Peter G Smith, George A Gates, J Gail Neely, G Robert Kletzker, Barry Brunsten, and Barbara Blocker. Ct-derived estimation of cochlear morphology and electrode array position in relation to word recognition in nucleus-22 recipients. *Journal of the Association for Research in Otolaryngology*, 3(3):332–350, 2002.
- [26] Kumiko Yukawa, Lawrence Cohen, Peter Blamey, Brian Pyman, Viruch Tungvachirakul, and Stephen O’Leary. Effects of insertion depth of cochlear implant electrodes upon speech perception. *Audiology and Neurotology*, 9(3):163–172, 2004.
- [27] Aayesha M Khan, Ophir Handzel, Barbara J Burgess, Doris Damian, Donald K Eddington, and Joseph B Nadol Jr. Is word recognition correlated with the number of surviving spiral ganglion cells and electrode insertion depth in human subjects with cochlear implants? *The Laryngoscope*, 115(4):672–677, 2005.

- [28] Joonhan Lee, Joseph B Nadol Jr, and Donald K Eddington. Depth of electrode insertion and postoperative performance in humans with cochlear implants: a histopathologic study. *Audiology and Neurotology*, 15(5):323–331, 2010.
- [29] World Health Organization, Global Campaign against Epilepsy, Programme for Neurological Diseases, Neuroscience (World Health Organization), International Bureau for Epilepsy, World Health Organization. Department of Mental Health, Substance Abuse, International Bureau of Epilepsy, and International League against Epilepsy. *Atlas: epilepsy care in the world*. World Health Organization, 2005.
- [30] Mark A Attiah, Danika L Paulo, Shabbar F Danish, Sherman C Stein, and Ram Mani. Anterior temporal lobectomy compared with laser thermal hippocampectomy for mesial temporal epilepsy: A threshold analysis study. *Epilepsy research*, 115: 1–7, 2015.
- [31] Patrick Kwan and Martin J Brodie. Early identification of refractory epilepsy. *New England Journal of Medicine*, 342(5):314–319, 2000.
- [32] Cristian Donos, Joshua Breier, Elliott Friedman, Patrick Rollo, Jessica Johnson, Lauren Moss, Stephen Thompson, Melissa Thomas, Omotola Hope, Jeremy Slater, et al. Laser ablation for mesial temporal lobe epilepsy: surgical and cognitive outcomes with and without mesial temporal sclerosis. *Epilepsia*, 59(7):1421–1432, 2018.
- [33] Jon T Willie, Nealen G Laxpati, Daniel L Drane, Ashok Gowda, Christina Appin, Chunhai Hao, Daniel J Brat, Sandra L Helmers, Amit Saindane, Sherif G Nour, et al. Real-time magnetic resonance-guided stereotactic laser amygdalohippocampotomy for mesial temporal lobe epilepsy. *Neurosurgery*, 74(6):569–585, 2014.
- [34] Hena Waseem, Andrew C Vivas, and Fernando L Vale. Mri-guided laser interstitial

thermal therapy for treatment of medically refractory non-lesional mesial temporal lobe epilepsy: outcomes, complications, and current limitations: a review. *Journal of Clinical Neuroscience*, 38:1–7, 2017.

- [35] Susan Spencer and Linda Huh. Outcomes of epilepsy surgery in adults and children. *The Lancet Neurology*, 7(6):525–537, 2008.
- [36] Joon Y Kang, Chengyuan Wu, Joseph Tracy, Matthew Lorenzo, James Evans, Maromi Nei, Christopher Skidmore, Scott Mintzer, Ashwini D Sharan, and Michael R Sperling. Laser interstitial thermal therapy for medically intractable mesial temporal lobe epilepsy. *Epilepsia*, 57(2):325–334, 2016.
- [37] Purvee Patel, Nitesh V Patel, and Shabbar F Danish. Intracranial mr-guided laser-induced thermal therapy: single-center experience with the visualase thermal therapy system. *Journal of neurosurgery*, 125(4):853–860, 2016.
- [38] Walter J Jermakowicz, Andres M Kanner, Samir Sur, Christina Bermudez, Pierre-François D’Haese, John Paul G Kolcun, Iahn Cajigas, Rui Li, Carlos Millan, Ramses Ribot, et al. Laser thermal ablation for mesiotemporal epilepsy: analysis of ablation volumes and trajectories. *Epilepsia*, 58(5):801–810, 2017.
- [39] Vejay N Vakharia, Rachel Sparks, Kuo Li, Aidan G O’Keeffe, Anna Miserocchi, Andrew W McEvoy, Michael R Sperling, Ashwini Sharan, Sebastien Ourselin, John S Duncan, et al. Automated trajectory planning for laser interstitial thermal therapy in mesial temporal lobe epilepsy. *Epilepsia*, 59(4):814–824, 2018.
- [40] Chengyuan Wu, David W Boorman, Richard J Gorniak, Christopher J Farrell, James J Evans, and Ashwini D Sharan. The effects of anatomic variations on stereotactic laser amygdalohippocampectomy and a proposed protocol for trajectory planning. *Operative Neurosurgery*, 11(2):345–357, 2015.

- [41] René H Gifford, Michael F Dorman, Sterling W Sheffield, Kate Teece, and Amy P Olund. Availability of binaural cues for bilateral implant recipients and bimodal listeners with and without preserved hearing in the implanted ear. *Audiology and Neurotology*, 19(1):57–71, 2013.
- [42] Berit M. Verbist, Johan H. M. Frijns, Jakob Geleijns, and Mark A. van Buchem. Multisection ct as a valuable tool in the postoperative assessment of cochlear implant patients. *American Journal of Neuroradiology*, 26(2):424–429, 2005.
- [43] George B. Wanna, Jack H. Noble, Matthew L. Carlson, René H. Gifford, Mary S. Dietrich, David S. Haynes, Benoit M. Dawant, and Robert F. Labadie. Impact of electrode design and surgical approach on scalar location and cochlear implant outcomes. *The Laryngoscope*, 124(S6):S1–S7, 2014.
- [44] Yiyuan Zhao, Benoit M. Dawant, Robert F. Labadie, and Jack H. Noble. Automatic localization of cochlear implant electrodes in ct. *Medical Image Computing and Computer-Assisted Intervention – MICCAI 2014*, Springer International Publishing, 2014. 331-338, 2014.
- [45] Jack H. Noble and Benoit M. Dawant. Automatic graph-based localization of cochlear implant electrodes in ct. *Medical Image Computing and Computer-Assisted Intervention – MICCAI 2015*, Springer International Publishing, 2015. 152-159, 2015.
- [46] Jin Xu, Shi-Ang Xu, Lawrence T Cohen, and Graeme M Clark. Cochlear view: postoperative radiography for cochlear implantation. *Otology & Neurotology*, 21(1):49–56, 2000.
- [47] Ge Wang, Margaret W Skinner, Jay T Rubinstein, MA Howard, and Michael W Vannier. Digital x-ray stereophotogrammetry for cochlear implantation. *IEEE transactions on biomedical engineering*, 47(8):1120–1130, 2000.

- [48] Hartmut W Husstedt, Antje Aschendorff, Bernhard Richter, Roland Laszig, and Martin Schumacher. Nondestructive three-dimensional analysis of electrode to modiolus proximity. *Otology & neurotology*, 23(1):49–52, 2002.
- [49] Darlene R Ketten, Margaret W Skinner, Ge Wang, Michael W Vannier, George A Gates, and J Gail Neely. In vivo measures of cochlear length and insertion depth of nucleus cochlear implant electrode arrays. *Annals of Otology, Rhinology & Laryngology*, 107(1):1B11, 1998.
- [50] Ge Wang, Michael W Vannier, Margaret W Skinner, Marcelo GP Cavalcanti, and Gary W Harding. Spiral ct image deblurring for cochlear implantation. *IEEE transactions on medical imaging*, 17(2):251–262, 1998.
- [51] Ming Jiang, Ge Wang, Margaret W Skinner, Jay T Rubinstein, and Michael W Vannier. Blind deblurring of spiral ct images. *IEEE transactions on medical imaging*, 22(7):837–845, 2003.
- [52] Jack H. Noble, Robert F. Labadie, René H. Gifford, and Benoit M. Dawant. Image-guidance enables new methods for customizing cochlear implant stimulation strategies. *Neural Systems and Rehabilitation Engineering, IEEE Transactions on*, 21(5): 820–829, 2013.
- [53] JL Farrell, JC Stuelpnagel, RH Wessner, JR Velman, and JE Brook. Problem 65-1: A least squares estimate of satellite attitude. *Siam Review*, 8(3):384–386, 1966.
- [54] J. Michael Fitzpatrick, Jay B. West, and Calvin R. Maurer Jr. Predicting error in rigid-body point-based registration. *IEEE Transactions on Medical Imaging*, 17(5): 694–702, 1998. doi: 10.1109/42.736021.
- [55] Frederik Maes, Andre Collignon, Dirk Vandermeulen, Guy Marchal, and Paul Suetens. Multimodality image registration by maximization of mutual information. *IEEE transactions on medical imaging*, 16(2):187–198, 1997.

- [56] Paul Viola and William M Wells III. Alignment by maximization of mutual information. *International journal of computer vision*, 24(2):137–154, 1997.
- [57] Bernard L Welch. The generalization of student’s’ problem when several different population variances are involved. *Biometrika*, 34(1/2):28–35, 1947.
- [58] George Casella and Roger L. Berger. *Statistical Inference*, volume 2. Pacific Grove CA: Duxbury, 2002.
- [59] Jacob Cohen. *Statistical power analysis for the behavioral sciences*. 1988.
- [60] Harald Hentschke and Maik C Stüttgen. Computation of measures of effect size for neuroscience data sets. *European Journal of Neuroscience*, 34(12):1887–1894, 2011.
- [61] Yiyuan Zhao, Srijata Chakravorti, Robert F. Labadie, Benoit M. Dawant, and Jack H. Noble. Automatic graph-based method for localization of cochlear implant electrode arrays in clinical ct with sub-voxel accuracy. *Medical Image Analysis*, 52:1 – 12, 2019. ISSN 1361-8415. doi: <https://doi.org/10.1016/j.media.2018.11.005>.
- [62] Ge Wang, Shiyong Zhao, Hengyong Yu, Charles A Miller, Paul J Abbas, Bruce J Gantz, Seung Wook Lee, and Jay T Rubinstein. Design, analysis and simulation for development of the first clinical micro-ct scanner. *Academic radiology*, 12(4): 511–525, 2005.
- [63] Jack H. Noble, Robert F. Labadie, Omid Majdani, and Benoit M. Dawant. Automatic segmentation of intracochlear anatomy in conventional ct. *Biomedical Engineering, IEEE Transactions on*, 58(9):2625–2632, 2011.
- [64] Jack H. Noble, René H. Gifford, Robert F. Labadie, and Benoit M. Dawant. Statistical shape model segmentation and frequency mapping of cochlear implant stimula-

tion targets in ct. pages 421–428. *Medical Image Computing and Computer-Assisted Intervention – MICCAI 2012*, Springer, 2012.

- [65] John F Knutson, Bruce J Gantz, James V Hinrichs, Helen A Schartz, Richard S Tyler, and George Woodworth. Psychological predictors of audiological outcomes of multichannel cochlear implants: Preliminary findings. *Ann Otol Rhinol Laryngol*, 1991.
- [66] Bruce J Gantz, George G Woodworth, John F Knutson, Paul J Abbas, and Richard S Tyler. Multivariate predictors of audiological success with multichannel cochlear implants. *Annals of Otolology, Rhinology & Laryngology*, 102(12):909–916, 1993.
- [67] Gitry Heydebrand, Sandra Hale, Lisa Potts, Brenda Gotter, and Margaret Skinner. Cognitive predictors of improvements in adults’ spoken word recognition six months after cochlear implant activation. *Audiology and Neurotology*, 12(4):254–264, 2007.
- [68] Joseph B Nadol Jr, Yi-Shyang Young, and Robert J Glynn. Survival of spiral ganglion cells in profound sensorineural hearing loss: implications for cochlear implantation. *Annals of Otolology, Rhinology & Laryngology*, 98(6):411–416, 1989.
- [69] Mohammad Seyyedi, Lucas M Viana, and Joseph B Nadol Jr. Within-subject comparison of word recognition and spiral ganglion cell count in bilateral cochlear implant recipients. *Otology & neurotology: official publication of the American Otological Society, American Neurotology Society [and] European Academy of Otology and Neurotology*, 35(8):1446, 2014.
- [70] Douglas C Fitzpatrick, Adam Campbell, Baishakhi Choudhury, Margaret Dillon, Mathieu Forgues, Craig A Buchman, and Oliver F Adunka. Round window electrocochleography just prior to cochlear implantation: relationship to word recognition outcomes in adults. *Otology & neurotology: official publication of the Ameri-*

*can Otological Society, American Neurotology Society [and] European Academy of Otology and Neurotology*, 35(1):64, 2014.

- [71] Brendan P O’Connell, Jourdan T Holder, Robert T Dwyer, René H Gifford, Jack H Noble, Marc L Bennett, Alejandro Rivas, George B Wanna, David S Haynes, and Robert F Labadie. Intra-and postoperative electrocochleography may be predictive of final electrode position and postoperative hearing preservation. *Frontiers in neuroscience*, 11:291, 2017.
- [72] Timothy J Davis, Dongqing Zhang, René H Gifford, Benoit M Dawant, Robert F Labadie, and Jack H Noble. Relationship between electrode-to-modiolus distance and current levels for adults with cochlear implants. *Otology & neurotology: official publication of the American Otological Society, American Neurotology Society [and] European Academy of Otology and Neurotology*, 37(1):31, 2016.
- [73] Paul J Abbas, Michelle L Hughes, Carolyn J Brown, Charles A Miller, and Heather South. Channel interaction in cochlear implant users evaluated using the electrically evoked compound action potential. *Audiology and Neurotology*, 9(4):203–213, 2004.
- [74] Fitsum A Reda, Jack H Noble, Robert F Labadie, and Benoit M Dawant. An artifact-robust, shape library-based algorithm for automatic segmentation of inner ear anatomy in post-cochlear-implantation ct. In *Medical Imaging 2014: Image Processing*, volume 9034, page 90342V. International Society for Optics and Photonics, 2014.
- [75] Fitsum A Reda, Theodore R McRackan, Robert F Labadie, Benoit M Dawant, and Jack H Noble. Automatic segmentation of intra-cochlear anatomy in post-implantation ct of unilateral cochlear implant recipients. *Medical image analysis*, 18(3):605–615, 2014.

- [76] Gordon E Peterson and Ilse Lehiste. Revised cnc lists for auditory tests. *Journal of Speech and Hearing Disorders*, 27(1):62–70, 1962.
- [77] John Bench, Åse Kowal, and John Bamford. The bkb (bamford-kowal-bench) sentence lists for partially-hearing children. *British journal of audiology*, 13(3):108–112, 1979.
- [78] O Adunka, J Kiefer, MH Unkelbach, A Radeloff, and W Gstoettner. Evaluating cochlear implant trauma to the scala vestibuli. *Clinical Otolaryngology*, 30(2):121–127, 2005.
- [79] Mary Hardy. The length of the organ of corti in man. *American Journal of Anatomy*, 62(2):291–311, 1938.
- [80] Alejandro Rivas, Ahmet Cakir, Jacob B Hunter, Robert F Labadie, M Geraldine Zuniga, George B Wanna, Benoit M Dawant, and Jack H Noble. Automatic cochlear duct length estimation for selection of cochlear implant electrode arrays. *Otology & neurotology: official publication of the American Otological Society, American Neurotology Society [and] European Academy of Otology and Neurotology*, 38(3):339, 2017.
- [81] Jianing Wang, Benoit M Dawant, Robert F Labadie, and Jack H Noble. Retrospective evaluation of a technique for patient-customized placement of precurved cochlear implant electrode arrays. *Otolaryngology–Head and Neck Surgery*, 157(1):107–112, 2017.
- [82] Robert F Labadie and Jack H Noble. Preliminary results with image-guided cochlear implant insertion techniques. *Otology & Neurotology*, 39(7):922–928, 2018.
- [83] Jack H Noble, René H Gifford, Andrea J Hedley-Williams, Benoit M Dawant, and Robert F Labadie. Clinical evaluation of an image-guided cochlear implant programming strategy. *Audiology and Neurotology*, 19(6):400–411, 2014.

- [84] Jack H Noble, Andrea J Hedley-Williams, Linsey Sunderhaus, Benoit M Dawant, Robert F Labadie, Stephen M Camarata, and René H Gifford. Initial results with image-guided cochlear implant programming in children. *Otology & neurotology: official publication of the American Otological Society, American Neurotology Society [and] European Academy of Otology and Neurotology*, 37(2):e63, 2016.
- [85] Isabelle Boisvert, Catherine M McMahon, Richard C Dowell, and Björn Lyxell. Long-term asymmetric hearing affects cochlear implantation outcomes differently in adults with pre-and postlingual hearing loss. *PloS one*, 10(6):e0129167, 2015.
- [86] Hosung Kim, Woo Seok Kang, Hong Ju Park, Jee Yeon Lee, Jun Woo Park, Yehree Kim, Ji Won Seo, Min Young Kwak, Byung Chul Kang, Chan Joo Yang, et al. Cochlear implantation in postlingually deaf adults is time-sensitive towards positive outcome: Prediction using advanced machine learning techniques. *Scientific reports*, 8(1):1–9, 2018.
- [87] Nahla A Gomaa, Jay T Rubinstein, Mary W Lowder, Richard S Tyler, and Bruce J Gantz. Residual speech perception and cochlear implant performance in postlingually deafened adults. *Ear and hearing*, 24(6):539–544, 2003.
- [88] Jafar Hamzavi, Wolf-dieter Baumgartner, Stefan Marcel Pok, Peter Franz, and Wolfgang Gstöttner. Variables affecting speech perception in postlingually deaf adults following cochlear implantation. *Acta oto-laryngologica*, 123(4):493–498, 2003.
- [89] Michael F Dorman, Tony Spahr, René Gifford, Louise Loiselle, Sharon McKarns, Timothy Holden, Margaret Skinner, and Charles Finley. An electric frequency-to-place map for a cochlear implant patient with hearing in the nonimplanted ear. *Journal for the Association for Research in Otolaryngology*, 8(2):234–240, 2007.
- [90] R Filippo, P Mancini, V Panebianco, M Viccaro, E Covelli, V Vergari, and R Passariello. Assessment of intracochlear electrode position and correlation with be-

- havioural thresholds in cii and 90k cochlear implants. *Acta oto-laryngologica*, 128(3):291–296, 2008.
- [91] F B van der Beek, P PBM Boermans, B M Verbist, J J Briaire, and J HM Frijns. Clinical evaluation of the clarion cii hifocus 1 with and without positioner. *Ear and hearing*, 26(6):577–592, 2005.
- [92] Gijs KA van Wermeskerken, Adriaan F van Olphen, and Kees Graamans. Imaging of electrode position in relation to electrode functioning after cochlear implantation. *European archives of oto-rhino-laryngology*, 266(10):1527–1531, 2009.
- [93] Jafar Hamzavi and Christoph Arnoldner. Effect of deep insertion of the cochlear implant electrode array on pitch estimation and speech perception. *Acta oto-laryngologica*, 126(11):1182–1187, 2006.
- [94] René H Gifford, Michael F Dorman, Henryk Skarzynski, Artur Lorens, Marek Polak, Colin LW Driscoll, Peter Roland, and Craig A Buchman. Cochlear implantation with hearing preservation yields significant benefit for speech recognition in complex listening environments. *Ear and hearing*, 34(4):413, 2013.
- [95] Jose F Téllez-Zenteno and Lizbeth Hernández-Ronquillo. A review of the epidemiology of temporal lobe epilepsy. *Epilepsy research and treatment*, 2012, 2012.
- [96] Samuel Wiebe and Nathalie Jetté. Epilepsy surgery utilization: who, when, where, and why? *Current opinion in neurology*, 25(2):187–193, 2012.
- [97] Robert E Gross, Matthew A Stern, Jon T Willie, Rebecca E Fasano, Amit M Sandane, Bruno P Soares, Nigel P Pedersen, and Daniel L Drane. Stereotactic laser amygdalohippocampotomy for mesial temporal lobe epilepsy. *Annals of neurology*, 83(3):575–587, 2018.

- [98] Daniel L Drane, David W Loring, Natalie L Voets, Michele Price, Jeffrey G Ojemann, Jon T Willie, Amit M Saindane, Vaishali Phatak, Mirjana Ivanisevic, Scott Millis, et al. Better object recognition and naming outcome with mri-guided stereotactic laser amygdalohippocampotomy for temporal lobe epilepsy. *Epilepsia*, 56(1): 101–113, 2015.
- [99] James X Tao, Shasha Wu, Maureen Lacy, Sandra Rose, Naoum P Issa, Carina W Yang, Katherine E Dorociak, Maria Bruzzone, Jisoon Kim, Ahmad Daif, et al. Stereotactic eeg-guided laser interstitial thermal therapy for mesial temporal lobe epilepsy. *J Neurol Neurosurg Psychiatry*, 89(5):542–548, 2018.
- [100] Sanjeet S Grewal, Richard S Zimmerman, Gregory Worrell, Benjamin H Brinkmann, William O Tatum, Amy Z Crepeau, David A Woodrum, Krzysztof R Gorny, Joel P Felmlee, Robert E Watson, et al. Laser ablation for mesial temporal epilepsy: a multi-site, single institutional series. *Journal of neurosurgery*, 130(6):2055–2062, 2018.
- [101] Scheherazade Le, Allen L Ho, Robert S Fisher, Kai J Miller, Jaimie M Henderson, Gerald A Grant, Kimford J Meador, and Casey H Halpern. Laser interstitial thermal therapy (litt): seizure outcomes for refractory mesial temporal lobe epilepsy. *Epilepsy & Behavior*, 89:37–41, 2018.
- [102] Pierre-François D’Haese, Peter E Konrad, Srivatsan Pallavaram, Rui Li, Priyanka Prasad, William Rodriguez, and Benoit M Dawant. Cranialcloud: a cloud-based architecture to support trans-institutional collaborative efforts in neurodegenerative disorders. *International journal of computer assisted radiology and surgery*, 10(6): 815–823, 2015.
- [103] Srijata Chakravorti, Walter J Jermakowicz, Chengyuan Wu, Rui Li, Raul Wirz-Gonzalez, Benoit M Dawant, and Pierre-François D’Haese. Evaluation of nonrigid

- registration around the hippocampus for the construction of statistical maps in a multicenter dataset of epilepsy laser ablation patients. In *Medical Imaging 2019: Image-Guided Procedures, Robotic Interventions, and Modeling*, volume 10951, page 109511J. International Society for Optics and Photonics, 2019.
- [104] Giovanni B Frisoni, Clifford R Jack Jr, Martina Bocchetta, Corinna Bauer, Kristian S Frederiksen, Yawu Liu, Gregory Preboske, Tim Swihart, Melanie Blair, Enrica Cavado, et al. The eadc-adni harmonized protocol for manual hippocampal segmentation on magnetic resonance: evidence of validity. *Alzheimer's & Dementia*, 11(2): 111–125, 2015.
- [105] Lisette Bosscher and Philip Scheltens. Mri of the medial temporal lobe for the diagnosis of alzheimer's disease. *Evidence Based Dementia Practice*, page 154, 2002.
- [106] Gustavo K Rohde, Akram Aldroubi, and Benoit M Dawant. The adaptive bases algorithm for intensity-based nonrigid image registration. *IEEE transactions on medical imaging*, 22(11):1470–1479, 2003.
- [107] Yuan Liu, Pierre-François D'Haese, and Benoit M Dawant. Effects of deformable registration algorithms on the creation of statistical maps for preoperative targeting in deep brain stimulation procedures. In *Medical Imaging 2014: Image-Guided Procedures, Robotic Interventions, and Modeling*, volume 9036, page 90362B. International Society for Optics and Photonics, 2014.
- [108] Srivatsan Pallavaram, Pierre-François D'Haese, Wendell Lake, Peter E Konrad, Benoit M Dawant, and Joseph S Neimat. Fully automated targeting using non-rigid image registration matches accuracy and exceeds precision of best manual approaches to subthalamic deep brain stimulation targeting in parkinson disease. *Neurosurgery*, 76(6):756–765, 2015.

- [109] Jugoslav Ivanovic, Pål G Larsson, Ylva Østby, John Hald, Bård K Krossnes, Jan G Fjeld, Are H Pripp, Kristin Å Alfstad, Arild Egge, and Milo Stanistic. Seizure outcomes of temporal lobe epilepsy surgery in patients with normal mri and without specific histopathology. *Acta neurochirurgica*, 159(5):757–766, 2017.
- [110] Brett E Youngerman, Justin Y Oh, Deepti Anbarasan, Santoshi Billakota, Camilla H Casadei, Emily K Corrigan, Garret P Banks, Alison M Pack, Hyunmi Choi, Carl W Bazil, et al. Laser ablation is effective for temporal lobe epilepsy with and without mesial temporal sclerosis if hippocampal seizure onsets are localized by stereoelectroencephalography. *Epilepsia*, 59(3):595–606, 2018.
- [111] Philippe Kahane and Fabrice Bartolomei. Temporal lobe epilepsy and hippocampal sclerosis: lessons from depth eeg recordings. *Epilepsia*, 51:59–62, 2010.
- [112] Barbara C Jobst and Gregory D Cascino. Resective epilepsy surgery for drug-resistant focal epilepsy: a review. *Jama*, 313(3):285–293, 2015.
- [113] Louis Maillard, Jean-Pierre Vignal, Martine Gavaret, Maxime Guye, Arnaud Biraben, Aileen McGonigal, Patrick Chauvel, and Fabrice Bartolomei. Semiologic and electrophysiologic correlations in temporal lobe seizure subtypes. *Epilepsia*, 45(12):1590–1599, 2004.
- [114] Zhenxing Sun, Huancong Zuo, Dan Yuan, Yaxing Sun, Kai Zhang, Zhiqiang Cui, and Jin Wang. Predictors of prognosis in patients with temporal lobe epilepsy after anterior temporal lobectomy. *Experimental and therapeutic medicine*, 10(5):1896–1902, 2015.
- [115] Ashalatha Radhakrishnan, Ramshekhar Menon, Sanjeev V Thomas, Mathew Abraham, George Vilanilam, Chandrashekharan Kesavadas, Bejoy Thomas, Ajith Cherian, and Ravi Prasad Varma. “time is brain”—how early should surgery be done in drug-resistant tle? *Acta Neurologica Scandinavica*, 138(6):531–540, 2018.

- [116] Eun Yeon Joo, Hyun Jung Han, Eun Kyung Lee, Sujung Choi, Ju Hee Jin, Jee Hyun Kim, Woo Suk Tae, Dae Won Seo, Seung-Chyul Hong, Munhyang Lee, et al. Resection extent versus postoperative outcomes of seizure and memory in mesial temporal lobe epilepsy. *Seizure*, 14(8):541–551, 2005.
- [117] Allen R Wyler, Bruce P Hermann, and Grant Somes. Extent of medial temporal resection on outcome from anterior temporal lobectomy: a randomized prospective study. *Neurosurgery*, 37(5):982–989, 1995.
- [118] Anne-Sophie Wendling, Edouard Hirsch, Ilona Wisniewski, Céline Davanture, Isabell Ofer, Josef Zentner, Sofia Bilic, Julia Scholly, Anke M Staack, Maria-Paula Valenti, et al. Selective amygdalohippocampectomy versus standard temporal lobectomy in patients with mesial temporal lobe epilepsy and unilateral hippocampal sclerosis. *Epilepsy research*, 104(1-2):94–104, 2013.
- [119] Johannes Schramm. Temporal lobe epilepsy surgery and the quest for optimal extent of resection: a review. *Epilepsia*, 49(8):1296–1307, 2008.
- [120] Johannes Schramm, TN Lehmann, J Zentner, CA Mueller, J Scorzin, R Fimmers, HJ Meencke, A Schulze-Bonhage, and CE Elger. Randomized controlled trial of 2.5-cm versus 3.5-cm mesial temporal resection in temporal lobe epilepsy—part 1: intent-to-treat analysis. *Acta neurochirurgica*, 153(2):209–219, 2011.
- [121] Claire Haegelen, Piero Perucca, Claude-Edouard Châtillon, Luciana Andrade-Valença, Rina Zelman, Julia Jacobs, D Louis Collins, François Dubeau, André Olivier, and Jean Gotman. High-frequency oscillations, extent of surgical resection, and surgical outcome in drug-resistant focal epilepsy. *Epilepsia*, 54(5):848–857, 2013.
- [122] Siming Bayer, Andreas Maier, Martin Ostermeier, and Rebecca Fahrig. Intraopera-

tive imaging modalities and compensation for brain shift in tumor resection surgery. *International journal of biomedical imaging*, 2017, 2017.

- [123] Marta S Vismer, Patrick A Forcelli, Mark D Skopin, Karen Gale, and Mohamad Z Koubeissi. The piriform, perirhinal, and entorhinal cortex in seizure generation. *Frontiers in neural circuits*, 9:27, 2015.
- [124] Dali Yin, John A Thompson, Cornelia Drees, Steven G Ojemann, Lidia Nague, Victoria S Pelak, and Aviva Abosch. Optic radiation tractography and visual field deficits in laser interstitial thermal therapy for amygdalohippocampectomy in patients with mesial temporal lobe epilepsy. *Stereotactic and functional neurosurgery*, 95(2):107–113, 2017.
- [125] Bertrand Mathon, Vincent Navarro, Franck Bielle, Vi-Huong Nguyen-Michel, Alexandre Carpentier, Michel Baulac, Philippe Cornu, Claude Adam, Sophie Dupont, and Stéphane Clemenceau. Complications after surgery for mesial temporal lobe epilepsy associated with hippocampal sclerosis. *World neurosurgery*, 102: 639–650, 2017.
- [126] Rachel Pruitt, Alexander Gamble, Karen Black, Michael Schulder, and Ashesh D Mehta. Complication avoidance in laser interstitial thermal therapy: lessons learned. *Journal of neurosurgery*, 126(4):1238–1245, 2017.
- [127] Ludvic Zrinzo, Thomas Foltynie, Patricia Limousin, and Marwan I Hariz. Reducing hemorrhagic complications in functional neurosurgery: a large case series and systematic literature review. *Journal of neurosurgery*, 116(1):84–94, 2012.
- [128] Joanne Wrench, Sarah J Wilson, and Peter F Bladin. Mood disturbance before and after seizure surgery: a comparison of temporal and extratemporal resections. *Epilepsia*, 45(5):534–543, 2004.

- [129] Barbara Schmeiser, Moritz Daniel, Evangelos Kogias, Daniel Böhringer, Karl Egger, Shan Yang, Niels Alexander Foit, Andreas Schulze-Bonhage, Bernhard Jochen Steinhoff, Josef Zentner, et al. Visual field defects following different resective procedures for mesiotemporal lobe epilepsy. *Epilepsy & Behavior*, 76:39–45, 2017.
- [130] Aaron A Cohen-Gadol, Jacqueline A Leavitt, James J Lynch, W Richard Marsh, and Gregory D Cascino. Prospective analysis of diplopia after anterior temporal lobectomy for mesial temporal lobe sclerosis. *Journal of neurosurgery*, 99(3):496–499, 2003.
- [131] Sonya Mehta, Kayo Inoue, David Rudrauf, Hanna Damasio, Daniel Tranel, and Thomas Grabowski. Segregation of anterior temporal regions critical for retrieving names of unique and non-unique entities reflects underlying long-range connectivity. *Cortex*, 75:1–19, 2016.